

*2<sup>nd</sup> Chitose International Forum on Photonics Science & Technology*  
*(CIF'2)*

International Forum on Nanotechnology: Toward the Organic Photonics

September 6-8, 2001

Chitose Institute of Science and Technology (CIST)

Chitose, Hokkaido, Japan



Sponsor: Japan Society for the Promotion of Science (JSPS)  
Co-sponsors: JSPS 142<sup>nd</sup> Committee  
Chitose Institute of Science and Technology (CIST)  
Photonics World Consortium (PWC)  
City of Chitose  
The Ogasawara Foundation for Promotion of Science & Engineering  
U.S. AFOSR/AOARD  
The Society of Polymer Science, Japan

**DISTRIBUTION STATEMENT A**  
Approved for Public Release  
Distribution Unlimited

20011023 030

<b>REPORT DOCUMENTATION PAGE</b>					<i>Form Approved</i> <b>OMB No. 0704-0188</b>	
<small>The public reporting burden for this collection of information is estimated to average 1 hour per response, including the time for reviewing instructions, searching existing data sources, gathering and maintaining the data needed, and completing and reviewing the collection of information. Send comments regarding this burden estimate or any other aspect of this collection of information, including suggestions for reducing the burden, to Department of Defense, Washington Headquarters Services, Directorate for Information Operations and Reports (0704-0188), 1215 Jefferson Davis Highway, Suite 1204, Arlington, VA 22202-4302. Respondents should be aware that notwithstanding any other provision of law, no person shall be subject to any penalty for failing to comply with a collection of information if it does not display a currently valid OMB control number.</small> <b>PLEASE DO NOT RETURN YOUR FORM TO THE ABOVE ADDRESS.</b>						
<b>1. REPORT DATE (DD-MM-YYYY)</b> 12-10-2001		<b>2. REPORT TYPE</b> Conference Proceedings			<b>3. DATES COVERED (From - To)</b>	
<b>4. TITLE AND SUBTITLE</b>  Chitose International Forum on Photonic Sciences (In Memory of Professor Sasaki)				<b>5a. CONTRACT NUMBER</b> F6256201M9086		
				<b>5b. GRANT NUMBER</b>		
				<b>5c. PROGRAM ELEMENT NUMBER</b>		
<b>6. AUTHOR(S)</b>  Conference Committee				<b>5d. PROJECT NUMBER</b>		
				<b>5e. TASK NUMBER</b>		
				<b>5f. WORK UNIT NUMBER</b>		
<b>7. PERFORMING ORGANIZATION NAME(S) AND ADDRESS(ES)</b> Chitose Institute of Science and Technology 758-65 Bibi Chitose 066-8655 Japan					<b>8. PERFORMING ORGANIZATION REPORT NUMBER</b>  N/A	
<b>9. SPONSORING/MONITORING AGENCY NAME(S) AND ADDRESS(ES)</b>  AOARD UNIT 45002 APO AP 96337-5002					<b>10. SPONSOR/MONITOR'S ACRONYM(S)</b>  AOARD	
					<b>11. SPONSOR/MONITOR'S REPORT NUMBER(S)</b> CSP-011019	
<b>12. DISTRIBUTION/AVAILABILITY STATEMENT</b>  Approved for public release; distribution is unlimited.						
<b>13. SUPPLEMENTARY NOTES</b>						
<b>14. ABSTRACT</b>  This is an interdisciplinary conference. Its aim is to achieve international cooperation among researchers and to stimulate the field of nonlinear polymers as photonic materials and devices. Topics to be covered include fundamental studies, novel molecu						
<b>15. SUBJECT TERMS</b>  Photonics, Polymer Chemistry, Surveillance, Nonlinear Optical Materials, Optoelectronic Materials, Optical Materials						
<b>16. SECURITY CLASSIFICATION OF:</b>			<b>17. LIMITATION OF ABSTRACT</b>  UU	<b>18. NUMBER OF PAGES</b>	<b>19a. NAME OF RESPONSIBLE PERSON</b> Joanne H. Maurice	
a. REPORT  U	b. ABSTRACT  U	c. THIS PAGE  U			<b>19b. TELEPHONE NUMBER (Include area code)</b> +81-3-5410-4409	

## ***2<sup>nd</sup> Chitose International Forum on Photonics Science & Technology (CIF'2)***

**International Forum on Nanotechnology: Toward the Organic Photonics**

**September 6-8, 2001**

**Chitose Institute of Science and Technology (CIST)**

**Chitose, Hokkaido, Japan**

**Chairman:** Naoya Ogata (CIST)

**Organizing Committee:**

Chihaya Adachi (CIST)  
Tomiki Ikeda (Tokyo Institute of Technology)  
Naoyuki Koide (Tokyo University of Science)  
Hachiro Nakanishi (Tohoku University)  
Masatsugu Shimomura (Hokkaido University)  
Kohei Uosaki (Hokkaido University)  
Tatsuo Wada (RIKEN)  
Hiroshi Yokoyama (National Institute of AIST)

**Local Committee:**

Suguru Horinouchi (CIST)  
Kuniharu Ijiri (Hokkaido University)  
Hiroshi Izumi (Chitose City)  
Olaf Karthaus (CIST)  
Yutaka Kawabe (CIST)  
Toshiharu Kobayashi (CIST)  
Masatsugu Shimomura (Hokkaido University)  
Junichi Yoshida (CIST)

**International Advisory Board:**

Jang Joo Kim (Kwangju Institute of Science & Technology, Korea)  
Wolfgang Knoll (Max-Planck Institute, Germany)  
Toyoki Kunitake (University of Kitakyushu, Japan)  
Jean Marie Lehn (College de France, France)  
Zongfan Liu (Peking University, China)  
Seth Marder (University of Arizona, USA)  
Andre Persoons (Lueven University, Belgium)  
Stephen Sligar (University of Illinois, USA)

**Secretary General:**

Hiroyuki Sasabe (CIST)

**Correspondence:**

Chitose Institute of Science & Technology  
758-65 Bibi, Chitose, Hokkaido 066-8655, Japan  
TEL&FAX: +81-123-27-6109 E-mail: [sasabeh@photon.chitose.ac.jp](mailto:sasabeh@photon.chitose.ac.jp)

## CIF'2 Program

### September 6 (Thu)

8:50-9:00            Opening Remarks            Prof. Naoya Ogata (CIST)

### Session 1: Molecular Design and Synthesis of Photonic Supramolecules

Chairman: Dr. Tatsuo Wada/ Prof. Jung Il Jin

9:00-10:30

S1-1      Toyoki Kunitake (FRS, RIKEN, Japan) *Invited*  
Molecular Design of Organized Nano-Films and their Functions

S1-2      Jung-Il Jin (Korea University, Korea) *Invited*  
Luminescence Properties of Substituted PPVs

S1-3      Yasuhiko Shirota, Motoi Kinoshita, Kenji Okumoto, Tetsuya Noda and Hidekaru Doi  
(Osaka University, Japan)  
Amorphous Molecular Materials for Organic Electroluminescent Devices

10:30-11:00            Coffee Break

S1-4      Stephen M. Kuebler, Kevin Braun, David Carrig, Seth R. Marder, Christopher K. Ober,  
Joseph W. Perry, Mariacristina Rumi, Toshiyuki Watanabe, Tianyue Yu and Wenhui Zhou  
(University of Arizona, USA) *Invited*  
Design, Characterization, and Application of High-Sensitivity Two-Photon Initiators for  
Three-Dimensional Lithographic Microfabrication

S1-5      Masaaki Iwata, Yoshihiro Imase, Atsushi Gunji, Tetsuya Aoyama and Tatsuo Wada  
(RIKEN, Japan) *Invited*  
Multifunctional Supramolecules for Photonic Application

S1-6      Takakazu Yamamoto (Tokyo Institute of Technology)  
Preparation of New  $\pi$ -Conjugated Polymers

12:30-14:00            Lunch

### Session 2: Control/Processing of Nanostructures

Chairman: Prof. Jong-Dal Hong/ Prof. Hachiro Nakanishi

14:00-15:30

S2-1      Hachiro Nakanishi (IMRAM, Tohoku University, Japan) *Invited*  
Preparation of Organic and Hybridized Nanocrystals for Photonics

S2-2      Masahiko Hara, Jaegun Noh, Keita Mitsui and Ken Nakajima (FRS, RIKEN, Japan) *Invited*  
Self-Assembled Monolayers and Optical Instability

S2-3      Olaf Karthaus, Toshiro Imai, Daisuke Miyakawa, Mariko Watanabe (CIST, Japan)

Dewetting-Assisted Controlled Crystallization of Dyes

15:30-15:45      **Coffee Break**

15:45-17:45

- S2-4      Gyoujin Cho, Sung-Gi Jung, Jongkwan Jang and Jae-Suk Lee  
(Sunchon National University, Korea)  
Natural Growth for the Formation of Complex Nanostructures Using Microphase Separated  
Block Copolymer as Template
- S2-5      Sang Woo Han, Inhyung Lee and Kwan Kim (CMC, Seoul National University, Korea)  
Chemical Lithography Via Visible Light
- S2-6      Yuhei Shimoyama (Hokkaido University of Education, Japan)  
Fabrication Techniques of Langmuir-Blodgett Films of Photonic Molecules
- S2-7      Seung-Sub Lee, Woo-Cheol Cheong, Myeon-Cheol Kim and Jong-Dal Hong  
(University of Incheon, Korea)  
Spin-Coated Multilayer Assemblies of Oppositely Charged Materials:  
From Bolaamphiphiles to Polyelectrolytes

18:00-20:00      **Poster Session** (Atrium)

**September 7 (Fri)**

**Session 3: Characterization of Nanostructures**

Chairman: Prof. Kohei Uosaki/ Prof. Hermann Gaub

9:00-10:30

- S3-1      Hermann Gaub (University of Munich, Germany) *Invited*  
Single Molecule Force Spectroscopy by AFM-Related Techniques
- S3-2      Satoshi Kawata (Osaka University, Japan) *Invited*  
Plasmon-Enhanced Near-Field Raman Spectroscopy for Nano-Imaging
- S3-3      Hiroshi Masuhara (Osaka University, Japan) *Invited*  
Femtosecond Spectroscopy and Photochemistry of Individual Organic Nanoparticles

10:30-11:00      **Coffee Break**

11:00-12:30

- S3-4      Masaya Mitsuishi, T. Tamura, J. Matui and T. Miyashita (Tohoku University, Japan)  
Spectroscopic Characterization of Polymer LB Films Assembled on Integrated Optical  
Waveguide
- S3-5      Agus Haryono, Satoru Shimada, Yuji Kaneko, Takashi Fukuda and Hiro Matsuda  
Surface Plasmon Resonance Effect on Polydiacetylene Conjugated Main Chain

S3-6 Tianxin Wei, H. Akiyama, Kaoru Tamada and Kiyoshi Yase  
PM-IRRAS Characterization of Highly Photoreactive SAMs on Gold

12:30 **Group Photo and Memorial Tree Planting**

**Special Lecture** (Hotel Nikko Chitose)

Chairman: Prof. Hiroyuki Sasabe (CIST)

14:00-14:10 Remarks Prof. Naoya Ogata (CIST)

14:10-14:20 Welcome Address Mr. Takashi Higashikawa (Mayor of Chitose City)

14:20-15:20

SL-1 Alan G. MacDiarmid (University of Pennsylvania, USA; Nobel Laureate)  
Synthetic Metals: A Novel Role for Organic Polymers

15:50-16:50

SL-2 Yasuhiro Koike (Keio University, Japan)  
Novel Photonics Polymer for Information Technology – Science and Dream of Future –

18:30-20:30 **Banquet** (Hotel Nikko Chitose)

## **September 8 (Sat)**

### **Session 4: Biophotonics**

Chairman: Prof. Masatsugu Shimomura/ Prof. Wolfgang Knoll

9:00-10:30

S4-1 Wolfgang Knoll, T. Neumann and D. Kambhampati  
(Max-Planck Institute, Germany) *Invited*  
Surface Plasmon Optical Techniques for the Quantitative Evaluation of Oligonucleotide Hybridization Reactions at Solid/Solution Interfaces

S4-2 Hiroyuki Tanaka and Tomoji Kawai (Osaka University, Japan) *Invited*  
Nanostructure of DNA and Formation of DNA Network

S4-3 K. Ijiro, R. Mitamura, S.-I. Nishimura, T. Sawadaishi and M. Shimomura  
(RIES, Hokkaido University, Japan)  
Controlled Immobilization of Single DNA Molecules Complexed with Cationic Lipid Monolayer at the Air-Water Interface

10:30-11:00 **Coffee Break**

11:00-12:30

S4-4 M. Shimomura, J. Matsumoto and K. Ijiro (RIES, Hokkaido University, Japan) *Invited*  
DNA-Mimetics. Novel Molecular Nanostructure for Molecular Photonics Devices

S4-5 Lili Wang and Naoya Ogata (CIST, Japan)

Molecular Design, Preparation and Characterization of Photonic Supramolecules,  
Functional Organic Dye-DNA-Surfactant Complex Film

- S4-6 Yoshio Okahata (Tokyo Institute of Technology, Japan) *Invited*  
Preparation and Anisotropic Electroconduction of a DNA-aligned Thin Film

12:30-14:00      **Lunch**

**Session 5: Nanophotonics Devices**

Chairman: Prof. Chihaya Adachi/ Prof. Jang Joo Kim

14:00-15:30

- S5-1 Jang-Joo Kim, C.-L. Lee, Yong-Young Noh, R. R. Das (K-JIST, Korea) *Invited*  
Polymer Electrophosphorescence Devices
- S5-2 Vladimir Bulovic (MIT, USA) *Invited*  
Dynamics of Electrostatic Molecular Interactions in Doped Organic Thin Films
- S5-3 Hiroshi Yokoyama, J. -H. Kim and M. Yoneya (AIST & ERATO, Japan) *Invited*  
Photonic Devices using Nanostructured Liquid Crystals

15:30-16:00      **Coffee Break**

16:00-17:30

- S5-4 Chihaya Adachi, S. R. Forrest and M. E. Thompson  
(CIST, Japan; Princeton University, USA; USC, USA) *Invited*  
Nearly 100% Internal Phosphorescence Efficiency in an Organic Light Emitting Diode
- S5-5 Kenji Harada, Masahide Itoh, Shinsuke Umegaki and Toyohiko Yatagai  
(Tsukuba University, Japan)  
Direct Fabrication Method of Surface Relief Structures on Azo-Polymer Films and its Application
- S5-6 Toshihiro Kondo, Masayuki Okamura, Takuya Masuda and Kohei Uosaki  
(Hokkaido University, Japan)  
Very Efficient Visible-Light-Induced Electron Transfer at Gold Electrodes Modified with Self-Assembled Monolayers of Various Metalporphyrin-Ferrocene-Thiol Linked Molecules

17:30      Closing Remarks

**Poster Presentation (September 6 18:00 – 20:00 Atrium, CIST)**

- P-1 Lili Wang, Hiroaki Takahashi, Gongjian Zhang, Junichi Yoshida and Naoya Ogata (CIST, Japan)  
Optical and Optoelectronic Materials Derived from Deoxyribonucleic Acid (DNA)
- P-2 Lili Wang, Masahiro Fukusima, Junichi Yoshida, Naoya Ogata (CIST, Japan)  
A Novel Photochromic Film Materials Derived from Supramolecules, DNA-Surfactant Complex: Spiropyran-DNA-CTMA Complex
- P-3 Inhyung Lee, Sang Woo Han, and Kwan Kim (LII, CMC, Seoul National University, Korea)  
Nanoparticle-Directed Crystallization of Calcium Carbonate
- P-4 Gongjian Zhang, Kanna Uchikoshi, Toshihiko Tanaka and Naoya Ogata (CIST, Japan)  
Nonlinear Optical Properties of Anisotropic Molecular Thin Films on Nanostructured Poly(tetrafluoroethylene) Surfaces
- P-5 Toshihiko Matsuura and Yuhei Shimoyama (Hokkaido University of Education, Japan)  
Langmuir-Blodgett Films of  $\beta$ -Carotene Fabricated by Flow-Orientation Method
- P-6 Toshihiko Matsuura, Hiroshi Sakaguchi and Yuhei Shimoyama (Hokkaido University of Education, Japan)  
Formation and Structure of Self-Assembled Films of Poly(3-alkylthiophene)
- P-7 Hiroyuki Kaji and Yuhei Shimoyama (Hokkaido University of Education, Japan)  
Langmuir-Blodgett Films of Nitrostilbene
- P-8 Yuukou Matsuda, Chimed Ganzorig and Masamichi Fujihira (TIT, Japan)  
Enhanced Electron Injection in Blue Organic Electroluminescent Devices
- P-9 Yasunori Taga (Toyota Central R&D Labs., Japan)  
Highly Efficient Organic Light-Emitting Diodes: Materials and Devices
- P-10 Limin Li, Kunihiro Kodama and Katsuo Aizawa (CIST, Japan)  
Photodynamics of Mono-L-aspartylchlorin E6 for Photodynamic Therapy
- P-11 Liming Li, Satoru Kusaka, Ryuji Morita and Mikio Yamashita (CIST, Hokkaido University, Japan)  
SPIDER and FROG Apparatuses for Phase Characterization of Few-Optical-Cycle Pulses
- P-12 Shinya Matsumoto, Tatsuo Wada and Masaru Matsuoka (RIKEN, Japan)  
Solid State Spectra and Intermolecular Interactions of Tetrathiobenzoquinone Derivatives
- P-13 Yoshihiro Imase, Tatsuo Wada, Atsushi Gunji (RIKEN, Japan)  
Development of Novel Carbazole Macrocycles



- P-14 T. Kobayashi, J. Hamazaki, M. Arakawa, H. Kunugita, T. Endo, M. Rikukawa, K. Sanui and K. Ema (Sophia University, Japan)  
Time-Resolved Photoluminescence Spectrum of Polythiophene Derivative
- P-15 Yasuo Toko, Masahiro Funahashi, Jun-ichi Hanna (Stanley Electric Co., Japan)  
Electro-Optical Characteristics of Self-Organizing Molecular Semiconductor Aligned by Polyimide Film
- P-16 Hidetomo Ashitaka, Kouki Ishihara and Naoya Ogata (CIST, Japan)  
Preparation of DNA Optical Fibers
- P-17 Yoshiaki Ito, Takayuki Fukagawa, Yuichiro Kumakura, Masahi Eguchi, Hiroyuki Sasabe and Suguru Horinouchi (CIST, Japan)  
Analysis of Mode Propagation in Plastic Optical Fibers
- P-18 Takayuki Fukagawa, Yoshiaki Ito, Masahi Eguchi, Hiroyuki Sasabe and Suguru Horinouchi (CIST, Japan)  
Development of Optical Module for Plastic Optical Fiber Link Systems
- P-19 Mitsuhiro Koda, Masatoshi Gyoten, Keitaro Koguchi, Masahi Eguchi, Kazuhito Fujii, Hiroyuki Sasabe and Suguru Horinouchi (CIST, Japan)  
New Model for CW Amplification in Plastic Optical
- P-20 Yasuteru Mawatari, Takeyuki Sone, Yoshikazu Sadahiro and Masayoshi Tabata (Hokkaido University, Japan)  
 $\pi$ -Conjugated Nanohole Columnar of Substituted Polyacetylene Prepared with a Rh Complex Catalyst
- P-21 Koichi Baba, Eiji Sarashina, Hitoshi Kasai, Shuji Okada, Hidetoshi Oikawa and Hachiro Nakanishi (IMRAM, Tohoku University, Japan)  
Improvement of Reprecipitation Method for Fabrication of Organic Microcrystals
- P-22 Masao Suzuki, Hitoshi Kasai, Shuji Okada, Hidetoshi Oikawa, Takayasu Nihira, Hiroyoshi Fukuro and Hachiro Nakanishi (IMRAM, Tohoku University, Japan)  
Fabrication of Polyimide Nanoparticles
- P-23 Nam Hoon Kim, Sang Woo Han, Inhyung Lee and Kwan Kim (LII, CMC, Seoul National University, Korea)  
Effect of Polymeric Stabilizers on the Catalytic Activity of Pt Nanoparticles
- P-24 Chimed Ganzorig and Masamichi Fujihara (TIT, Japan)  
Surface Potential Difference Measurements on Indium-Tin-Oxide Substrates Modified with Various Organic Molecules
- P-25 Masayuki Okamura, Toshihiro Kondo and Kohei Uosaki (Hokkaido University, Japan)  
Construction and Electron Transfer Characteristics of Multilayers of Au Nanoclusters

Modified with Self-Assembled Monolayers Containing Ferrocene Group

- P-26 Toshihiro Kondo, Toshihito Kanai and Kohei Uosaki (Hokkaido University, Japan)  
Control of the Charge Transfer Rate at a Gold Electrode Modified with a Self-Assembled Monolayer Containing Ferrocene and Azobenzene by Electro- and Photochemical Structural Conversion of *cis*- and *trans*-forms of the Azobenzene Moiety
- P-27 Tetsuro Sawadaishi, Kuniharu Ijiri and Masatsugu Shimomura  
(RIES, Hokkaido University, Japan)  
Preparation and Characterization of Mesoscopic Patterns of Nanoparticles
- P-28 Jin Matsumoto, Kuniharu Ijiri, Shinichiro Nishimura and Masatsugu Shimomura  
(RIES, Hokkaido University, Japan)  
Template Polymerization of Diacetylene Assemblies Based on DNA-Mimetics at the Air-Water Interface
- P-29 Satoshi Nihonyanagi, S. Ye and Kohei Uosaki (Hokkaido University, Japan)  
Sum Frequency Generation Study on the Structure of Interfacial Molecules and Dynamics
- P-30 Ichizo Yagi, Kojiro Ebina, Satoru Idojiri and Kohei Uosaki (Hokkaido University, Japan)  
Dynamics of Photogenerated Carriers at Surface -Modified GaAs
- P-31 Hiroyuki Sasabe, Hirofumi Hokai, Masahisa Osawa and Takashi Isoshima (RIKEN, Japan)  
Rigid Dendrimers for Light Harvesting
- P-32 Okihiro Sugihara (Shizuoka University, Japan)  
Nanoimprint Technology for the Formation of High Resolution Periodic Structure in Electrooptic Polymers

## *Molecular Design of Organized Nano-Films and their Functions*

Toyoki Kunitake,  
Frontier Research System, RIKEN

Organized nano-films of organic molecules may be prepared by either transfer techniques or by adsorption techniques. Representative cases of the former are Langmuir-Blodgett technique and micro-contact printing. The latter includes polymerization-induced epitaxy/adsorption, electrostatic alternate adsorption and the surface sol-gel process. We discuss in this lecture preparation of nano-precision films by the use of alternate electrostatic adsorption of polyelectrolytes and the surface sol-gel process of metal alkoxides.

The electrostatic layer-by-layer adsorption technique has been commonly applied to oppositely-charged polyions including linear synthetic polymers and DNA. We extended this technique to polyions of spherical shapes such as globular proteins, nano-particles and inorganic nano-plates. As an example, multi-enzyme films that sequentially catalyze hydrolysis and oxidation are prepared by this procedure through ordering of multiple enzyme layers. Ordered nano-composites of organic polyions and clay nano-plates are similarly obtainable (1).

The surface sol-gel process is useful for preparing ultrathin metal oxide films with ease. In this method, molecular multi-layers of metal oxide gel are formed by repeating chemi-sorption of metal alkoxides and subsequent hydrolysis of the adsorbed layers (2). For example, TiO<sub>2</sub> layers with nanometer thickness can be grown repeatedly for at least 20 cycles, as monitored by quartz crystal microbalance and scanning electron microscopy. It is also possible to use hydroxylated organic and inorganic compounds such as poly(acrylic acid), porphyrin carboxylic acids, cyclodextrins and surface-modified gold nano-particles, in combination with metal alkoxides, for fabrication of organic/inorganic alternate nanolayers. The alternate layers are also produced by taking advantage of electrostatic attraction between metal oxide layer and cationic organic polymers and metal clusters, since metal oxide layers are negatively charged due to deprotonation. In the case of weakly bound hydroxyl species such as monocarboxylic acids and derivatized amino acids, the organic components can be washed out after formation of alternate film (3). The remaining films exhibit imprinting effects for the template organic molecule. The template

effects are found not only for different monocarboxylic acids but also for regio-isomers and enantiomers.

Another extension of the surface sol-gel process is molecular wrapping which is performed by using the structural flexibility of metal oxide gel. Thus, a fluorescent molecule is wrapped by ultrathin  $\text{TiO}_2$  gel layer, although the wrapped molecular object is not stable enough and further capping is required for enhanced stability (4). The physical isolation of fluorescein molecule from the surrounding medium is ascertained by quenching experiment with iodine. The wrapping technique has been applied to linear and spherical molecules.

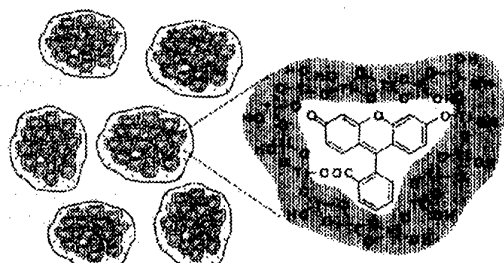
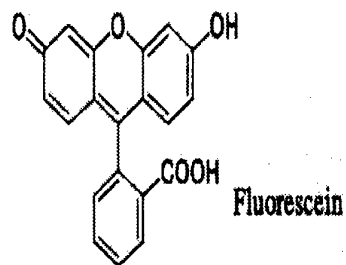


Figure: A schematic illustration of fluorescein /  $\text{TiO}_2$ -gel particles coated with capping reagents.



- (1) M. Sano, Y. Lvov, T. Kunitake, *Ann. Rev. Mater. Sci.*, 26, 153(1996)
- (2) I. Ichinose, H. Senzu, T. Kunitake, *Chem. Mater.*, 9, 1296(1997)
- (3) S-W. Lee, I. Ichinose, T. Kunitake, *Langmuir*, 14, 2857(1998)
- (4) I. Ichinose, T. Kunitake, *Chem. Lett.*, 2001(7), 626

## Luminescence Properties of Substituted PPVs

Jung-Il Jin

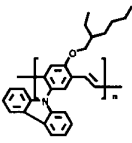
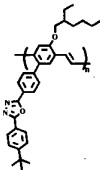
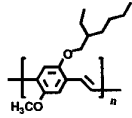
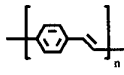
*Department of Chemistry and Center for Electro- and Photo- Responsive Molecules,*

*Korea University, Seoul 136-701, Korea*

*E-mail : jijin@mail.korea.ac.kr*

A series of poly(p-phenylenevinylene) (PPV) derivatives bearing a wide variety of pendants were synthesized, and their photo- (PL) and electroluminescence (EL) properties were studied in order to establish their structure – luminescence properties relationship [1-5]. Better understanding of EL characteristics of the polymers requires utilization of many analytical tools including various spectroscopic methods such as UV-vis absorption, UPS, XPS, NEXAFS, and measurement of carrier mobilities, and morphological studies.

In this presentation, EL properties of the following two polymers are discussed in detail in comparison with unsubstituted PPV and the well-known dialkoxy substituted PPV, MEh-PPV.

Materials				
	CzEh-PPV	OxdEh-PPV	MEh-PPV	PPV
$\lambda_{\text{max.}}^{\text{abs.}}$ (nm)	470	450	500	430
$\lambda_{\text{max.}}^{\text{EL}}$ (nm)	536	541	576	540
Opt. bandgap (eV)	2.3	2.3	2.1	2.5
E (T.O.) (MV/cm) <sup>a</sup>	0.63	2.3	0.43	1.1
$\Phi_{\text{EXT.}}(\%)^a$	$1.0 \times 10^{-2}$	$1.5 \times 10^{-2}$	$6.6 \times 10^{-4}$	$1.7 \times 10^{-4}$

a. Device configuration : ITO/ Polymer/ Al.

For the ITO/ PEDOT/ Polymer/ Ca/ Al devices, photometric efficiency (cd/A) and maximum luminescence (cd/m<sup>2</sup>) decrease in the order of CzEh-PPV (4.4) > OxdEh-PPV (1.2) ≥ MEh-PPV (1.1) and CzEh-PPV (39,000) > MEh-PPV (20,000) > OxdEh-PPV (5,700), respectively. Turn-on electric field of the devices are 0.4 – 0.5 MV/cm for CzEh-PPV and MEh-PPV and 1.2 MV/cm for OxdEh-PPV device.

The HOMO and LUMO levels of the polymers determined by UPS do not provide us with a clear

clue why MEh-PPV and CzEh-PPV devices exhibit lower turn-on electric fields than the OxdEh-PPV devices. The near-edge X-ray absorption fine structure spectroscopy, however, appears to give us some answers for the difference in the turn-on electric field of the EL devices fabricated with the polymers. When NEXAFS spectra of the polymer films are collected as calcium metal is deposited, it is observed for CzEh-PPV and MEh-PPV that a new peak appears within the leading edge of the  $\pi^*$  resonance indicating the formation of a new valence state (intragap state) within the band gap. In contrast, the OxdEh-PPV polymer does not show similar phenomenon. This tells us that charge injection from Ca into polymer is enhanced for the former two polymers by providing additional sites for electron transfer near the Fermi level of the metal. Formation of additional unoccupied states on contact with Ca metal should lower the threshold electric field for EL emission.

As far as the dependence of external quantum efficiency of light-emitting diodes (LEDs) based on the polymers is concerned, a combination of balance in carrier mobility and low threshold electric field is judged to be the most important factor. We measured the mobilities of holes and electrons of the polymers by the time-of-flight and electrical methods. In the later, we employed the space-charge limited conduction model. According to the results, the hole mobility in MEh-PPV is about 200 times the electron mobility whereas the mobilities of the two carriers are in balance in CzEh-PPV and OxdEh-PPV. Electrical measurements reveal that mobilities of both carriers in CzEh-PPV and OxdEh-PPV are greatly reduced when compared with those in MEh-PPV. Dissymmetrical electron distribution along the main chain of the two polymers appears to be responsible for the reduced mobilities of the carriers.

In addition, XPS analysis of surface compositions of polymer films spin-coated onto ITO-coated glasses strongly suggests that the hydrophobic groups in the two polymers are richer on the air-side surface than in bulk. In other words, the polar groups tend to orient themselves toward ITO-glass surface. This will promote the hole injection in CzEh-PPV, whereas both hole and electron injections are hampered in OxdEh-PPV.

Acknowledgment : This work is supported by the Korea Science and Engineering Foundation through CRM of Korea University.

## References

1. Burroughes, J. H.; Bradley, D. D. C.; Brown, A. R.; Marks, R. N.; Mackay, K.; Friend, R. H.; Burn, P. L.; Holmes, A. B. *Nature* **1990**, *347*, 539.
2. Gustafsson, G.; Gao, Y.; Treacy, G. M.; Klavetter, F.; Colaneri, N.; Heeger, A. J. *Nature* **1992**, *357*, 477.
3. Chung, S.-J.; Kwon, K.-Y.; Lee, S.-W.; Jin, J.-I.; Lee, C.-H.; Lee, C.-E.; Park, Y.-S. *Adv. Mater.* **1998**, *10*, 1112.
4. Lee, D. W.; Kwon, K.-Y.; Jin, J.-I.; Park, Y.; Kim, Y.-R.; Hwang, I.-W. *Chem. Mater.* **2001**, *13*, 565.
5. Kim, K.; Hong, Y.-R.; Lee, S.-W.; Jin, J.-I.; Park, Y.; Sohn, B.-H.; Kim, W.-H.; Park, J.-K. *J. Mater. Chem.* in press.

### Amorphous Molecular Materials for Organic Electroluminescent Devices

Yasuhiko Shirota, Motoi Kinoshita, Kenji Okumoto, Tetsuya Noda, and Hidekaru Doi  
Department of Applied Chemistry, Faculty of Engineering, Osaka University, Yamadaoka,  
Suita, Osaka 565-0871, Japan

The performance of organic electroluminescent (EL) devices depends on materials functioning in various specialized roles, including emitting, charge-transporting and charge-blocking materials. Therefore, creation of high-performance materials based on molecular design concepts is of great importance. Amorphous molecular materials that readily form stable amorphous glasses have demonstrated their suitability and versatility as materials for organic EL devices.<sup>1)</sup>

We report here the molecular design and synthesis of amorphous molecular materials and the fabrication and performance of organic EL devices using these materials. The concept of  $\pi$ -electron starburst molecules has led to the creation of various charge-transporting and emitting amorphous molecular materials for organic EL devices. Amorphous molecular materials with very low solid-state ionization potentials such as the 4,4',4''-tris(diphenylamino)triphenylamine (TDATA) family have been found to serve as hole-transporting materials that facilitate hole injection from the ITO electrode. Based on the concept of the incorporation of rigid moieties such as carbazolyl and fluorenyl groups to make nonplanar molecules for increasing the glass-transition temperature, we have developed thermally stable charge-transporting and emitting amorphous molecular materials. These materials permitted the fabrication of thermally stable organic EL devices which can operate even at 180 °C. We have proposed boron-containing compounds as candidates for electron-transporting materials and have shown that  $\alpha,\omega$ -bis(dimesitylboryl)oligothiophenes (BMB-nT) function well as electron transporters that facilitate electron injection from the cathode. 1,3,5-Tris[5-(dimesitylboryl)thiophen-2-yl]benzene (BMB-TB) functions as electron transporters with better hole-blocking character than Alq<sub>3</sub>. The design concept of molecules that form stable bipolar radicals for emitting amorphous molecular materials has led to the synthesis of new materials with desired properties. They function not only as emitting materials but also are expected to function as host materials that serve as a recombination center of injected holes and electrons.

1) Y. Shirota, *J. Mater. Chem.*, **10**, 1 (2000) and references cited therein.

## Design, Characterization, and Application of High-Sensitivity Two-Photon Initiators for Three-Dimensional Lithographic Microfabrication

Stephen M. Kuebler, Kevin Braun, David Carrig, Seth R. Marder, Christopher K. Ober<sup>(a)</sup>,  
Joseph W. Perry, Mariacristina Rumi, Toshiyuki Watanabe<sup>(b)</sup>, Tianyue Yu<sup>(a)</sup>, and  
Wenhui Zhou

Department of Chemistry, University of Arizona, Tucson, Arizona, 85721  
e-mail for SMK: kuebler@u.arizona.edu

<sup>(a)</sup>Materials Science and Engineering, Cornell University, Ithaca, New York, 14853

<sup>(b)</sup>Department of Applied Chemistry, Faculty of Technology, Tokyo University of Agriculture & Technology, 2-24-16 Nakamachi, Koganei-shi, Tokyo 184-8588, Japan

### Abstract

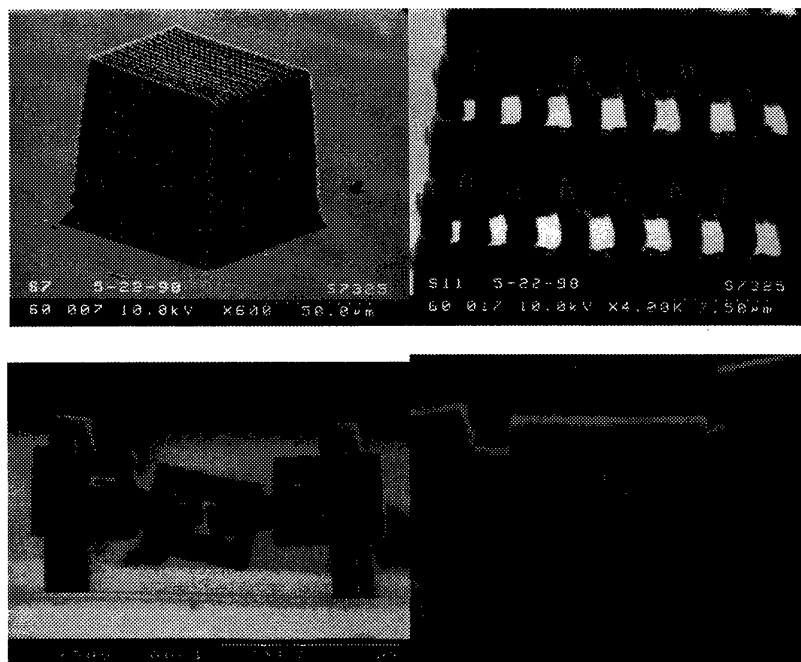
Two-photon excitation provides a means of activating chemical or physical processes with high spatial resolution in three dimensions and has enabled the development of 3D fluorescence imaging, 3D optical data storage, and 3D lithographic microfabrication.<sup>1,2</sup> Each of these applications takes advantage of the fact that the two-photon absorption probability depends quadratically on intensity. Under tight-focusing conditions, the absorption is confined at the focus to a volume of the order of  $\lambda^3$ , where  $\lambda$  is the excitation wavelength. Any subsequent process, such as fluorescence or a photo-induced chemical reaction, can be localized in this small volume.

We have developed a wide array of chromophores which hold great promise for 3D microfabrication, as well as other applications, such as two-photon fluorescence imaging and 3D optical data storage.<sup>3,6</sup> These materials are based on a donor- $\pi$ -donor, donor-acceptor-donor, or acceptor-donor-acceptor structural motif. The magnitude of the two-photon absorption cross-section,  $\delta$ , and the position of the two-photon absorption maximum,  $\lambda_{\text{max}}^{(2)}$ , can be controlled by varying the length of the conjugated bridge and by varying the strength of the donor/acceptor groups. In this way, chromophores have been developed which exhibit strong two-photon absorption in the range of 500 - 975 nm, in some cases as high as  $4400 \times 10^{-50} \text{ cm}^4 \text{ s/photon-molecule}$ .

For many of the donor- $\pi$ -donor molecules, two-photon excitation populates a state which is sufficiently reducing that a charge transfer reaction can occur with acrylate monomers. Under suitable conditions, such reactions can initiate radical polymerization of acrylate resins. Polymerization growth rates have been measured, and we show that these two-photon chromophores display increased sensitivity over conventional photoinitiators. Complex 3D structures can be fabricated in acrylate films doped with these chromophores using tightly focused near-infrared femtosecond laser pulses (see figure). A 3D periodic array of polymeric columns has been produced for use in photonic bandgap applications, and tapered waveguide structures have been fabricated, which could be used to interconnect disparate-sized microoptical components. More traditional MEMS structures, such as cantilevers, have also been produced.<sup>5,6</sup> The two-photon photopolymerization process can be extended to other material systems, such as metallic, ceramic, and composite materials, by templating the photopolymer structures.

Our long-term strategy is to develop new multi-photon activatable photochemical systems which will allow two-photon techniques to be extended to a wider range of materials. For two-photon-activated chemistry to be efficient, an initiator must be a strong two-photon absorber and have a mechanism for effectively generating the desired reactive species following excitation. We have applied this design strategy to the development of two-photon-activatable photoacid generators. Chromophores have been synthesized which offer strong two-photon absorption and large quantum yields for acid generation. These new initiators have made it possible to extend easily the process of two-photon microfabrication to acid-activated chemical systems, such as polymerizable epoxides and chemically amplified resist materials.





Microstructures fabricated by two-photon induced polymerization of a cross-linkable acrylate using a donor- $\pi$ -donor polymerization initiator.

## References

1. Denk *et al.*, *Science* **1990**, 248, 73.
2. Maruo *et al.*, *Opt. Lett.* **1997**, 22, 132.
3. Albota *et al.*, *Science* **1998**, 281, 1653.
4. Rumi *et al.*, *J. Am. Chem. Soc.* **2000**, 122, 9500.
5. Cumpston *et al.*, *Nature* **1999**, 398, 51.
6. Kuebler *et al.*, *J. Photopolym. Sci. Tech.* **2001**, 14, 657.

**Keywords:** Microfabrication, two-photon absorption, photopolymerization, micro-electromechanical systems (MEMS), photonic bandgap.

## Acknowledgements

We gratefully acknowledge support for this research from the Office of Naval Research (CAMP-MURI), the National Science Foundation, and the Air Force Office of Scientific Research. We thank Sartomer, Inc. for providing us with various acrylate monomer materials used in this study.

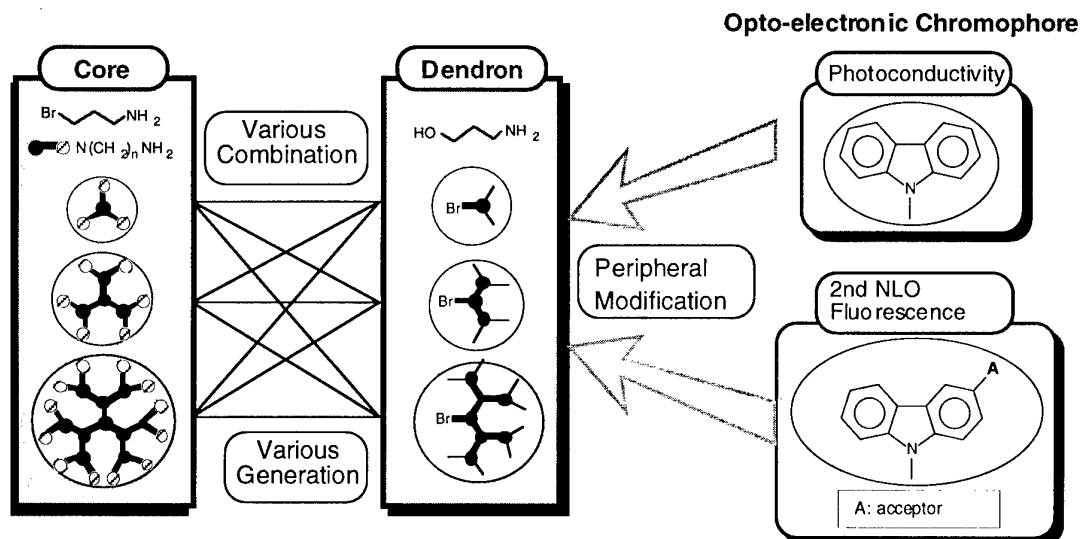
## Multifunctional Supramolecules for Photonic Application

Masaaki Iwata<sup>a</sup>, Yoshihiro Imase<sup>b</sup>, Atsushi Gunji<sup>a</sup>, Tetsuya Aoyama<sup>a</sup>  
and Tatsuo Wada<sup>a,b</sup>

<sup>a</sup>Supramolecular Science Laboratory, RIKEN (The Institute of Physical and  
Chemical Research), 2-1 Hirosawa, Wako, Saitama 351-0198, Japan

<sup>b</sup>Graduate School of Science and Engineering, Saitama University,  
255 Shimookubo, Saitama, Saitama 338-8570, Japan

Supramolecular chemistry has been developed in terms of molecular recognition, especially macromolecular chemistry associated with molecular biology. Supramolecular systems can be expected to be superior to simple functional molecules or polymers because of their multifunctionality. Three types of carbazole supramolecular systems were studied: cyclic oligomers, calix[4]arenes and dendrimers. Systems exhibiting multifunctional opto-electronic properties such as photoconductivity, electro-optic activity, photorefractive effects and electroluminescent responses, were designed and investigated. Amorphous molecular solid films were prepared by spin-coating without a polymer matrix and can be poled above the glass transition temperature. We have also developed the new general synthetic method for polyamine-based dendrimers. We successfully synthesized the core-dendrons with  $\text{NH}_2$ -terminal and peripheral-dendrons with a bromo-substituent by the repeated addition-transformation reactions. By combination of a core-dendron with peripheral dendrons, it is possible to prepare multifunctional dendrimers with terminal carbazole groups in one step as shown in scheme 1. Nano-scale dendrimers containing carbazole-based opto- and electro-active units were found to serve for prototypal molecular photonic devices.



Scheme 1 Development of novel polyamine-dendrimers.

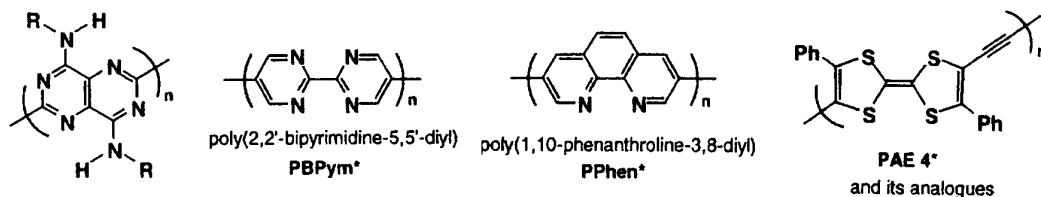
Preparation of New  $\pi$ -Conjugated Polymers

Takakazu Yamamoto

Chemical Resources Laboratory, Tokyo Institute of Technology,

4259 Nagatsuta, Midori-ku, Yokohama 226-8503, Japan

The following new  $\pi$ -conjugated polymers have been prepared according to organometallic dehalogenative polycondensation of dihaloaromatic compounds.



PPympym(4,8-NHR)\*

PPympym(4,8-NHR) ( $R$  = butyl-hexadecyl) is considered to have a planar structure since it does not receive *o*-hydrogen repulsion due to the presence of nitrogen at the all four *o*-positions. Actually, PPympym(4,8-NHR) gives its UV-vis absorption peak at the longest wavelength among similar poly(naphthalene)-type polymers. XRD data and solution properties of the polymer reveal a strong tendency for the polymer molecules to stack.

PBPym and PPhen and its derivatives form metal complexes with various transition metals, and the metal complexes show catalytic activity, e.g. for photoevolution of hydrogen from aqueous media.

Light scattering analysis of PPhen indicates that it assumes a stiff structure in formic acid. All of the  $\pi$ -conjugated polymers are soluble in organic solvents and their cast films are electrochemically active; PPympym(4,8-NHR), PBPym, and PPhen containing the electron-accepting imine nitrogen undergo electrochemical reduction. On the other hand,  $\pi$ -conjugated polymers constituted of tetrathiafulvalene (e.g., the above shown PAE 4) are susceptible to electrochemical oxidation. The electrochemical redox reactions are accompanied with color change (electrochromism).

The  $\pi$ -conjugated polymers usually show photoluminescence.

## Reference

Bull. Chem. Soc. Jpn., 72, 621 (1999).

## Preparation of Organic and Hybridized Nanocrystals for Photonics

Hachiro Nakanishi, Institute of Multidisciplinary Research for Advanced Materials, Tohoku University, Kataira, Aoba-ku, Sendai 980-8577, Japan, Fax:81-22-217-5645, E-mail:hnakanis@tagen.tohoku.ac.jp

### 1. Introduction

During the past decade, we have been demonstrating that microcrystals of variety of organic compounds, in the range of tens nm to several hundreds nm in size, can easily be fabricated by reprecipitation method, and reported the novel size dependent optical properties of conjugated compounds which occurs in the size range one order of magnitudes larger than those of metal and semiconductor nanocrystals (1,2). One of the most extensively investigated compounds in our nanocrystal studies is the polydiacetylene because of their high third-order optical nonlinearity and stability. The polydiacetylene can be obtained by a solid-state polymerization of diacetylene monomer crystal. Among many diacetylene monomers, our focus is made on 1,6-di(N-carbazolyl)-2,4-hexadiyne (DCHD) due to quantitative conversion and high melting point. We have succeeded in the thin-film fabrication of poly(DCHD) nanocrystals by means of electrostatic deposition technique, and purely optical ultra-fast switching has been demonstrated (3).

The enhancement of optical nonlinearity of polydiacetylene in a composite nanostructures with metals was theoretically predicted (4,5), and was claimed to be actually realized in the gold fine particles-dispersed polydiacetylene thin film (6). However, nothing about their ground state absorption spectra and structural details was presented. Thus, in order to clarify the electronic interaction in this composite materials, we have tried to prepare well defined composite structures, composed of nanocrystals of poly(DCHD) and metals.

### 2. Hetero-multilayered thin films (7)

The  $\zeta$ -potential of poly(DCHD) nanocrystals (ca. 100nm in size, and ca. 20 to 30nm in thickness) was ca.-40mV, and those of Au and Ag fineparticles (ca. 13 and 15nm in size) were -27 and -36mV, respectively. Since all these particles were negatively charged in their water dispersion, all combinations of multi-layered thin film formation were possible by an electrostatic layer-by-layer deposition technique with polycations. The thickness of polyelectrolytes layer was 2 to 3nm in average of one-time deposition. In the case of homo-multilayered thin films of metals, plasmon

absorption peaks made longer wavelength shift with increasing layer numbers. This shift is explained quantitatively on the basis of resonance energy transfer induced by dipole-dipole interaction, not within but between adjacent layers.

On the other hand, in the case of hetero-multilayer deposition with poly (DCHD) nanocrystals, no such shifts were observed. The absorption spectra of silver and poly (DCHD) hetero-multilayers were the simple additives of both components. Interestingly, however, the spectra of gold and poly (DCHD) were deformed from the simple additives; that is, the absorbance of poly (DCHD) became so weak, suggesting a certain electronic interactions between both particles.

### 3. Hybridized nanocrystals (8)

In order to enhance the electronic interactions between the nanocrystals of poly (DCHD) and metals, we have prepared their composite nanocrystals, i.e. spherical crystals where metal particles were covered with poly (DCHD), by means of co-reprecipitation method.

Surprisingly, in the case of silver composite, the plasmon absorption disappeared and only the excitonic absorption of poly (DCHD) appeared at longer wavelengths, compared with pure poly (DCHD)'s spectra of the same size. Of course, no such phenomena were observed when both components were simply mixed up in a dispersion or in a thin film.

Thus, it was revealed experimentally for the first time that the core domain of metal fine particles interact optoelectronically with the shell layer of polydiacetylene in the composite nanocrystals to give different (i.e. hybridized !) electronic states, compared with those of original components. Further studies on a variety of combinations of metals and organics in the composite nanocrystals are in progress.

- 1) H.Kasai et al., Jpn. J. Appl. Phys., 32 (8A), 1132 (1992).
- 2) H.Kasai et al., "Organic Mesoscopic Chemistry", ed. by H.Masuhara et al., Blackwell Science, 145 (1999).
- 3) M.Bakarezos et al., Electronics Letts, 35 (13), 1078 (1999).
- 4) A.E.Neeves et al., J. Opt. Soc. Am., B6, 787 (1989).
- 5) J.W.Haus et al., J. Appl. Phys., 73, 1043 (1993).
- 6) A.W.Olsen et al., J. Am. Chem. Soc., 113, 7758 (1991).
- 7) A. Masuhara et al., J. Macromol. Sci., in press.
- 8) A. Masuhara et al., Jpn. J. Appl. Phys., in press.

## Self-Assembled Monolayers and Optical Instability

Masahiko Hara, Jaegeun Noh, Keita Mitsui and Ken Nakajima

Local Spatio-Temporal Functions Laboratory, Frontier Research System, RIKEN  
Wako, Saitama 351-0198, Japan  
E-Mail: masahara@postman.riken.go.jp

### 1. STM for Self-Assembled Monolayers

Growth processes of self-assembled monolayers (SAMs) were studied by scanning tunneling microscopy (STM), surface plasmon spectroscopy (SPS), thermal desorption spectroscopy (TDS) and x-ray photoelectron spectroscopy (XPS). A new equilibrium state for alkanethiol SAMs different from previously reported phase was confirmed for the first time. While the conventional final equilibrium state was interpreted as the homogeneous adsorption sites on three-fold hollow on Au(111), the existence of a new equilibrium state shows that there are three adsorption sites: hollow, bridge and on-top sites on Au(111), suggesting that the previously accepted phase is still under nonequilibrium. As a result of this study, temporal development of interfacial reaction and dimerization problems were discussed in more detail.

### 2. AFM for Single Molecular Nano-Rheology

We have studied protein stretching event using force curve measurement mode of atomic force microscopy (AFM). Protein molecules were sandwiched between Au(111) and a gold-coated AFM tip through thiol-gold chemisorption. Thiol groups were introduced by adding cysteine residues at both N- and C-terminal to facilitate chemisorption. We have established a newly assembled piezo controller of AFM system and programmed a software to unfold and fold protein molecules. Although the length of the protein molecule responded in-phase to the applied movement in most case, we found a novel out-of-phase response around a certain stretching length where the second domain unfolded. Applying the measured force in quasi-static experiment, the out-of-phase response was reproduced in simple calculation, which suggested that the unfolding and the refolding of the protein were taking place repeatedly.

### 3. SNOM for Optical Proximity Effect

The hybridization of scanning near-field optical microscopy (SNOM) with scanning tunneling microscopy (STM) was realized by introducing a doubly metal-coated optical fiber tip with an extremely small aperture ( $<100$  nm), where the second metal-coating to the aperture was performed to obtain a half-transparent conducting tip after the fabrication of aperture probe. A simultaneous SNOM/STM observation and the identical channel transport for both electrons and photons were achieved. For the life time measurement of dye molecules in SAMs, the measured luminescence decay time was variable against the intrinsic (macroscopic) decay time, mainly due to the existence of the metal layer as an optical boundary in the proximity of the luminescent center.

### References

- (1) "Nanoscopic Evidence for Dissociative Adsorption of Asymmetric Disulfide Self-Assembled Monolayers on Au(111)" J. Noh and M. Hara: *Langmuir*, 16 (2000) 2045-2048.; "Nanoscopic Investigation of Self-Assembly Processes of Dialkyl Disulfides and Dialkyl Sulfides on Au(111)" J. Noh, T. Murase, K. Nakajima, H. Lee and M. Hara: *J. Phys. Chem. B*, 104 (2000) 7411-7416.
- (2) "Development of a Hybrid Scanning Near-Field Optical/Tunneling Microscope (SNOM/STM) System" K. Nakajima, R. Micheletto, K. Mitsui, T. Isoshima, M. Hara, T. Wada, H. Sasabe and W. Knoll: *Jpn. J. Appl. Phys.*, 38 (1999) 3949-3953.
- (3) "Dynamic Measurement of Single Protein's Mechanical Properties" K. Mitsui, K. Nakajima, H. Arakawa, M. Hara and A. Ikai: *Biochem. Biophys. Res. Comm.*, 272 (2000) 55-63.

## Dewetting-Assisted Controlled Crystallization of Dyes

Olaf KARTHAUS<sup>1,2</sup>, Toshiro IMAI<sup>1</sup>, Daisuke MIYAKAWA<sup>1</sup>, and Mariko WATANABE<sup>1</sup>

<sup>1</sup> Chitose Institute of Science and Technology, Faculty of Photonics  
Science066-8655 Hokkaido, Chitose, Bibi 758-65, Tel/fax 0123-27-6102  
karthaus@photon.chitose.ac.jp  
<sup>2</sup> JST, PRESTO

## Introduction:

Aromatic organic compounds which are substituted with electron-donor and -acceptor groups may exhibit second order non-linear responses to light. The non-linear response depends significantly on the macroscopic orientation of the molecules. Either the compound is incorporated into a polymer thin film which is then corona-poled, or non-centrosymmetric crystals have to be produced. In the first case, crystallization leads to a decrease in performance, while in the latter case high quality crystals are needed. Thus it is of crucial importance to control the crystallinity of the material.

Here we present the first results of a novel way to control the crystallinity of low molar mass compounds by casting from dilute solution. The investigated compounds, push-pull substituted thienyl dyes, are summarized in Fig. 1.

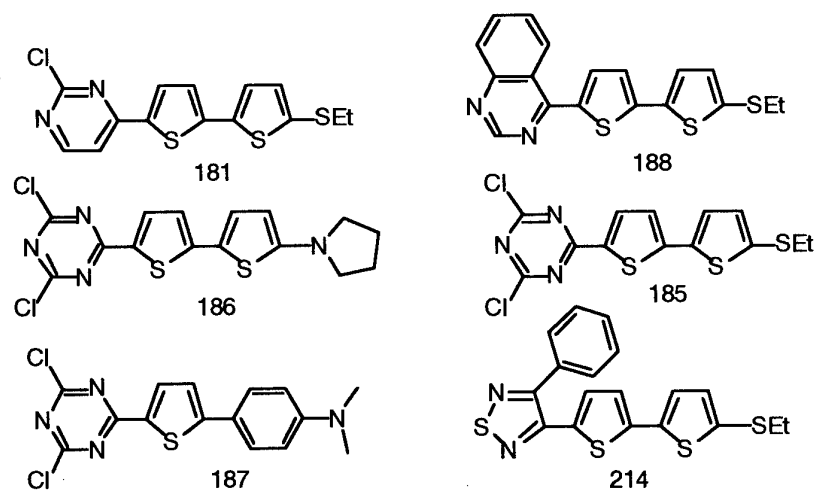


Fig. 1: chemical formulae of the investigated compounds

### Experimental:

Upon casting from dilute solution (typically 1 g/L), the hydrophobic compounds dewet from the substrate (slide glass or mica) and form micrometer-sized amorphous "domes". This method to produce micron-size structures has been intensively studied in the past for polymers. Low molar mass compounds usually crystallize during solvent evaporation and thus are not suitable for the preparation of micronsize domes. The amorphous domes are annealed, either thermally at 20°C below their bulk melting point, or by subjecting the sample to solvent vapor. The morphological change is monitored by optical and fluorescence microscopy.

### Results:

A clear melting-point dependence of the crystallization has been observed. Compounds 181 and 214 with melting points below 80°C do not crystallize even after prolonged annealing. Compound 186 and 187 with melting points above 200°C crystallize during casting. Only compounds with intermediate melting points form amorphous domes that can efficiently be crystallized in a subsequent annealing process.

A second approach to control crystallinity is the co-casting of the dye and a polymer, e.g. polystyrene from solution. In this case, the polymer also dewets from the surface and forms microdomes.

In these cases the crystallization of the dye depends not only on its melting point, but also on its solubility in the polymer matrix. By choosing the various parameters, e.g. dye/polymer ratio and annealing conditions, the crystallization of the dyes, and the crystal size can be fine-tuned.

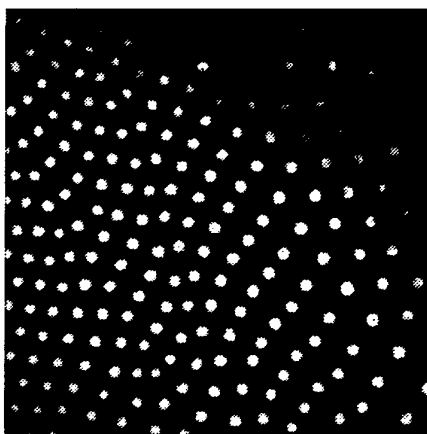


Fig. 2: Fluorescence micrograph of 187 crystals in polystyrene microdomes



# Natural Growth for the Formation of Complex Nanostructures Using Microphase Separated Block Copolymer as Template

Gyujin Cho,<sup>1\*</sup> Sung-Gi Jung,<sup>1</sup> Jongkwan Jang,<sup>1</sup> and Jae-Suk Lee<sup>2</sup>

<sup>1</sup>Department of Chemical Engineering, Sunchon National University, 315 Maegok Sunchon, Chonnam 540-742 Korea

<sup>2</sup>Department of Materials Science and Engineering, Kwangju Institute of Science and Technology (K-JIST), Kwangju 506-712 Korea

We report a new method to control both the nucleation and the growth of  $\text{SiO}_2$  to form nanopatterns. Preparing inorganic materials with 3-dimensional and nano-size periodic patterns is the essential steps in designing miniature devices.<sup>1</sup> A simple micron-size periodic pattern can be prepared using conventional photolithography.<sup>2</sup> On the other hand, complex materials with periodic patterns having sizes below  $0.1 \mu\text{m}$  cannot be simply constructed using conventional photolithography. Recently, an alternative approach to attain complex nanostructures has been developed by using microphase separated block copolymer as a template.<sup>3</sup> The block copolymer can self-assemble to produce periodic nanodomains, such as lamellar, hexagonal, and spherical phases.<sup>4</sup> These self-assembled structures with length scales of 10-100 nm are ideally suited to control the nucleation, growth, and morphology of inorganic materials,<sup>5</sup> and are used for nanoscale patterning.<sup>6</sup> To do this, regioselective nucleation is regulated by the difference in interfacial energy between the reaction medium and different nanodomains of the block copolymer.<sup>7</sup> Usually, heterogeneous nucleation is favored for the nanodomains which have a lower interfacial energy. Although these methods were successful for two-dimensional nanopatterning, we found that the influence of the morphology of the block copolymer on the nanostructures becomes weaker as the structures build up, so that the boundaries between the patterns become blurred gradually as the thickness increases. To overcome this problem, we have developed a new method to promote the nucleation and growth of  $\text{SiO}_2$  regioselectively.

To regioselectively nucleate and grow  $\text{SiO}_2$  for nanopatterning, we prepared poly(styrene-*b*-4-vinylpyridine) (PS-*b*-4PV) with Mw of 20,000 g/mol and polydispersity of 1.1 using anionic polymerization. The ratio of PS/4PV was 0.95 calculated from integrating the  $^1\text{H-NMR}$  peaks of PS and 4PV. A main reason for using PS-*b*-4PV is that the pyridine rings can be easily protonated, so that there is a large difference in the surface energy between the PS and 4PV blocks. Furthermore, the protonated 4PV can act as acid catalyst sites for the hydrolysis of tetraethoxysilane (TEOS). Thus  $\text{SiO}_2$  can nucleate onto only the 4PV block and grow from the surface. After the regioselective nucleation, the direction of  $\text{SiO}_2$  growth can be controlled by using an oil instead of aqueous medium.

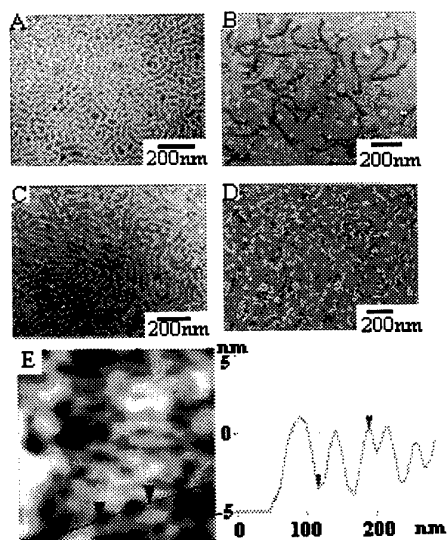


**Figure 1.** TEM image of stained PS-*b*-4PV (A) with  $\text{OsO}_4$ , and TEM images of  $\text{SiO}_2$  on PS-*b*-4PV without staining after 10 (B), 20 (C), and 300 (D) minutes of immersion into aqueous solution for  $\text{SiO}_2$  growth. (E) AFM image with cross sectional analysis for 20 min growth of  $\text{SiO}_2$

The morphology of the microphase-separated PS-*b*-4PV on the grid was investigated using TEM. Figure 1A shows a plain TEM image of the resulting thin film after staining with  $\text{OsO}_4$ . The nanodomains of 4PV in the PS-*b*-4PV appear as dark lamellar periodic nanodomains with 30 nm interspacing. After the growth of  $\text{SiO}_2$  onto the PS-*b*-4PV template in an aqueous or an oil phase for 10 to 300 min, TEM images of the samples were taken without staining. Figure 1B, C, and D show TEM images of  $\text{SiO}_2$  nanopatterning grown in an aqueous phase with 10, 20, and 300 min growth, respectively. It can be seen that  $\text{SiO}_2$  starts to nucleate following the nanodomains of 4PV after 10 min (Figure 1B) and completely nucleates onto all of the 4PV nanodomains after 20 min (Figure 1C). The reason for the fast regioselective nucleation onto only the protonated hydrophilic 4PV block is that the interfacial energy between water and the nanodomains of protonated 4PV is lower than that for the PS nanodomains. However, because the heterogeneous nucleation of  $\text{SiO}_2$  was very fast, there is no favored growth

direction to decrease interfacial energy. Furthermore, at longer growth time,  $\text{SiO}_2$  can also nucleate on the PS nanodomains because the nucleation with less selectivity is promoted by longer growth time. As the result, the patterning becomes blurred after 60 min of growth time, and is completely lost after 300 min (Figure 1D). To check the height of  $\text{SiO}_2$  nanopatterns of Figure 1C,  $\text{SiO}_2$  nanopatterns were grown onto a PS-*b*-4PV coated graphite plate under the same conditions for AFM studies with contact mode (Nanoscope III, Digital Instruments). Based on the crosssectional analysis of AFM image (Figure 1E), the height of the nanopatterns were 3–4 nm with 30 to 40 nm width. On the other hand, a longer time (60 min) was required to complete regioselective nucleation in an oil phase, and clear nanopatterns could be observed for all samples with 60 to 300 min growth time. As an example, the TEM image of a sample with 300 min growth is shown in Figure 2A, in which the definition of the grown  $\text{SiO}_2$  pattern is as sharp as the PS-*b*-PV template (Figure 1A). For further characterization,  $\text{SiO}_2$  nanopatterns were also grown onto a graphite plate under the same conditions for AFM studies with contact mode. The AFM image (Figure 2B) shows that the nanodomains are similar to those observed from TEM, and much more definitive than those obtained for samples with growth in an aqueous medium (Figure 1E). Based on the cross-sectional analysis of the AFM image (Figure 2C), the height of  $\text{SiO}_2$  patterning is estimated to be about 5–15 nm with 40 nm width for samples prepared with 300 min of growth.

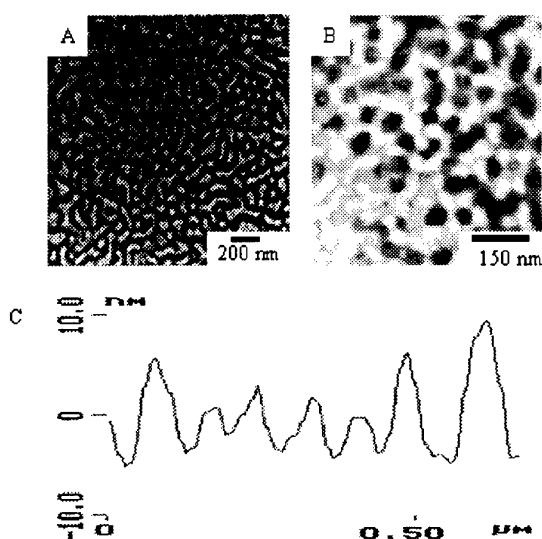


**Figure 2.** (A) TEM image of  $\text{SiO}_2$  on PS-*b*-4PV without staining after 300 minute of immersion into the oil phase, (B) AFM image and (C) cross-sectional analysis of  $\text{SiO}_2$  on a PS-*b*-4PV coated graphite plate prepared under the same condition as the sample in (A).

The remarkable difference in the nanopatterning growth of  $\text{SiO}_2$  in the two phases can be explained by the following consideration. Because protonated pyridine rings are hydrophilic, each micro domain of 4PV may be covered by a very thin water layer, which does not mix with the surrounding medium in an oil phase. It may be compared to the liquid-flux in both vapor-liquid-solid (VLS) and solution-liquid-solid (SLS) methods of crystal growth. The thin strips of water film can act as acid catalyst to let  $\text{SiO}_2$  nucleate regioselectively on the surface of P4V block. After the nucleation,  $\text{SiO}_2$  can further grow only along the vertical direction because the thin water strips do not mix with oil and stay on top of the  $\text{SiO}_2$  columns. During the growth, more TEOS from the oil phase is slowly fed into the thin water strips and hydrolyze into  $\text{SiO}_2$  following only the patterns of the 4PV block in the template. This explanation is substantiated by the observation that, without the acid treatment, bulk  $\text{SiO}_2$  with sizes of a few  $\mu\text{m}$  grow randomly on the substrates coated with PS-*b*-4PV.

In summary, we have demonstrated a new method to copy the nanostructures of micro-phase separated copolymer thin films to form silica thin films up to a height of 15 nm with 40 nm width. Detailed studies of morphological changes and growing mechanism relating to changes in interfacial tensions of the medium are being carried out.

**Acknowledgment.** The work of GC was supported by the Ministry of Science and Technology (MOST) of Korea.

## References.

- (1) Chou, S. Y.; Krauss, P. R.; Renstrom, P. *J. Vac. Sci. Technol.*, **B1996**, *14*, 4129.
- (2) Moreau, M. *Semiconductor Lithography: Principles and Materials*; Plenum, New York, 1988.
- (3) Meiners, J. C.; Ritz, E. A.; Mlynek, J.; Krausch, G. *J. Appl. Phys.* **1996**, *80*, 2224. Lee, T.; Yao, N.; Aksay, I. *Langmuir* **1997**, *13*, 3866. Tsutsumi, K.; Funaki, Y.; Hirokawa, Y.; Hashimoto, T. *Langmuir* **1999**, *15*, 5200. Zehner, R. W.; Sita, L. R. *Langmuir* **1999**, *15*, 6139. Rosa, C. D.; Park, C.; Thomas, E.; Lotz, B. *Nature* **2000**, *405*, 433.
- (4) Abetz, V.; Goldacker, T. *Macromol. Rapid Commun.* **2000**, *21*, 16 and references therein.
- (5) Swift, D. M.; Wheeler, A. P. *J. Phys. Chem.* **1992**, *96*, 202. Wolber, P. K.; Warren, G. J. *Trends Biochem. Sci.* **1989**, *14*, 179. Mann, S.; Archibald, D. D.; Didymus, J. M.; Douglas, T.; Heywood, B. R.; Meldrum, F. C.; Reeves, N. *Science* **1993**, *261*, 1286.

## CHEMICAL LITHOGRAPHY VIA VISIBLE LIGHT

Sang Woo Han, Inhyung Lee, and Kwan Kim

*Laboratory of Intelligent Interface, School of Chemistry and Molecular Engineering  
and Center for Molecular Catalysis, Seoul National University, Seoul 151-742, Korea*

Site-selective alternations of surface chemistry provide a means of engineering surfaces that can be used in sensitive optoelectronic devices, sensors, and devices that mimic biological functions. Formation of patterned self-assembled monolayers (SAMs) is an excellent strategy for preparing such templates with selectable surface chemical properties,<sup>[1,2]</sup> and they can be manufactured by utilizing conventional optical methods using UV light as an excitation source and other lithographic schemes based on state-of-the-art technologies as well as by a destructive atomic-beam and proximal-probe lithographic processes relying on the local degradation of portions of a monolayer. Searching for alternative systems that could allow the controlled chemical modification of SAMs preserving the overall structural integrity of the primary monolayer, we found that nitro groups on aromatic SAMs were selectively converted to amino groups under irradiation with visible light. Using this surface induced photoreaction, we could prepare patterned binary SAMs on silver surfaces. The locally modified monolayer surfaces thus prepared can be used to direct the site-selective self-assembly of a number of different organic (Fig. 1) and inorganic materials (Fig. 2), subjected to a predefined geometric pattern and a pre-selected type of chemical functionality.

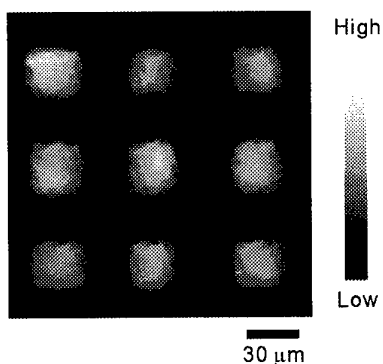


Fig. 1

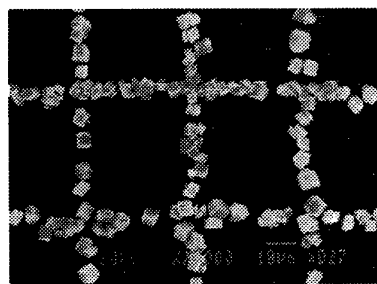


Fig. 2

This novel surface modification method may open up new possibilities of chemical

lithography, allowing the inscription of chemical information on a functionalized organic monolayer. Since the amine-terminated surfaces are widely used in the development of biomolecule adsorption sensors,<sup>[3]</sup> enzyme-coated electrodes,<sup>[3]</sup> biomolecular templates to create novel nanostructured materials,<sup>[4]</sup> and DNA computer,<sup>[5]</sup> the present strategy must be beneficial.

#### REFERENCES

1. R. J. Collins, I. T. Bae, D. A. Scherson, C. N. Sukenik, *Langmuir* **1996**, *12*, 5509.
2. (a) R. Maoz, R. Yam, G. Berkovic, J. Sagiv, in *Thin Films*, Vol. 20, (Ed: A. Ulman), Academic Press, San Diego, CA, **1995**, p 41. (b) C. Duschl, M. Liley, G. Corradin, H. Vogel, *Biophys. J.* **1994**, *67*, 1229.
3. C. D. Bain, G. M. Whitesides, *Science* **1988**, *240*, 62.
4. M. Mertig, R. Kirsch, W. Pompe, H. Engelhardt, *Eur. Phys. J. D* **1999**, *9*, 45.
5. Q. Liu, L. Wang, A. G. Frutos, A. E. Condon, R. M. Corn, L. M. Smith, *Nature* **2000**, *403*, 175.

# Fabrication Techniques of Langmuir-Blodgett films of Photonic Molecules

Yuhei SHIMOYAMA

*Department of Physics, Hokkaido University of Education,  
Hakodate 040-8567, Japan.*

*E-mail: yuhei@cc.hokkyodai.ac.jp*

Recently, ultrathin films of organic pigments such as  $\beta$ -carotene and phthalocyanine derivatives have drawn much attention as nonlinear optical devices. The Langmuir-Blodgett (LB) technique produces ultrathin organic films with a high molecular order at ambient temperatures and at atmospheric pressures. So far, few techniques for the well-ordered Langmuir (L) monolayers of  $\beta$ -carotene and phthalocyanine derivatives have been reported [1, 2]. The primary problem with existing LB techniques is that the molecules cannot form a well-defined monolayer on the surface. Therefore, it is desirable to establish a technique for fabrication of well-ordered L-monolayers at the subphase surface. In order to enhance the molecular orientation of the L-monolayers, we have developed the flow-orientation method [3-5]. The method allows to control the flow of the developing solution on the subphase surface. A constant surface area is normally used during the deposition of a developing solution on the subphase in the conventional techniques for preparing L-monolayers. On the other hand, our technique forces to spread the developing solution on the subphase while the surface area on trough is increased by the moving barrier. Simultaneously, the barrier produces a laminar flow, which allows the film molecules to flow along the finite direction, and hence to form the well-ordered monolayers [6]. We shall present the detailed techniques of LB films for organic pigment molecules.

## References

- [1] R. M. Leblanc and B. H. Orger, *Biochim. Biophys. Acta.* **275** (1972) 102.
- [2] S. Baker, M. C. Petty, G. G. Roberts and M. V. Twigg, *Thin Solid Films* **99** (1983) 53.
- [3] T. Matsuura, T. Komatsu, E. Hatta and Y. Shimoyama, *Jpn. J. Appl. Phys.* **39** (2000) 1821.
- [4] T. Matsuura, A. Nishimura and Y. Shimoyama, *Jpn. J. Appl. Phys.* **39** (2000) 3557.
- [5] H. Kaji and Y. Shimoyama, *Jpn. J. Appl. Phys.* **40** (2001) 1396.
- [6] S. Yamada and Y. Shimoyama, *Jpn. J. Appl. Phys.* **35** (1996) 4480.

## Spin-Coated Multilayer Assemblies of Oppositely Charged Materials: From Bolaamphiphiles to Polyelectrolytes

Seung-Sub Lee, Woo-Cheol Cheong, Myeon-Cheol Kim and Jong-Dal Hong\*

Dept. of Chemistry, University of Incheon 177 Dohwa-dong Nam-ku,  
402-749 Incheon, sKorea. Tel. +82-32-770-8234; Fax. +82-32-770-8238  
e-mail. [hong5506@lion.incheon.ac.kr](mailto:hong5506@lion.incheon.ac.kr)

Jinhan Cho and Kookheon Char \*

School of Chemical Engineering, Seoul National University,  
San 56-1, Shinlim-dong, Kwanak-gu, Seoul 151-742, Korea

Chang Hwan Kim and Kwan Kim

Division of Chemistry and Molecular Engineering and Center for Molecular Catalysis, Seoul  
National University, Seoul 151-742, Korea

During past several years, the electrostatic self-assembly (ESA) technique has been devoted to realization of a variety of multilayer heterostructures on a solid substrate, especially, ultrathin films and coatings of polymers [1-6]. This technique was developed based on a solution-dipping method. Recently, A spin-coating technique is successfully applied to the build-up of multilayer assemblies of polyelectrolytes. Figure 1 (a) shows the maximum  $\pi\pi^*$  absorbance of PAZ-6 at 360 and 363 nm as a function of the number of bilayers for both the spin-coated and solution-dipped multilayers, respectively. In accordance of the UV/visible absorbance, the ellipsometric thickness of bilayers increased also linearly with the number of PAZ-6/CAG bilayers, as can be seen in Figure 1(b).

Also, we demonstrate the build-up of organic/inorganic multilayer films composed of cationic poly(allylamine hydrochloride) (PAH) and negatively charged inorganic cadmium sulfide (CdS) nanoparticles using the spin-coating method. By structural analysis of the multilayer assemblies using x-ray diffraction, we have observed Bragg reflection peaks originating from the internal structure and Kissig fringes that indicate the relatively smooth surface, as shown in Figure 2.

Compared with the conventional solution-dipping method, the spin-coating electrostatic self-assembly (SCESA) technique greatly reduces the preparation time per monolayer film (10-20 sec versus 20 min), along with the creation of much smoother surfaces that can be evidenced from X-ray reflectivity and AFM measurements. We also demonstrate that thicknesses of the polymer bilayers can be manipulated at the molecular level by adjusting the spin speed, and the concentration of the polymer solution, i.e. PSS, PAH, PAA etc.

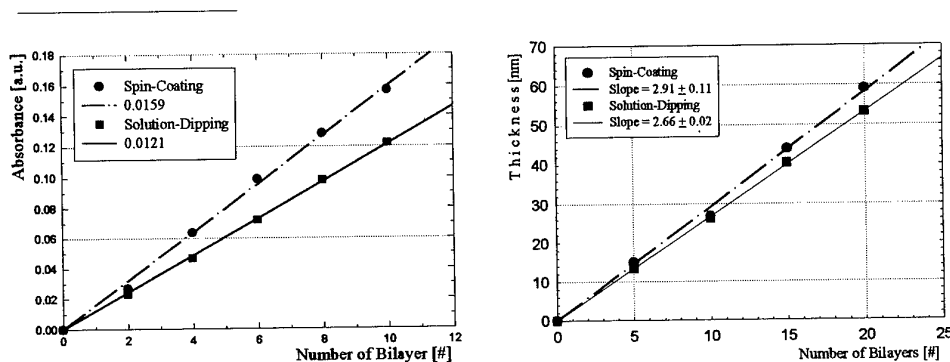


Figure 1. Plot of the absorbance (a) and the ellipsometric thickness (b) vs. the number of deposition cycles of PAZ-6/CAG bilayer on the precoating 5 bilayers film of PAH/CAG that were prepared by spin-coating and solution-dipping techniques.

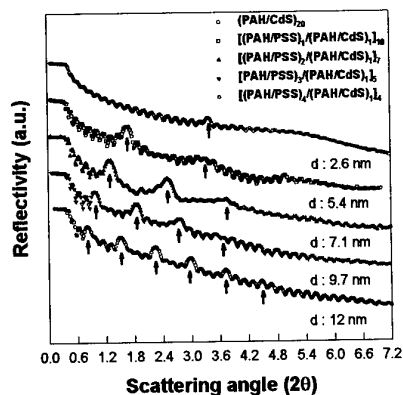


Figure 2. X-ray reflectivity curves of  $[(\text{PAH/PSS})_n/(\text{PAH/CdS})_1]_m$  ( $[n+1] \times m = 20$  or  $21$ ) films prepared by the spin SA method. The increase of bilayer number of (PAH/PSS) from 0 to 4 causes the increase of d-spacing between polyelectrolyte and nanoparticle from 2.6 to 12 nm. The arrow symbols in the figure indicate the Bragg peaks of such internal structure.

## References

- (1) Decher, G.; Hong, J. -D. *Makromol. Chem. Macromol. Symp.* **1991**, *46*, 321. Decher, G.; Hong, J. -D. *US patent* **1993**, Nr.: 5,208,111.
- (2) Arys, X.; Jonas, A. M. Laschewsky, A.; Legras, R. "Supramolecular Polymers"; Albertociferri; editor; Marcel Dekker, New York, **2000**, pp 505-563.

## Single Molecule Force Spectroscopy by AFM-Related Techniques

M. Seitz, T. Hugel, N. Holland & H.E. Gaub

Applied Physics and Center for Nanoscience, University Munich, Amalienstr. 54, 80799 Munich

The rapid development of novel experimental tools allowing the precise application and measurement of minute forces has opened exciting new perspectives in material- and life sciences. Particularly scanned probe techniques, which combine unparalleled spatial resolution with superb sensitivity, have allowed the development of a fundamental understanding of bio-molecular interactions and their nano-mechanical properties. Mechanical experiments with single molecules have become possible, and for the first time, intramolecular and intermolecular forces could be studied directly at the molecular level. Molecular recognition processes between many different ligand-receptor systems were meanwhile investigated and these studies have provided detailed insight in the underlying fundamental mechanisms. Even adhesion between live cells was resolved at the single molecule level. The option to investigate mechanical properties of biomolecules, such as polysaccharides, proteins and nucleic acids, attracted the interest of researchers, and in turn stimulated new developments in instrumentation. Proteins were unfolded at the resolution of individual helices with the precision of single amino acids. With the accessible force window, the whole range from entropic forces at several piconewtons (pN) to the rupture of covalent bonds at several nanonewtons (nN) can now be investigated. As single-molecule force spectroscopy continues to be a rapidly evolving field and now emerges as a widely used tool for the structural and functional investigation of bio-molecules in their native environment, this lecture will highlight the advances of the recent years.

Particular emphasis will be given to recent developments, which allowed the measurement of the adhesion forces of individual polyelectrolyte molecules to surfaces of different nature. Contributions of surface charge density, dissociation degree of the polymer and Ionic strength could be separated from non-Coulombic effects. Also a report on first experiments where opto-mechanical experiments were performed with single molecules will be given.

### References

- Engel, A., H. Gaub, and D.J. Müller, *Atomic force microscope: A forceful way with single molecules*. Curr. Biol., 9: p. R133-138. (1999)
- Clausen-Schaumann, H., M. Seitz, R. Krautbauer & H. E. Gaub, *Force spectroscopy with single bio-molecules*, Current Opinion in Chemical Biology 4:524-530, (2000)
- T. Hugel, M. Grosholz, H. Clausen-Schaumann, A. Pfau, H. Gaub and M. Seitz, *Elasticity of single polyelectrolyte chains and their desorption from solid supports studied by AFM based single molecule force spectroscopy* Macromolecules, 34 : p 1039-1047 (2001)



## Plasmon-enhanced near-field Raman spectroscopy for nano-imaging

Satoshi Kawata

Department of Applied Physics, Osaka University

Suita, Osaka, 565 -0871, JAPAN

kawata@ap.eng.osaka-u.ac.jp

Experimental study of super resolving near-field optical microscopy (NSOM) has started with the demonstration of topographic imaging in the 1970's and 80's, and then extended to the molecular imaging using fluorescence spectroscopy technology in the 1990's.

In this presentation, we will talk about another spectroscopical approach to observe molecular images[1]. A molecule can be directly observed as an absorption of infrared light at a specific wavelength or a spectral shift in light scattering as Raman scattering. Compared with fluorescence spectroscopy, vibration spectroscopy including infra-red absorption spectroscopy and Raman scattering spectroscopy directly excites the molecule vibration, so that the staining of a molecule with a dye is not necessary to label a specific molecule. There does not occur photobleaching or quenching with the metal coating on fiber probe or apertureless metal tip.

However, there are not many reports on infrared NSOM [2-4] because of lacking of high-intensity tunable lasers in mid-infrared region. Raman scattering is even more difficult than infrared absorption spectroscopy to couple with NSOM due to the extremely small scattering cross section. We recently overcame this problem with aid of field enhancement at the metallic probe tip [5]. Figure 1 shows the Raman spectral mapping of Rhodamine 6G molecule excited at the silver-coated AFM tip with an interval of 30nm [6]. Shift of the vibrational peaks and revealing of new vibrational peaks are observed due to chemical interaction of the tip with the adsorbate molecules.

I predict that one of the main topics of NFO research in the next decade will be the vibration spectroscopy coupled with a near-field probe, to which nonlinear spectroscopy such as multi-photon processes, second harmonic generation, and coherent anti-Stokes Raman scattering could also contribute.

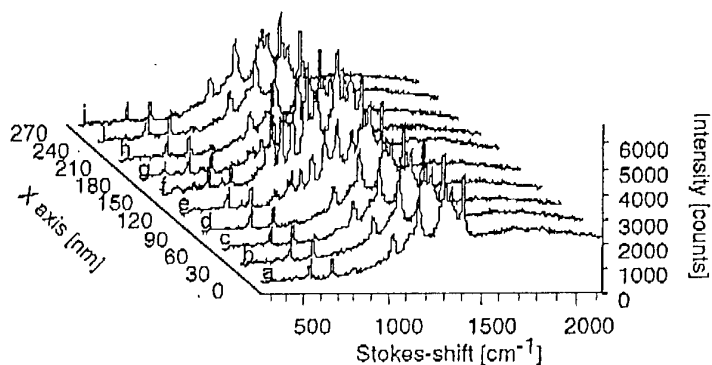


Fig. 1 Near-field Raman spectral mapping

- [1] S. Kawata. Ed. "Near Field Optics and Surface Plasmon Polariton," Springer, Heidelberg, 2001.
- [2] T. Nakano and S. Kawata, *Optik*, 94, 19-162 (1993).
- [3] T. Nakano and S. Kawata, *Scanning*, 16, 368-371 (1994).
- [4] S. Kawata, H. Takaoka, and . Inouye, *Near Field Optics-3*, European Optical Society Topical Meetings Di-gest Series, 8, 19-160 (1995 ).
- [5] N. Hayazawa, Y Inouye, Z. Sekkat, and S. Kawata, *Opt. Commun.*, 183, 333-336 (2000).
- [6] N. Hayazawa, Y Inouye, Z. Sekkat, and S. Kawata, *Chem. Phys.* 369-374. (2001).

## Femtosecond Spectroscopy and Photochemistry of Individual Organic Nanoparticles

Hiroshi MASUHARA

Department of Applied Physics, Osaka University, Suita, Osaka 565-0871, Japan  
masuhara@ap.eng.osaka-u.ac.jp

Nanoparticles are just between molecules/atoms and bulk materials and show very important and interesting physical and chemical properties due to confinement of electrons, holes, and energies, large surface-to-volume ratio, and so on. Already many reports have been presented, and observation of their size and shape by SEM, TEM, and AFM, and their spectroscopic analysis have been published. However, most studies are concerned with metal and semiconductor particles and conducted for an ensemble of the nanoparticles. Without any doubt spectroscopy, photochemistry, and manipulation of individual nanoparticles are important and indispensable to advance the research on the relevant field. Considering the situation, we have developed some novel methods which are useful for studying single nanoparticles in air at room temperature and applied them to organic ones. We believe our approach will be a basis for developing organic photonics and present here some of our recent results.

### 1. Femtosecond surface light scattering spectroscopy of single gold nanoparticles.

Size-dependent electronic absorption spectra have been widely reported for metals, semiconductor, and organic molecular systems, however the conventional spectroscopy gives information on an ensemble average of many particles. Scatters in particle size and shape lead to inhomogeneous broadening in the spectra and non-exponential decay in dynamics. To solve these problems a simple and reliable spectroscopic technique has been developed for the first time using a conventional optical microscope and a femtosecond pump-probe method. Far-field light scattering from individual gold nanoparticles dispersed in a PVA film was detected in dark field of a microscope, and the spectra were measured with a CCD / spectrometer. A femtosecond white-light continuum pulse is used as a probe light, which allows us to measure not only steady-state spectra in the whole visible region (400-750 nm) but also the transient spectra as a function of delay time after femtosecond UV pulse excitation.

Surface plasmon resonance spectra of individual nanoparticles were successfully measured, and the relation between the peak intensity and wavelength was well explained on the basis of the Mie theory using optical parameters of bulk gold. Also time-resolved scattering intensity after 390 nm fs laser excitation was examined, and the observed dynamics can be explained in terms of electron heating by excitation pulse and thermalization of absorbed light energy due to electron-phonon interactions in a gold nanoparticle.

## 2. Picosecond near-field fluorescence microspectroscopy of single anthracene microcrystals in evaporated anthracene-tetracene film.

Topographies, fluorescence images, fluorescence spectra, and fluorescence decay curves of anthracene-tetracene two component evaporated films were observed by ps near-field fluorescence microspectroscopy. Individual anthracene microcrystals were formed on tetracene microcrystalline films, although layer-on-layer film was expected. The central part of individual anthracene microcrystals shows intense tetracene monomer fluorescence, while edge parts give relatively weak fluorescence. This means that energy transfer from anthracene to tetracene took place more preferably in the central part of the anthracene crystal than in the surrounding area. This inhomogeneity can not be simply explained as an energy transfer at interface between anthracene and tetracene crystals. The characteristic position dependence of energy transfer dynamics was analysed by measuring ps fluorescence decay curves from position to position by 200 nm distance, on which special crystal growth and molecular diffusion mechanisms was considered.

## 3. Optical patterning and photochemical fixation of individual polymer nanoparticles.

By utilizing laser manipulation method, nanoparticles can be transferred from position to position, arranged, patterned, and fixed on the substrate as we demonstrated for  $\mu\text{m}$ -sized particles. The nanoparticles were identified by fluorescence spectroscopy and back scattering light imaging.

One fixation method deals with photopolymerization around localized nanoparticles on a substrate. Polymer nanoparticles are gathered at the focal point by photon pressure of a trapping beam, and patterned onto the glass substrate. Local photopolymerization within and around the nanoparticles assembly was induced by additional irradiation of pulsed-laser beam (355 nm), resulting in generation of polyacrylamide containing nanoparticles. The polymerized assembly was evaluated by atomic force microscope observation. By scanning both trapping and excitation laser beams, patterned nanoparticles could also be fixed on a glass substrate. Also single polymer and gold nanoparticles were trapped, transferred, and fixed on the substrate.

## 4. Nanoparticle preparation of phthalocyanines by laser ablation in solution.

Water suspension of  $\mu\text{m}$ -sized vanadyl phthalocyanine (VOPc) crystals was converted into VOPc aqueous colloid by irradiation with an excimer laser (351 nm, 30 ns, 5 Hz). VOPc nanoparticles with nearly equilateral triangular and hexagonal shapes were obtained from a VOPc aqueous colloid, and their mean height and width of the nanoparticles are 17 nm and 51 nm, respectively. Laser fluence dependence was examined and laser ablation of the microcrystals in water is considered to be responsible to the nanoparticle formation. A threshold laser fluence of the conversion was determined to be  $\sim 20 \text{ mJ/cm}^2$ . Nanoparticle formation processes and their phase transition during standing were analyzed by electronic absorption spectroscopy.

## Spectroscopic Characterization of Polymer LB Films Assembled on Integrated Optical Waveguide

M. Mitsuishi, T. Tanuma, J. Matsui, and T. Miyashita

Institute of Multidisciplinary Research for Advanced Materials,  
Tohoku University, Katahira 2-1-1, Aoba-ku, Sendai 980-8577, Japan  
Tel: +81-22-217-5639, Fax: +81-22-217-5639, e-mail: masaya@tagen.icsr.tohoku.ac.jp

For fabrication of photonic devices at the nanometer scale, it is important to understand the photochemical and/or photophysical behavior of chromophores confined in the nanoassemblies. Herein we describe in situ monitoring of the absorption spectra for the anthracene chromophore incorporated in polymer LB films by integrated optical waveguide technique.

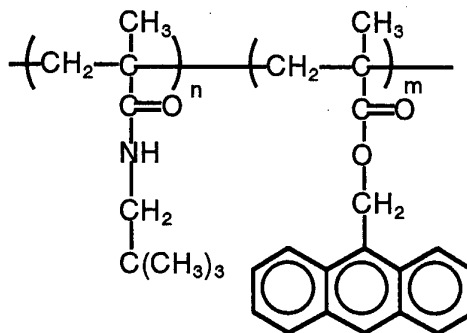


Figure 1. Chemical structure of p(nPMA/AMMA)s.

The copolymers of 9-anthrylmethyl methacrylate (AMMA) with neopentyl methacrylamide (nPMA) were synthesized by free radical polymerization (Fig. 1). From the surface pressure – area isotherms, it was found that the copolymer (p(nPMA/AMMA)) forms a condensed monolayer and the anthracene ring orients almost parallel to the monolayer plane. The monolayers were deposited on the surface of a 200  $\mu\text{m}$  thick quartz slab optical waveguide. A Xe lamp was utilized as a signal. This allows us to monitor absorption spectra in the range from 250 to 800 nm.

First, we measured UV-Vis absorption spectra for p(nPMA/AMMA) monolayer. The characteristic absorption bands for anthracene (solid line) were observed with enhanced sensitivity (Fig. 2). The sensitivity increased by a factor of ca. 200 compared with those of transmitted UV-Vis spectrometer (dashed line).

The anthracene chromophore undergoes a photocrosslinking reaction when irradiated with a near-UV light. The spectral change due to the photocrosslinking reaction was precisely monitored by this technique. This means that the technique provides us with detailed information about monolayer spectroscopic properties. We will discuss the photochemical processes in view of the LB layer structures.

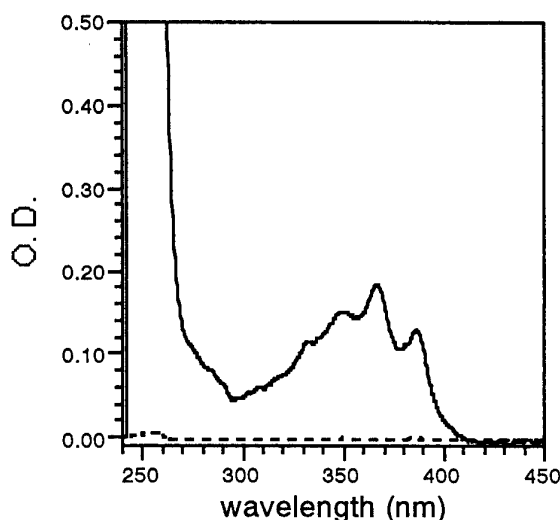


Figure 2. Absorption spectra for p(nPMA/AMMA) monolayer (5 % AMMA content).

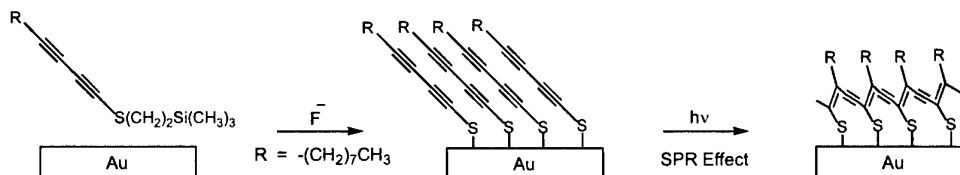
## Surface Plasmon Resonance Effect on Polydiacetylene Conjugated Main Chain

Agus Haryono<sup>2</sup>, Satoru Shimada<sup>1</sup>, Yuji Kaneko<sup>3</sup>, Takashi Fukuda<sup>1</sup>, Hiro Matsuda<sup>1,3</sup>

<sup>1</sup> National Institute of Advance Industrial Science and Technology (AIST), 1-1 Higashi, Tsukuba, Ibaraki 305-8565, JAPAN. <sup>2</sup> Japan Science and Technology Corporation (JST).

<sup>3</sup> Core Research for Evolutional Science and Technology (CREST)

Polydiacetylenes (PDAs) have lately attracted considerable attention because of their applications in 3<sup>rd</sup>-order nonlinear optical materials. The increasing electron density of the polymer unit is important in order to improve their nonlinear optical properties. We have determined that the alkylthio groups electron donation effect could raise the PDA backbone electron density.<sup>1</sup> Composite materials containing metal particles and PDAs are promising materials to enhance the optical nonlinearities, in which an electromagnetic resonance effect, the so-called surface plasmon-resonance, plays an important role. On the other hand, thiol and disulfide compounds covalently bond with gold resulting in a self-assembled monolayer (SAM) on the gold surface. The distance between the conjugated polymer and metal surface was considered to be important due to the interaction between them. We expected that PDAs adjacent to the gold surface could exhibit greatly enhanced optical nonlinearities.



**Scheme 1**

Therefore, we prepared PDA-SAM which has sulfur atoms directly bonded to the conjugated main chain (Scheme 1). However the thiol and disulfide compounds having acetylene groups adjoining the sulfur atoms are unstable because of the 1,3-sigmatropic rearrangement. To solve this problem, we designed a stable precursor, which can release 1,3-alkadiynethiolate under mild conditions for preparing the SAM without isolation, using a protecting group. We have already found that the 2-(trimethylsilyl)ethyl group serves as a promising protecting group for 1-alkynethiols.<sup>2</sup> 2-(Trimethylsilyl)ethyl sulfide is easily converted to the corresponding thiolate anion, ethylene, and trimethylsilyl fluoride by treatment with tetrabutylammonium fluoride (TBAF). Diacetylenic SAMs were formed on 200 nm-Au films on mica substrates. Freshly prepared gold films were immersed for 2 days in a 2 mM 1,3-dodecadiynyl-2-(trimethylsilyl)ethyl sulfide THF solution with two equimolar

amounts of TBAF in the presence of a protonic acid. The formation of DA-SAMs was characterized by the cyclic voltammetry, AFM investigation and SPR spectroscopy.

We measured the UV-vis reflection spectra of the DA-SAM during exposure to a 254 nm UV light. A fairly well-developed peak appeared at 740 nm and increased gradually during the exposure until 30 minutes. In our previous work, we found that the exciton absorption maximum of the PDAs having dodecylthio groups directly bound to the conjugated main chain was observed at 750 nm, which is longer than those of the conventional PDAs.<sup>1</sup> The absorption peak detection at 740 nm suggest that the PDA backbone was formed, and it has a similar structure to the previously reported ones. On the basis of the PDA-SAM preparation results from Crooks et. al.<sup>3</sup>, we expect a stronger electron donation of the thioether group to the PDA backbone. The cyclic voltammogram of the PDA-SAM modified gold electrode also shows the inhibition to electron transfer between the underlying gold surface and  $\text{Fe}(\text{CN})_6^{3-}$  aqueous solution. This suggests that no defect occurred during the polymerization caused by UV irradiation, even though the SAMs prepared by *n*-alkanethiols are easily removed from the Au substrate because of the photooxidation of sulfur in the *n*-alkanethiols.

Surface Plasmon Resonance (SPR) spectroscopy is a technique where changes in the refractive index near an interface can be readily detected. SPR can be used to monitor the assembly and the photo-polymerization of DA-SAM after UV light irradiation. The SPR curve was shifted slightly toward higher angle, owing to the monolayer refractive index increasing. The resulting monolayer refractive index ( $n_f$ ) was obtained as 2.32, after curve fitting. This means the polymerization of diacetylene monolayer was occurred. On the contrary, in the case of DA-SAM having long-chain alkyl group spacer, there is no SPR curve shift even the photo-polymerization was occurred. The refractive index change was not occurred, because of the presence of alkyl group spacer. The formation of the PDA having a high electron density adjacent to the gold surface could enhance the surface plasmon-resonance effect.

It is important to know the interaction between a metal and  $\pi$ -conjugated polymer not only in nonlinear optics but also in a contiguous position in the development of electronic devices. The examination of its electrical behavior and the evaluation of the nonlinear optical properties are under investigation using attenuated total reflection with enhancement of surface plasmon-resonance.

## References

1. Takeda, H.; Shimada, S.; Masaki, A.; Hayamizu, K.; Matsuda, H.; Nakanishi, F.; Okada, S.; Nakanishi, H. *Macromol. Chem. Phys.*, **1999**, *200*, 1240.
2. Takeda, H.; Shimada, S.; Ohnishi, S.; Nakanishi, F.; Matsuda, H. *Tetrahedron Letters*, **1998**, *39*, 3701.
3. Kim, T.; Crooks, R. M.; Tsen, M.; Sun, L. *J. Am. Chem. Soc.*, **1995**, *117*, 3963.

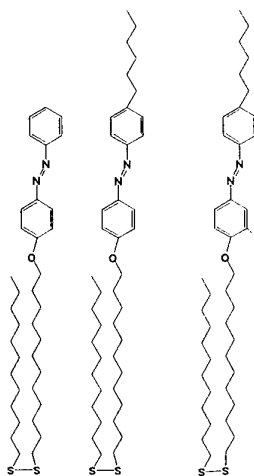
## PM-IRRAS Characterization of Highly Photoreactive SAMs on Gold

T. Wei H. Akiyama K. Tamada K. Yase

National Institute of Advanced Industrial Science and Technology (AIST)

1-1-1 Higashi, Tsukuba, Ibaraki 305-8565 Japan Email: [t.wei@aist.go.jp](mailto:t.wei@aist.go.jp)

An advantage of using a polarization modulation infrared (PM-IR) beam is that the modulated reflectivity is independent of isotropic absorption on gold surface, i.e. experimentally we do not need another bare substrate as reference. This makes in situ measurements possible even in thin film. PM-IRRAS is deemed to be most promising to obtain the richest and the most decisive information about dynamics for the structural order in thin films<sup>1,2</sup>



HAzSSC12 C6AzSSC12 C6Az(Me)SSC12

Figure 1

exhibited alterations in spectra, where the intensities of  $\nu(\text{benzene ring})$  and  $\nu_{\text{as}}(\text{c-o-ph})$  vibration modes clearly decreased after UV irradiation. These changes indicated that photo-isomerization reactions took place in these SAMs. (Fig 2) These transforms are reversible under the irradiation of proper visible light, however spectrum of HAzSSC12 is not completely reversible. The thermal stabilities of SAMs of C6AzSSC12 and C6Az(Me)SSC12 are investigated by IR measurement after annealing in oven at 100°C for three hours. These results were compared with our SPR and AFM data.

In this paper, we will discuss the film structures of three unsymmetrical azobenzene disulfides (Fig 1) compared with a similar thiol azobenzene. Furthermore, we will continue structural change due to photoreaction *in situ* observation with PM-IRRA. We performed in situ PM-IRRAS measurements under irradiation of 365nm UV light for cis form measurement, and 440nm visible light for trans form recovered from cis form. Fujishima and his coworker<sup>3</sup> found that SAMs made from azobenzene thiol derivatives are almost not photoreactive. In agreement with their result, we can not get notable alteration after UV irradiation for our thiol derivative either, while the unsymmetrical disulfide SAMs

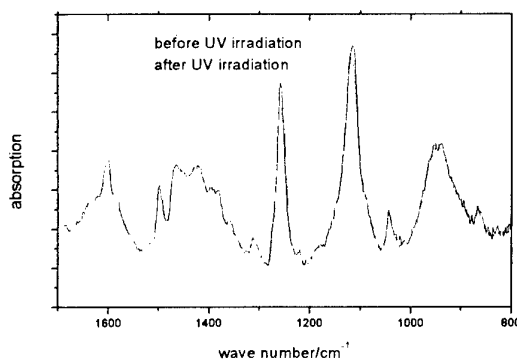


Figure 2 In situ measurements of C6Az(Me)SSC12.

<sup>1</sup> R.A. Dluhy, *J. Phys. Chem.* **90** (1986), p. 1373.<sup>2</sup> C.R. Flach, A. Gericke and R. Mendelsohn, *J. Phys. Chem. B* **101** (1997), p. 58.<sup>3</sup> R. Wang, A. Fujishima, *J. Electro. Chem.* **438**(1997), 213.



## Synthetic Metals: A Novel Role for Organic Polymers

Alan G. MacDiarmid,  
Department of Chemistry,  
University of Pennsylvania, Philadelphia PA 19104-6323 USA

The applicability of the concept of "doping" is the unifying theme which distinguishes polymers that form intrinsically conducting materials, called "synthetic metals," from all other types of polymeric materials. Chemical or electrochemical doping of electronic polymers results in dramatic electronic and magnetic changes with a concomitant increase in conductivity that can enter the metallic regime. Doping phenomena and the chief types of dopable organic polymers will be discussed.

Potential new science/technology by combining the now well-established field of electronic polymers (intrinsically conducting polymers—"synthetic metals," when doped) with the emerging field of nanoscience (one dimension <100 nm) will be discussed. We can consistently produce by simple, electrostatic dispersion ("electrospinning") methods nanofibers of polyaniline or its blends in conventional polymers<sup>1</sup>. Current/voltage curves of single fibers can be obtained. Nanofibers of, for example, polyacrylonitrile can act as high surface area substrates upon which thin films (~30 nm) of gold or polypyrrole may be deposited from aqueous solution<sup>1</sup>. Thermal treatment results in their conversion to carbon nanofibers. Diodes, p/n junctions, Schottky junctions, transistors, etc have already been constructed using electronic polymers in macroscopic form<sup>2</sup>. The basic scientific groundwork is, therefore, already in place for the construction of true nano-scale electronic devices.

A very simple and inexpensive method has been developed for producing conducting patterns of electronic polymers on plastic and paper of e.g. "PEDOT", poly (3-4-ethylene dioxythiophene polystyrene sulfonate), polyaniline, etc. and of metals such as silver from computer-designed patterns. This method, "Line Patterning,"<sup>3</sup> does *not* involve printing of the conducting polymer or of a metal. The difference in hydrophobicity/hydrophilicity between a substrate and a line of regular toner printed on it by a non-modified, standard office laser printer results in conducting polymer or metal areas (deposited by electroless printing) separated by insulating toner lines. Examples of application in liquid crystal displays, transistors and simple electronic devices will be demonstrated.

### References

<sup>1</sup>MacDiarmid et al., *Synth. Met.*, **119**, 27 (2001).

<sup>2</sup>Handbook of Organic Conductive Materials and Polymers, H.S., Nalwa, Ed., Wiley (1997); Handbook of Conducting Polymers, 2<sup>nd</sup> Ed. Marcel Dekker, T. Skotheim, R. Elsenbaumer, J. Reynolds, Ed., (1998).

<sup>3</sup>MacDiarmid and D. Hohnholtz, *Synth. Met.*, **121**, 1327, (2001).

## Novel Photonics Polymer for Information Technology - Science and Dream of Future -

Yasuhiro Koike

Faculty of Science and Technology, Keio University 3-14-1, Hiyoshi, Kohoku-ku, YOKOHAMA 223-8522, JAPAN  
Japan Science and Technology Corporation ERATO, 144-8, Ogura, Saiwai-ku, KAWASAKI 211-0054 JAPAN

### Introduction

The convergence of information transmission, storage, and display is increasingly pervading most industrial and social activities and becoming key factors of the hardware part of information technology (IT). Large capacity of information transmission by optical fiber which offers ever increasing capacity meeting bandwidth demand, is presently under deployment in telecom and data-com. area. Single mode silica fiber is widely utilized in the long haul telecommunication network, while many of short distance data link favor less expensive multimode fiber technology. Increasing demand to access to Internet even from home, the high-speed and low cost optical data transmission medium is strongly required.

We have proposed a high-bandwidth GI polymer optical fiber (POF) as one of the promising candidates for the high-speed data transmission medium. We reported the interfacial-gel polymerization technique to fabricate the GI POF for the first time in 1980's, and over gigabit data transmission through the GI POF was succeeded in the beginning of 1990's. Recently, more interests have been focused on the bandwidth characteristics of the GI POF. It is well known that the bandwidth characteristics of the multimode fiber, including POF, are dominated by the modal dispersion which strongly depends on the fiber structure i.e. refractive index profile. In the case of the silica based multimode fiber (MMF) fabricated by typical MCVD method, the refractive index profile perturbation was observed due to the stepwise concentration difference of the  $\text{GeO}_2$  in each deposited layers. Therefore, the modal dispersion of the silica based MMF has not necessarily been minimized and achieved bandwidth has been much lower than that expected. On the other hand, the refractive index profile of the GI POF is formed by the interfacial-gel polymerization process. The index profile of the GI POF can be controlled by the polymerization reaction rate to minimize the modal dispersion.

In this paper, not only the modal dispersion but also the other factors affecting the bandwidth characteristics of the GI POF are quantitatively investigated in order to clarify the bandwidth potential of the GI POF.

### 2. What is GI POF?

Great advantage of the PF polymer is low intrinsic absorption loss. Because of the low intrinsic loss, very wide wavelength range from visible to near infrared region (for instance 1.3- $\mu\text{m}$ ) can be adopted for signal wavelength in the PF polymer based GI POF link. Currently the lowest attenuation of the PF polymer based GI POF is approximately 15 dB/km at 1.0 - 1.3- $\mu\text{m}$ . On the other hand, we found another advantage in the PF polymer, that is the low material dispersion.

Recent trend in the optical data communication is adopting 0.85- $\mu\text{m}$  signal wavelength with using GaAs VCSEL because of the low cost of optical transceiver. In fact, combined data link of silica based MMF and VCSEL was already standardized for one of the PMDs of gigabit Ethernet, and very recently, IEEE 802.3 meeting issued the 0.85- $\mu\text{m}$  PMD draft for 10gigabit Ethernet standard. In this case, the dispersion issue of the MMF greatly affects the link performance. In the case of the silica based MMF fabricated by typical MCVD method, rippled refractive index profile perturbation was observed due to the stepwise concentration difference of the  $\text{GeO}_2$  in each deposited layers. On the other hand, the index profile of the GI POF can be tightly controlled by the polymerization reaction rate without any such a perturbation. Furthermore, it is noted that the material dispersion becomes serious in the silica base MMF in 0.85- $\mu\text{m}$  use. So, the material dispersions of silica and PF polymer were quantitatively investigated. In the case of the PF polymer, the material dispersion at 0.85- $\mu\text{m}$  wavelength is 0.054 ns/nm $\cdot$ km which is lower than that (0.084 ns/nm $\cdot$ km) of the silica at the same wavelength. Furthermore, the material dispersion of the PF polymer at 1.3- $\mu\text{m}$  wavelength decreases to 0.009 ns/nm $\cdot$ km. These are material dispersions of undoped PF polymer and silica. In the core of the fiber, PF dopant or  $\text{GeO}_2$  is doped for PF polymer based GI POF and silica based MMF, respectively to form the refractive index profile. Therefore, the material dispersion of doped PF polymer and silica should be evaluated to precisely analyze the bandwidth potential. Figure 1 shows the material dispersions of both  $\text{SiO}_2$  and PF polymer. Since the dopant concentration should be high in order to obtain high NA, the material dispersions of doped silica and PF polymer are degraded compared with those of pure silica and undoped PF polymer that are corresponding to the cladding. However, it is noteworthy that the material dispersion of doped PF polymer at 0.85- $\mu\text{m}$  wavelength is much lower than that of  $\text{GeO}_2$  doped silica even when the NA is sufficiently high. These outstanding results indicate that the bit rate theoretically achieved by the PF polymer based GI POF is higher than that of the silica based MMF. Calculated bandwidth properties of the PF polymer based GI POF

with respect to the wavelength are shown in Fig. 2. For PF polymer based GI POF, several kinds of dopants were investigated to represent the high performances such as low attenuation, high mechanical strength, and high temperature resistance, etc.

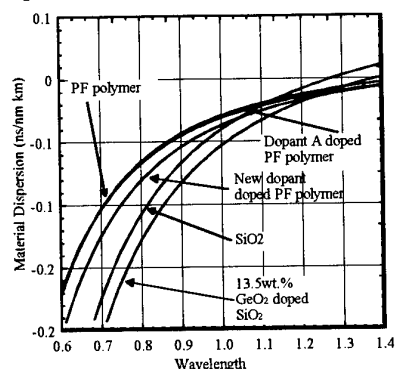


Fig. 1 Material dispersion comparison between the PF polymer and silica.

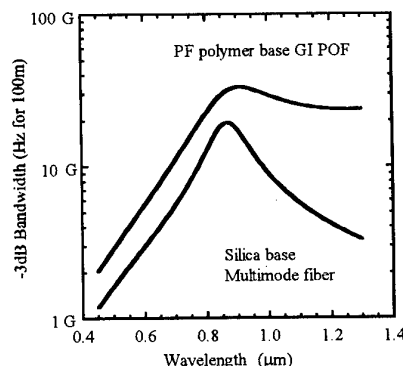


Fig. 2 Calculated bandwidth potential of 1-km PF polymer based GI POF compared with that of silica based MMF.

In the bit rate calculation process, the material dispersion of the PF polymer including the best dopant which can satisfy the requirements for the POF mentioned above was taken into consideration.

In Fig. 2, it was assumed that the refractive index profiles of both silica based MMF and PF polymer based GI POF were designed to be optimum for 0.85- $\mu\text{m}$  use. It was already confirmed that if the index exponent  $g$  is controlled to around 2.0, several Gb/s for 100 m could be achieved by PF polymer based GI POF in wide wavelength range from 0.6 to 1.3  $\mu\text{m}$ . On the other hand, in the case of the  $\text{SiO}_2$ - $\text{GeO}_2$  based MMF, accurate index profile control for specified wavelength is necessary to achieve several Gb/s for 100 to 300 m, since the wavelength dependence of the bandwidth is much stronger than that of the PF polymer as shown in Fig. 2. In Fig. 2, the bit rate performance of the PF polymer based GI POF link was also shown when the spectral source width was assumed to be 0.3 nm which corresponds to the VCSEL. It is obvious that with using the light source with narrow spectral width, the maximum bandwidth at 0.85- $\mu\text{m}$  wavelength increases and higher than 10 GHz·km of bandwidth can be achieved. This is because the effect of material dispersion is more serious in short wavelength range. As shown in Fig. 2, in the case of PF polymer based GI POF, use of VCSEL having narrow line width enables over gigabit transmission in very wide wavelength range (0.6–1.6  $\mu\text{m}$ ), which cannot be realized by the silica based MMF having larger material dispersion than PF polymer. Furthermore, since the PF polymer based GI POF has low attenuation in wide wavelength range from visible to near infrared region, not only serial high speed data transmission system but also WDM system can be realized. When the coarse WDM system is applied, the wavelength dependence of the bit rate performance which was observed in silica based MMF link was concerned in POF link. However, if the PF polymer based GI POF is fabricated to have approximately optimum index profile, it can be expected that higher than the order of Gbps for 1km can be covered in 0.8 – 1.3  $\mu\text{m}$  wavelength region. Such a high bit rate cannot be achieved by the silica based MMF link in wide wavelength range.

### 3. Challenges of GI POF

The PF polymer based GI POF was officially commercialized in June, 2000. The PF polymer based GI POF was installed in the new buildings of Keio University opened from April 2000, prior to its commercialization. Figure 3 shows K2 town campus which is the newly developed campus of Keio University. The PF polymer base GI POFs are introduced in this campus as the first trial of high-speed POF campus LAN. These GI POFs are directly distributed to the desk-top computer having giga-bit Ethernet optical network card. Such a POF data-com system installed in Keio University will be introduced at the conference in detail.

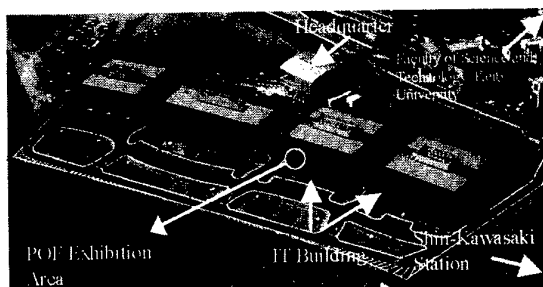


Fig. 3 Photograph of K2 Town Campus realizing first gigabit POF Campus LAN.

## Surface-plasmon optical techniques for the quantitative evaluation of oligonucleotide hybridization reactions at solid/solution interfaces

W. Knoll, T. Neumann, D. Kambhampati

Max-Planck-Institut für Polymerforschung, Ackermannweg 10, 55128 Mainz, Germany

The development and characterization of DNA sensor formats based on Surface Plasmon Fluorescence Spectroscopy (SPFS) will be discussed.

Firstly, we give a brief introduction to the use of evanescent surface plasmon waves at a metal/dielectric interface for the excitation of fluorophores near that interface. The field-enhancement mechanisms operating at resonant surface plasmon excitation can be used to increase the detection sensitivity provided the Förster energy transfer mechanisms (quenching) between the excited chromophores and the broad-band acceptor states of the metallic substrate are under control. This can be achieved by a careful design of the supramolecular architecture built at the transducer surface in order to provide the bio-recognition sites for the binding of the analyte.

In our examples, this surface coating is based on a biotinylated mixed thiol (self-assembled) monolayer to which a layer of streptavidin is bound. Biotinylated oligonucleotides with 15 thymine units as spacers and another 15 nucleotides of a specific base sequence are then coupled as the catcher strands. Complementary target strands from solution are hybridizing to these surface-attached catcher sequences. The association and dissociation kinetics, as well as, the affinity (binding) constants can be monitored on-line in real time provided the target strands carry a chromophore label.

This mode of SPFS has been used to quantitatively determine the  $k_{\text{on}}$  and  $k_{\text{off}}$  rate constants of hybridizing 15mer-oligonucleotides as a function of temperature, ionic strength, number and position of mismatches between probe and target, etc.

In another version of SPFS the catcher strands are labeled with a fluorophore. Upon hybridization of unlabeled target sequences the resulting double strands with their enhanced mechanical stiffness push the chromophores further away from the metal surface, resulting in an enhanced photon emission because less quenching occurs (although other mechanisms may contribute to the observed intensity increase, e.g., a change in the orientation distribution of the labels).

If both strands are labeled, e.g., the catcher probe carries a donor dye and the target is modified with an acceptor chromophore resonant energy transfer mechanisms allow for other modes of observation of these hybridization reactions at interfaces (cf. Figure 1).

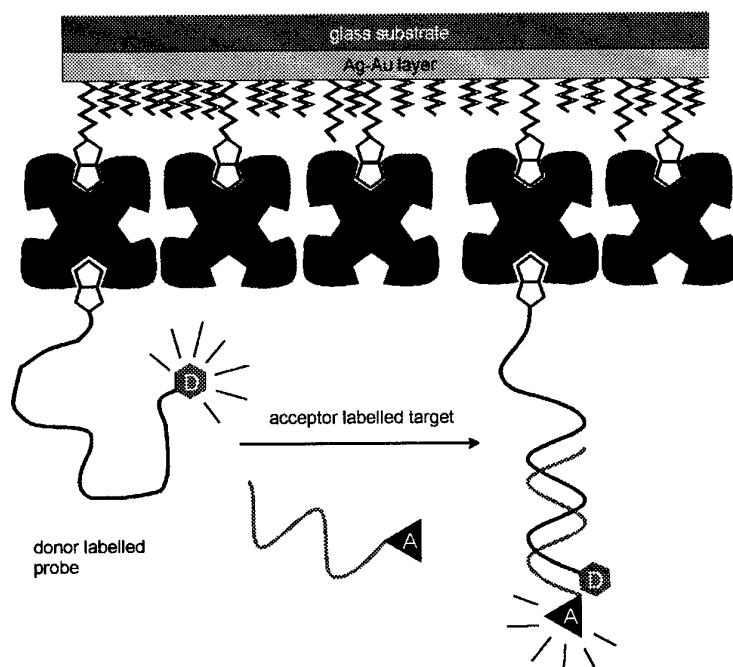


Figure 1

And finally, examples will be given for the binding and competitive replacement by target strands of single-strand binding proteins to the surface-attached probe oligonucleotides. It will be demonstrated that this way an enhanced mismatch discrimination (which is the basis for SNP detection) can be achieved.

#### References:

- Liebermann, T., Knoll, W. *Surface-Plasmon Field-Enhanced Fluorescence Spectroscopy*. Colloids & Surfaces A **171**, 115-130 (2000)
- Liebermann, T., Knoll, W., Sluka, P., Herrmann, R. *Complement Hybridization from Solution to Surface-Attached Probe-Oligonucleotides Observed by Surface-Plasmon-Field-Enhanced Fluorescence Spectroscopy*. Colloids & Surfaces A **169**, 337-350 (2000)

# Nanostructure of DNA and Formation of DNA Network

Hiroyuki Tanaka and Tomoji Kawai

The Institute of Scientific and Industrial Research, Osaka University, Mihogaoka, Ibaraki, Osaka 567 -0047, Japan  
<http://www.sanken.osaka-u.ac.jp/labs/kawai-lab/>

DNA has been studied as a highly specific functional material for measuring electric conductivity and for network fabrication. However, it has rarely been employed in industrial applications since a uniform DNA film or network is difficult to fabricate on solid surfaces. We have already fabricated large-scale ( $12 \times 12 \text{ mm}^2$ ) DNA networks on mica surfaces by dropping a linear-DNA solution on freshly cleaved mica and blowing it off with air (T. Kanno, et. al., Jpn. J. Appl. Phys., Part 1 **39**, (2000) 269) This report describes how we fabricated a variety of network structures by changing the type of DNA, and then controlled the network structure using ethanol treatment. (T. Kanno, et. al., Appl. Phys. Lett., Vol. **77**, No. 23, 4 December 2000)

To investigate the variations in network structure statistically by changing the kind of DNA, we studied the network structures of four kinds of DNA (poly(dA-dT)-poly(dA-dT), poly(dG-dC)-poly(dG-dC), poly(dA)-poly(dT), and poly(dG)-poly(dC)), all observed by AFM. Figures 1(a)–1(d) show a series of AFM images and histograms of measured height for DNA networks. These AFM images indicate that all four linear-DNA types can fabricate a network regardless of the DNA bases, suggesting that the variations in network structure depend on the kind of DNA used. Figure 2(a) shows an AFM image observed at the spot where the ethanol was dropped, together with a height histogram. The DNA network remains on the surfaces after ethanol treatment. Compared with the histogram of poly(dA)-poly(dT) (Fig. 1(a)), the heights appear to be truncated above 2.5 nm. Figure 2(b) shows the AFM image and the height histogram observed at the off-center spot where the ethanol was not dropped directly, with a new peak of 2.9 nm. We speculate that the DNA adsorbing directly on the mica surfaces does not move, whereas the DNA adsorbing onto the DNA is carried away from the center to the off-center spot on the sample by the flow of rt-ethanol. Next, we dropped two drops of 20 ml  $60^\circ\text{C}$  ethanol on a DNA network. Figure 2(c) is a large-scale ( $20000 \times 20000 \text{ nm}^2$ ) AFM image observed on the spot where the  $60^\circ\text{C}$  ethanol was dropped. This image revealed many widened ditches made by the DNA network by the  $60^\circ\text{C}$  ethanol. Figure 2(d) shows that the fiber became thick as a result of movement and cohesion by the flow and drying of the ethanol. This means that strongly fixed DNA (adsorbing on surfaces) is moved by  $60^\circ\text{C}$  ethanol. Thus, the height of a DNA network can be controlled by rt-ethanol, whereas its frame structure can be controlled using hot ethanol.

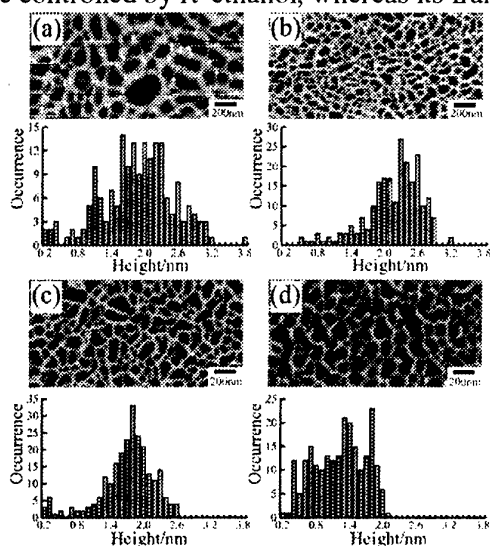


FIG. 1. AFM images of the DNA networks and histograms of measured height for DNA networks. (a) poly(dA)-poly(dT); (b) poly(dG)-poly(dC); (c) poly(dA-dT)-poly(dA-dT); and (d) poly(dG-dC)-poly(dG-dC). All images share the same scale ( $2000 \times 1000 \text{ nm}^2$ ). poly(dA)-poly(dT) had thick fiber and the distribution of height varies from DNA to DNA.

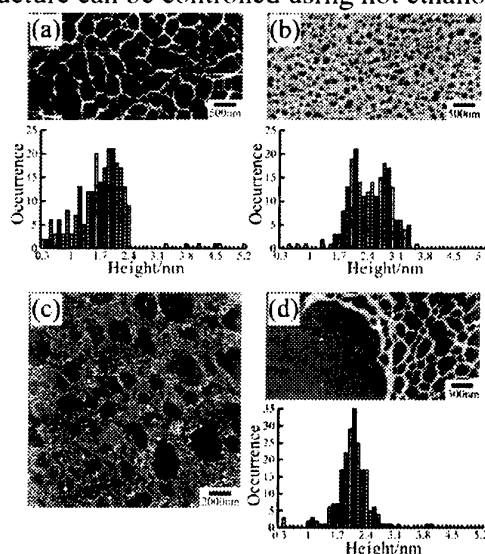


FIG. 2. AFM images of poly(dA)-poly(dT) networks and histograms of measured height for poly(dA)-poly(dT) networks. (a) At the spot where room temperature ethanol was dropped ( $5000 \times 2500 \text{ nm}^2$ ). (b) At the spot where the ethanol spread and evaporated on the DNA network ( $5000 \times 2500 \text{ nm}^2$ ). (c) At the spot where  $60^\circ\text{C}$  ethanol was dropped ( $20000 \times 20000 \text{ nm}^2$ ). (d) A magnified image ( $5000 \times 2500 \text{ nm}^2$ ) of (c) and the height histogram.

# Controlled Immobilization of Single DNA Molecules Complexed with Cationic Lipid Monolayer at the Air-Water Interface

K. Ijiro<sup>1,2</sup>, R. Mitamura<sup>4</sup>, S.-I. Nishimura<sup>4</sup>, T. Sawadaishi<sup>3</sup>, M. Shimomura<sup>1,3</sup>

<sup>1</sup>Research Institute for Electronic Science, Hokkaido University, <sup>2</sup>PRESTO, Japan Science and Technology Corporation (JST), <sup>3</sup>Frontier Research Program, The Institute of Physical and Chemical Research (RIKEN),

<sup>4</sup>Graduate School of Science, Hokkaido University

<sup>1</sup>N12W6 Kita-ku, Sapporo 060-0812, Japan E-mail: ijiro@poly.es.hokudai.ac.jp

Double-stranded DNA molecules have attracted attention as a potential building block for molecular devices due to electron and hole transfer through stacking structure of  $\pi$ -electron-rich nucleobases. From the viewpoint of a new functional material of DNA, investigation of the electric characterization of a single DNA molecule is very important<sup>1</sup>. Therefore development of technique for immobilization of stretched single DNA molecules on a substrate is desired. It is known that DNA molecules, which is a kind of anionic polyelectrolytes, can be bound to a cationic lipid monolayer to form a polyion complex at the air-water interface by electrostatic interaction (Figure 1). When the cationic lipid was spread on an aqueous DNA solution, the cationic lipid monolayer complexed with DNA molecules can be transferred on a solid substrate by vertical lifting method. We report, herein, that fluorescence labeled DNA molecules in the polyion complex monolayers transferred on glass substrates were observed by conventional fluorescence microscopy and scanning near-field optical microscopy (SNOM). When the polyion complex monolayer was transferred, bright line structure was observed by fluorescence microscopy (Figure 2). Length of each line of the fluorescence image gives good agreement with a molecular length calculated from number of base pairs of DNA in the experiment. This indicates that the single line corresponds to the stretched single DNA molecule.

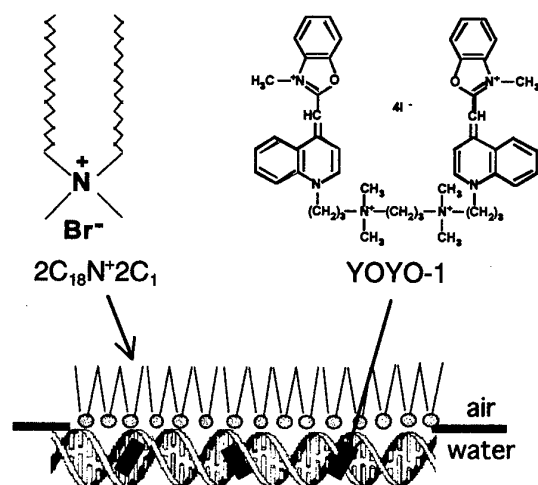


Figure 1. Schematic illustration of DNA-lipid polyion complex monolayer at the air-water interface.

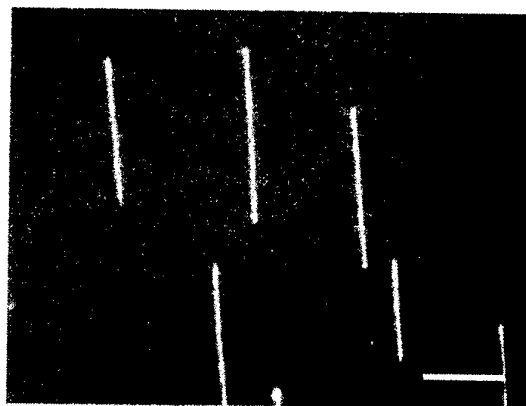


Figure 2. Fluorescence image of a Lambda DNA-2C18N+2C1 complex monolayer deposited on a glass substrate (bar:10 $\mu$ m).

[1] M. Shimomura, J. Matsumoto, F. Nakamura, T. Ikeda, T. Fukasawa, K. Hasebe, T. Sawadaishi, O. Karthaus and K. Ijiro, *Polymer Journal*, **31**, 1115 (1999).

# DNA-Mimetics. Novel Molecular Nanostructure for Molecular Photonics Devices

M. Shimomura, J. Matsumoto and K. Ijiri

Research Institute for Electronic Science, Hokkaido University,

N12W6, Kita-ku, Sapporo 060-0812, Japan

DNA has a double helical supramolecular structure composed of complementary base pairs between adenine-thymine and guanine-cytosine and is a carrier of genetic information. We have already reported that the surface monolayer of simply alkylated nucleobase amphiphiles formed base pair and base trimer with polynucleotides dissolved in water subphase at the air-water interface<sup>[1-4]</sup>. We have coined these monolayers as DNA-mimetics and proposed them as novel functional nanostructured molecular-information materials with precise molecular structure, e.g. controlled molecular weight, regulated sequence of molecular units, and controlled molecular orientation. To confirm the sequenced molecular arrangement transcribed by the template oligonucleotides added in the subphase, a polymerizable part, diacetylene group, is introduced into the alkyl chain of the adenine and thymine amphiphiles (DA-Ade, DA-Thy)<sup>[5]</sup>. Diacetylene group is chosen as a polymerizable spectral probe because of its photopolymerization with remarkable color change.

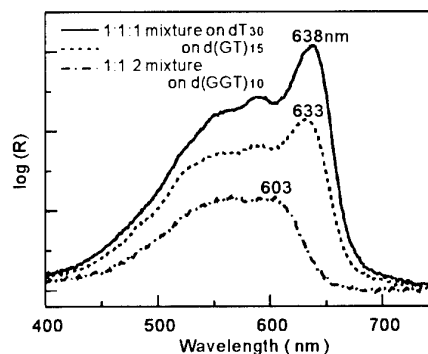
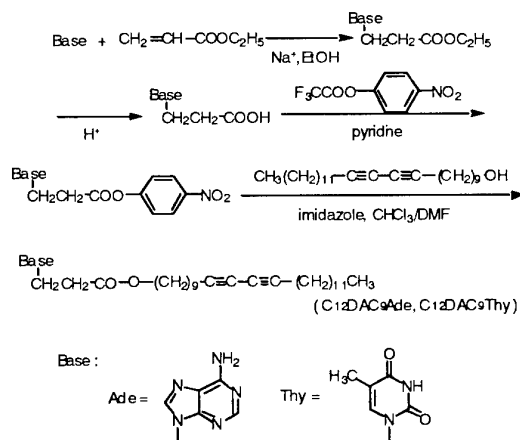


Figure 1. Reflection spectra of the mixed monolayer on various oligonucleotide subphases after UV irradiation for 20min.

Ternary mixtures of DA-Ade, DA-Thy, and C<sub>18</sub>-Cyt were spread on aqueous subphases containing oligonucleotide, d(GT)<sub>15</sub> or d(GGT)<sub>10</sub>. The non-polymerizable cytosine amphiphile is expected to be a spacer molecule mixing into the one-dimensional diacetylene arrays to suppress the polymerization because the cytosine amphiphile can form Watson-Crick base pair with guanine of the template oligonucleotide. Figure 1 shows the reflection spectra of the mixed monolayers on various oligonucleotide subphases after 20min UV irradiation. These spectra are normalized by the contents of the diacetylene amphiphiles at the molecular area of 15mN/m. The monolayer formed on dT<sub>30</sub> solution



shows "blue form" of polydiacetylene with absorption maximum at 638nm, which is identical with that of the polymerized DA-Ade/DA-Thy monolayer without the C<sub>18</sub>-Cyt spacer. On the contrary the photopolymerization of the 1:1:1 mixture spread on the d(GT)<sub>15</sub> subphase was suppressed and the spectral shift to 633nm was observed. Drastic suppression of polymerization was found when the 1:1:2 mixture was spread on the d(GGT)<sub>10</sub> subphase. It is suggested that the DA-Ade/DA-Thy base pair and C<sub>18</sub>-Cyt can recognize dT and dG in the oligonucleotides, respectively. Owing to the inter-chain polymerization the complete suppression of the diacetylene photopolymerization was not achieved in this system.

Isolation of the single oligonucleotide chain complexed with the ternary mixed monolayer is required to the complete suppression of the polymerization. The ternary mixture of the DA-Ade/DA-Thy/C<sub>18</sub>-Cyt (1:1:10) was spread on polyG subphase containing the template origonucleotide. Dilution of the diacetylene complex by polymeric monolayer matrix, complementary complex of polyG-C<sub>18</sub>-Cyt, clearly indicates the template effects on polymerization reaction. As shown in Figure 2a, the reflection spectrum clearly shows the template polymerization of the diacetylene group complexed with the homogeneous sequence of d(T)<sub>30</sub>. While on the d(GT)<sub>15</sub> subphase including excess amount of poly G, complete suppression of the polymerization was observed Figure 2b).

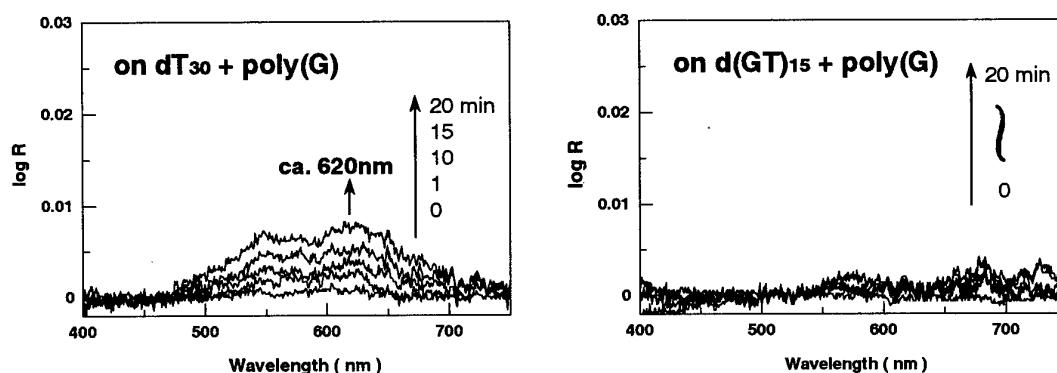


Figure 2. Isolation effect on polymerization of the diacetylene complex. Excess amount of the polymeric complex of polyG-C<sub>18</sub>-Cyt can act as polymer matrix to suppress inter chain polymerization.

#### References

- [1.] M. Shimomura *et al*, *Thin Solid Films*, **284-285**, 691 (1996).
- [2.] M. Shimomura *et al*, *J. Am. Chem. Soc.*, **119**, 2341 (1997).
- [3.] F. Nakamura *et al*, *Thin Solid Films*, **327-329**, 603 (1998).
- [4.] M. Shimomura *et al*, *Polym. J.*, **31**, 1115 (1999).
- [5.] J. Matsumoto *et al*, *Chem. Lett.*, 1280 (2000).

## **Molecular Design, Preparation and Characterization of Photonic Supramolecules, Functional Organic Dye-DNA-Surfactant Complex Film**

Wang Lili and Ogata Naoya\*

Faculty of Photonic Sciences, Chitose Institute of Science and Technology,  
758-65 Bibi, Chitose, Hokkaido 066-8655, Japan,

We report the formation of an ordered supramolecular structure between photonic functional dye and DNA in aqueous solution, and in solid film matrix of DNA-CTMA (cetyltrimethylammonium) complex. Spectroscopic studies indicate that the dye can bind to DNA, and orient on minor groove of DNA in aqueous solution or in solid DNA-cationic surfactant complex films, based on the following observation: firstly, in aqueous solution, (1) the electron absorption peak of the dye shifts to red or blue; (2) exciton splitting are observed in the induced circular dichroism spectrum at high dye/b.p. (about 1:1 to 1: 2.5); and (3) fluorescence from the dyes are strongly enhanced. Circular dichroism analysis for the dsDNA-dye complex revealed that a characteristic feature of chromophore was its ability to bind to minor groove of A/T of double helical DNA, or sandwiched between A/T, depending on molar ratio of DNA to dye. Oriented combination on I/C, but not G/C sequences suggests that the functional dye insert preferably into the minor groove of A/T in high-level loading DNA-CTMA film (dye:b.p.=1:10). And the functional dye intercalates preferably in pocket between A/T base-pairs in low-level loading DNA-CTMA film. Therefore, optical properties of the functional dye-DNA-CTMA complex films can be tuned by changing molar ratio of dye to DNA. Secondly, comparison studies on induced CD spectra in ethanol solution and solid film states of the dye-DNA-CTMA complex demonstrated an orientation of the dye on the chiral nanotemplates of DNA which was observed mainly in the films of DNA-CTMA complex. Therefore, the film formation with slow evaporation of solvent molecules resulted in ordered structure with self-assembly and self-organization. Functional dye ( such as laser, NLO, and photochromic dyes)-DNA-surfactant complex materials, with good processability, photostability and thermostability, will show promise in molecular optical and optoelectric fields.

**\*To whom all correspondence should be addressed (phone: +81-123-27-6001, Fax: + 81-123-27-6007)**

from water-soluble DNA to functional dye-doped dye-DNA-surfactant complex film.

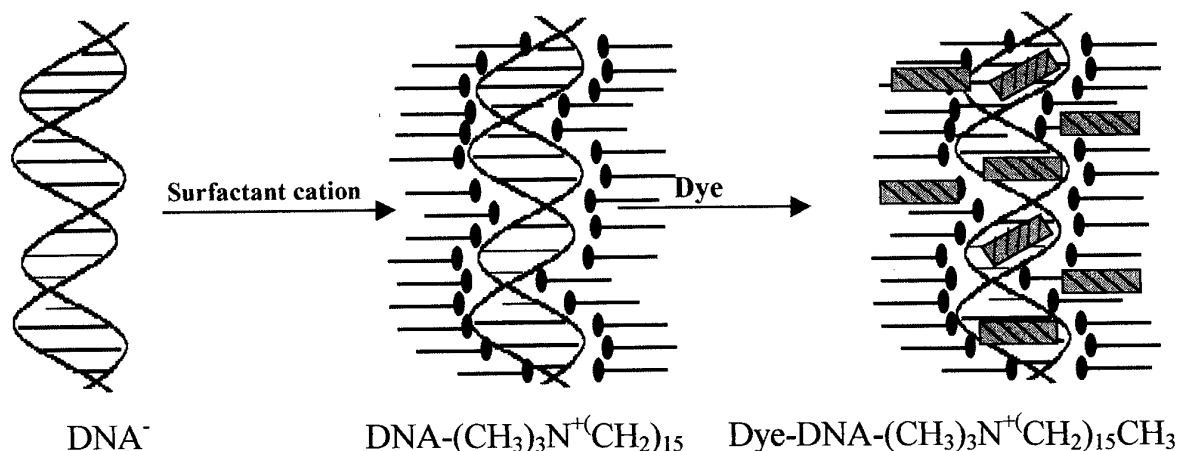
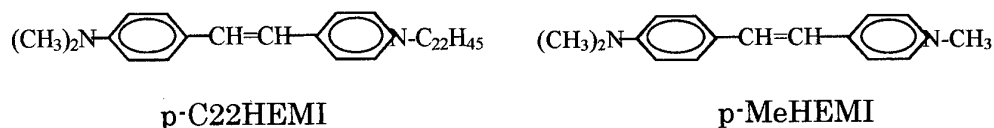


Fig.1 A schematic road from water-soluble DNA-Na to functional dye-doped dye-DNA-surfactant complex film

In this presentation, we further study on optical and optoelectronic properties of DNA-surfactant complex film and a famous NLO dye, C22HEMI-doped DNA-surfactant complex film. Refractive indices and film thickness of the thin film were determined by using the prism coupling method. The results indicated that the self-assembled DNA-Na thin film has anisotropic structure; DNA-CTMA thin film is isotropic in two-dimension. The NLO dye-doped DNA-CTMA thin film displayed enhancement of fluorescence above 3 orders. But it did not display a strong SHG despite of the orientation of organic chromophores doped in DNA-CTMA film which was achieved by inserting the NLO dye to helical minorgrooves.



Therefore, the strongly fluorescence of the NLO dye-doped DNA-CTMA thin film is very promising for application as solid dye laser materials.

**\*To whom all correspondence should be addressed (phone: +81-123-27-6001, Fax: +81-123-27-6007)**

**S4-6**

**Preparation and Anisotropic Electroconduction of a DNA-aligned Thin Film**

Yoshio Okahata (Tokyo Institute of Technology, Japan)

## Polymer electrophosphorescence devices

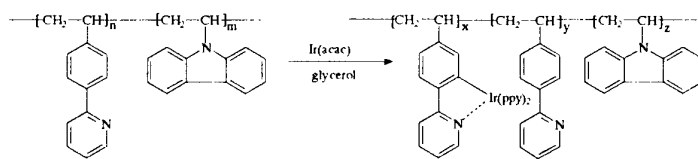
J.-J. Kim, C.-L. Lee, Yong-Young Noh, and R. R. Das

*Department of Materials Science and Engineering, Kwangju Institute of Science and Technology (K-JIST), 1 Oryong-dong, Puk-gu, Kwangju 500-712, Korea*

We have investigated the effect of host polymers for electrophosphorescent light emitting devices (EPLEDs) doped with *fac* tri(phenylpyridine) iridium ( $\text{Ir}(\text{ppy})_3$ ). We selected host materials of poly(N-vinylcarbazol) (PVK), poly(2-vinylnaphthalene) (PVN), polyacenaphthalene (PAN), and polyfluorene derivative poly[9,9'-di-n-hexyl-2,7-fluorene-alt-1,4-(2,5-di-n-hexylo-xy)phenylene] (PFHP), which have almost same spectrum overlaps for efficient Förster energy transfer. However, the PL spectra of these films are remarkably different for different host materials. PVK, PAN and PVN films showed PL from  $\text{Ir}(\text{ppy})_3$ , but PFHP showed emission only from PFHP with little emission from  $\text{Ir}(\text{ppy})_3$  even with high doping concentrations when host polymers are excited. In contrast, the EL spectra from devices showed almost the same characteristics for different polymer hosts. The device with PVK host showed emission from  $\text{Ir}(\text{ppy})_3$  even at the very low concentrations. PFHP device also showed emission from  $\text{Ir}(\text{ppy})_3$ , which is significantly different from PL. The differences in EL and PL for different host polymers will be discussed based on the energy levels, I-V-L, time resolved PL and EL characteristics for various concentrations of the dopant. Contributions from energy transfers and charge confinement effects will also be discussed.

The maximal performance of the electrophosphorescent LED using transition metal complexes is not only dependent on the optimal conditions but also controlled by the coordinating ligands to Ir(III). We have investigated the effect of the fine-tuning brought in by the introduction of a methyl substituent in the pyridine ring of 2-phenylpyridine on the HOMO and emitting  $^3\text{MLCT}$  states of its Ir(III) complex and the subsequent impact on the energy transfer from the host to the guest in EPLEDs. We have synthesized a new green emitting Ir (III) complex with 3-methyl-2-phenyl pyridine,  $\text{Ir}(\text{mpp})_3$  and fabricated polymer based electrophosphorescence devices furnishing good quantum yield. Again, the emissive state, emissive state's lifetime, quantum yield of emission and subsequent performance of the device are greatly influenced by a decrease in the number of the orthometalating ligand and introduction of nonorthometalating uninegative bidentate ligands. We have investigated these effects in mixed ligand complexes utilising 3-methyl-2-phenyl pyridine along with other uninegative bidentate ligands.

Up to now, most of the works on electrophosphorescence devices from transition metal complexes have adopted doping systems either in organic molecules [1] or in polymers [2]. In this study we report, for the first time to the best of our knowledge, electrophosphorescent devices from a polymer where a transition metal phosphorescent dye is attached to a polymer backbone as a side group. For the purpose we synthesized a new polymer, poly( $\text{Ir}(\text{ppy})_2(2-(4\text{-vinylphenyl})\text{pyridine})$ )-*co*-vinylcarbazole), containing both carbazole and iridium (Ir) complex as side groups. The absorption spectra of



Scheme 1. Synthetic routes for Ir complex copolymer.

Ir-complex copolymer showed the  $^1\text{MLCT}$  peak at 370 nm. The  $^1\text{MLCT}$  peak of Ir complex copolymer observed at 370 nm is slightly shifted when compared to that of  $\text{Ir}(\text{ppy})_3$  doped PVK solution ascribed to VPPy a different ligand. In the PL spectra, the emission maximum was observed at 512 nm by effective energy transfer from carbazole to Ir complex. In the EL spectra, the emission maximum was also observed at 512 nm with a little emission from carbazole at 410 nm. The reason for incomplete energy transfer from carbazole to Ir complex is to be explored. The device shows the maximum external quantum efficiency of 0.38 % and the peak luminance of 2000  $\text{cd/m}^2$ . These quantum efficiency and luminescence value is quite lower compared to Ir complex doped system. However, our device demonstrates that this strategy of finding out novel materials incorporating both phosphorescent and fluorescent material will invoke new concepts in electroluminescent material used in OLEDs. Further work is being carried out to optimize the structural aspect of the Ir-complex copolymer, so as to effect total transfer of energy from the carbazole unit to the Ir-complex.

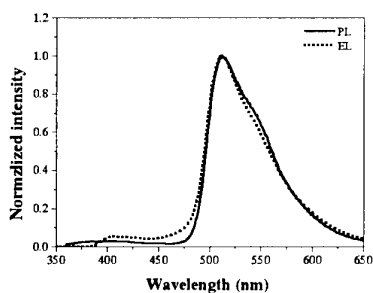


Fig.1. The PL and EL spectra of Ir-complex copolymer.

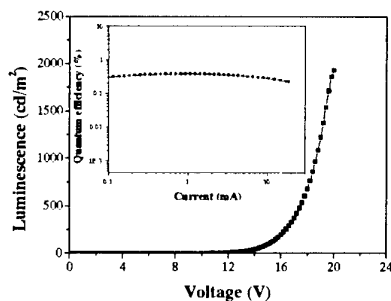


Fig.2. Quantum efficiency and luminescence characteristics.

## Acknowledgements

This work was performed with the support from Ministry of Education of Korea through BK21 program and Center for Electro and Photo Responsive Molecules.

## Dynamics of Electrostatic Molecular Interactions in Doped Organic Thin Films

Vladimir Bulović

Emission and absorption spectra of many organic dyes in liquid solutions depend on the local electric fields generated by the surrounding polar solvent molecules. This "solvation effect" is a result of intermolecular solute-solvent interaction forces (such as dipole-dipole or dipole-induced dipole) that tend to stretch molecular bonds and shift charge distribution on molecules, altering the energy difference between the ground and excited states of the solute.

We have shown that the solvation effect is also present in molecular solids where closely packed polar molecules can generate large local electric fields. We previously observed luminescence shifts in excess of 35 nm (changing emission from yellow to orange to red) for DCM laser dye doped in  $\text{Alq}_3$  host matrix [1,2]. Our recent measurements of time resolved luminescence of polar luminescent dyes indicate that spectral shifts also take place during the luminescent process. The lower panel of Fig. 1 shows a typical contour trace of luminescence intensity as a function of wavelength and time for DCM dye in  $\text{Alq}_3$ . Most of the spectral shifting takes place during the first 2 ns and has tentatively been assigned to molecular reorganization induced by the sudden change in the

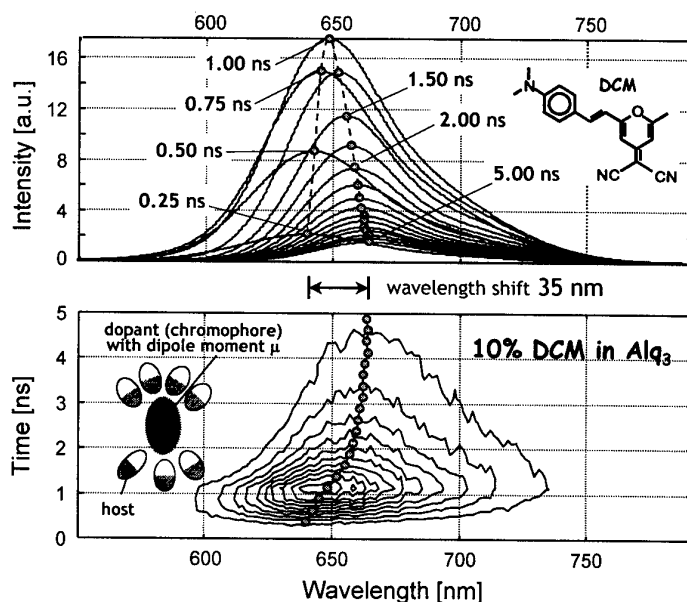


FIGURE 1 (Bottom) Contour plot of photoluminescence intensity of 10% DCM in  $\text{Alq}_3$  500 Å thick film as a function of wavelength and time. (Top) Time resolved spectra of the same sample, where each spectrum is integrated over 0.2 ns window, with an average time indicated in the figure.

lumophores' dipole moment upon excitation. The remaining shift can be associated with an exciton thermalization process, due to exciton diffusion through the doped molecular structure. The observed phenomenon is general in nature and provides insight into exciton dynamics during the luminescence process.

- 
- [1] V. Bulović, A. Shoustikov, M.A. Baldo, E. Bose, V.G. Kozlov, M.E. Thompson, and S.R. Forrest, "Bright, Saturated, Red-to-Yellow Organic Light Emitting Devices Based on Polarization Induced Spectral Shifts," *Chem. Phys. Lett.* **287**, 455 (1998).
  - [2] V. Bulović, R. S. Deshpande, and S. R. Forrest, "Tuning the Color Emission of Thin Film Molecular Organic Light Emitting Devices by the Solid State Solvation Effect," *Chem. Phys. Lett.* **308**, 317 (1999).



## Photonic devices using nanostructured liquid crystals

H. Yokoyama<sup>1,2)</sup>, J.-H. Kim<sup>2)</sup>, J. Yamamoto<sup>2)</sup> and M. Yoneya<sup>2)</sup>

<sup>1</sup>Nanotechnology Research Institute  
National Institute of Advanced Industrial Science and Technology  
1-1-1 Umezono, Tsukuba, Ibaraki 305-8568, Japan

<sup>2</sup>Nanostructured Liquid Crystal Project, ERATO  
Japan Science and Technology Corporation  
5-9-9 Tokodai, Tsukuba, Ibaraki 300-2635, Japan

Deliberate introduction of nanostructures in otherwise homogeneous liquid crystals can potentially be a powerful approach to create naturally nonexistent phases, structures and functions based on the liquid crystallinity. Owing to the microscopic molecular orientational order and the associated long range curvature elasticity, indigenous liquid crystal structures interact strongly with extrinsic objects on the nanometer scale.

Our rapidly evolving ability to create, manipulate and characterize nanometer scale objects, *i.e.* Nanotechnology, is opening up a new field of liquid crystal science and technology by allowing us to realize, in part at least, the above scenario. Since it consists in a mesoscale combination of the self-organizing character of liquid crystalline states and the nanostructure design based on the top-down engineering, I refer to it as a “directed bottom-up approach”, emphasizing the role of human directive intervention put into the self-organization of a materials system.

In this talk, I present the results of our recent efforts along the directed bottom-up approach as applied to artificial two-dimensional nanostructuring of liquid crystals with a view to developing novel photonic devices. I will focus here on the use of the stylus of the atomic force microscope to nanoscopically treat the surface anchoring in such a way as to implement an orientationally patterned surface<sup>1)</sup>. By properly designing the symmetry and the degree of orientational frustrations as shown in Fig.1, we succeeded in realizing a truly bistable alignment, which has never been realized by other means, despite its apparent technical utility. Over the checkerboard pattern, the two diagonal axes become equally stable orientations for the liquid crystal director in contact with this patterned surface. When the

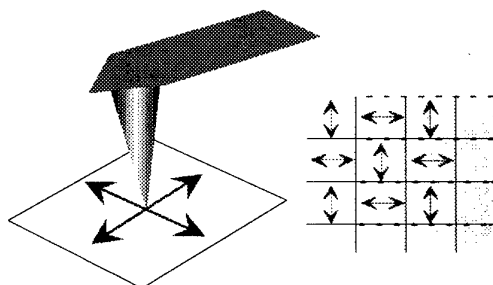


Fig.1 Nanoscopic rubbing of the aligning surface with the atomic force microscope.

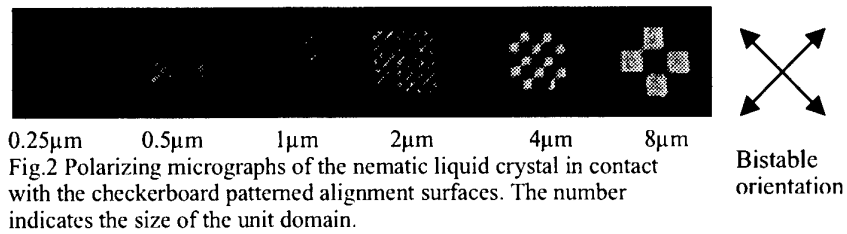


Fig.2 Polarizing micrographs of the nematic liquid crystal in contact with the checkerboard patterned alignment surfaces. The number indicates the size of the unit domain.

size of the unit domain is smaller than the wavelength of visible light, individual domains are no longer visible in the far field and only the average liquid crystal orientation becomes what matters (Fig.2). The alignment can be switched from one stable orientation to the other by applying a sufficiently strong in-plane electric field (Fig.3), and each of the orientations remains stable even after the electric field is removed. Such a true bistability is hard to achieve in nematic liquid crystals, and the present success should be a clear indicative of the potentiality of nanostructuring.

The bistable orientation should be useful in any low-power consumption electrooptic applications of liquid crystals. Apart from the flat panel displays, in particular, the bistable structure should be valuable in telecommunication device applications of liquid crystals where a great demand exists for dynamically reconfigurable networking switches.

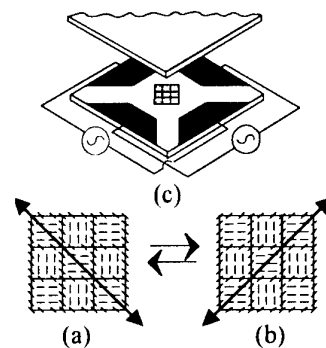


Fig.3 Bistable orientations on the checkerboard patterned surface (a) & (b). The electrode configuration for in-plane switching.

(1) J.-H. Kim, J. Yamamoto, M. Yoneya and H. Yokoyama, Appl. Phys. Lett. **78**, 3035(2001).

E-mail: yokoyama-hiroshi@aist.go.jp

## Nearly 100% internal phosphorescence efficiency in an organic light emitting diode

Chihaya Adachi<sup>a)</sup>, S. R. Forrest<sup>b)</sup> and M. E. Thompson<sup>c)</sup>

<sup>a)</sup>Department of Photonics Materials Science, Chitose Institute of Science and Technology,  
Chitose, Hokkaido 066-8655, Japan

<sup>b)</sup>Department of Electrical Engineering, Princeton University, Princeton, NJ 08544, USA

<sup>c)</sup>Department of Chemistry, USC, LA, CA 90089, USA

We demonstrate very high efficiency electrophosphorescence in organic light emitting devices employing a green phosphorescent molecule doped into a wide energy gap host. Using bis(2-phenylpyridine)iridium(III) acetylacetonate [ $(\text{ppy})_2\text{Ir}(\text{acac})$ ] doped into 3-phenyl-4-(1'-naphthyl)-5-phenyl-1,2,4-triazole (TAZ), a maximum external quantum efficiency ( $\eta_{\text{ext}}$ ) of  $(19.0 \pm 1.0)\%$  and luminous power efficiency ( $\eta_p$ ) of  $(60 \pm 5)\text{lm/W}$  are achieved. This corresponds to an internal quantum efficiency ( $\eta_{\text{int}}$ ) of  $(87 \pm 7)\%$ . Further, the temperature dependences of the electrophosphorescence and photoluminescence efficiencies indicate an absence of thermally activated non-radiative processes, leading to an internal phosphorescent quantum efficiency of 100%. Very high external quantum efficiencies are due to the 100% internal phosphorescence efficiency of  $(\text{ppy})_2\text{Ir}(\text{acac})$  coupled with balanced hole and electron injection and transport into, and triplet exciton confinement within the light emitting layer.

Furthermore, we demonstrate high-efficiency red electrophosphorescent OLEDs employing bis(2-(2'-benzo[4,5-a]thienyl)pyridinato- $\text{N},\text{C}^3$ )iridium(acetylacetonate) [ $\text{Btp}_2\text{Ir}(\text{acac})$ ] as a red phosphor. A maximum external quantum efficiency of  $\eta_{\text{ext}} = (7.0 \pm 0.5)\%$  and power efficiency of  $\eta_p = (4.6 \pm 0.5)\text{lm/W}$  are achieved at  $J = 0.01\text{mA/cm}^2$ . The EL spectrum has a maximum at  $\lambda_{\text{max}} = 616\text{nm}$  with additional intensity peaks at  $\lambda_{\text{sub}} = 670\text{nm}$  and  $745\text{nm}$ . The CIE coordinates of  $(x=0.68, y=0.32)$  are close to meeting video display standards. The short phosphorescence lifetime ( $\sim 4\mu\text{s}$ ) of  $\text{Btp}_2\text{Ir}(\text{acac})$  leads to a significant improvement in  $\eta_{\text{ext}}$  at high currents. Further, we demonstrate that the mechanism of endothermic energy transfer from a conductive molecular organic host to an organometallic phosphor can result in highly efficient blue organic light emitting device. This demonstration of endothermic transfer employs iridium(III)bis(4,6-di-fluorophenyl)-pyridinato- $\text{N},\text{C}2'$  picolinate, **FIrpic**, as the phosphor. Due to the comparable energy of the phosphor triplet state relative to that of the 4,4'-N,N'-dicarbazole-biphenyl (CBP) conductive host molecule into which it is doped, the exothermic transfer of energy from phosphor to host, and subsequent endothermic transfer from host back to phosphor is clearly observed. Employing this process, a very high maximum  $\eta_{\text{ext}} = (5.7 \pm 0.3)\%$  and  $\eta_p = (6.3 \pm 0.3)\text{lm/W}$  are achieved. The EL spectrum has a maximum at  $\lambda_{\text{max}} = 470\text{nm}$  with additional peaks at  $\lambda_{\text{sub}} = 495\text{nm}$  and  $540\text{nm}$ , leading to the CIE coordinates of  $x=0.16$  and  $y=0.29$ .

<sup>a)</sup> c-adachi@photon.chitose.ac.jp

# Direct fabrication method of surface relief structures on azopolymer films and its device application

Kenji Harada, Masahide Itoh, Shinsuke Umegaki\* and Toyohiko Yatagai

*Institute of Applied Physics and Tsukuba Advanced Research Alliance (TARA), University of Tsukuba, Tsukuba 305-8573, Japan*

*Phone +81-298-53-5217 Fax +81-298-53-5205 E-mail harada@optlab2.bk.tsukuba.ac.jp*

*\*Faculty of Science and Technology, Keio University, Hiyoshi, Yokohama 223, Japan*

Polymeric materials are the most promising organic materials for electro-optic devices and memory devices. In the past several years, direct fabrication of surface relief structures in azo-polymers has been reported. This method is a one-step fabrication technique. A surface relief structure is fabricated by means of irradiation of interference fringes. It can be fabricated only upon azobenzene functionalized polymers such as side-chain-type and main-chain-type azo-polymers. The diffraction efficiency and the surface relief depth depend on the writing energy and the polarization of the writing laser beam. This structure is very stable at temperatures under glass transition temperature  $T_g$  and can be erased by heating above  $T_g$ . Surface relief grating fabrication and the modulation of a surface relief electro-optic grating has been reported.

We proposed a new technique to increase the surface relief structure. The electric charge was deposited on the surface relief grating in a corona-depositing poling setup in an oven. Figure 1 shows typical examples of the three dimensional view of the surface relief gratings observed from atomic force microscopy before and after corona discharge. The first-order diffraction efficiency measured before and after corona discharge increased from about 0.24 % to about 28 %. This diffraction efficiency increase is mainly caused by the increase of the relief depth caused by the electric charge. The relief depth is increased from 20 nm to 350 nm by corona discharge.

We fabricated the Fresnel and Fourier transform hologram on polymer film. Figure 2 show a reconstructed image of a Fresnel hologram. Diffraction efficiency is increased by corona discharge. This material can be applied for new recording materials and optical devices

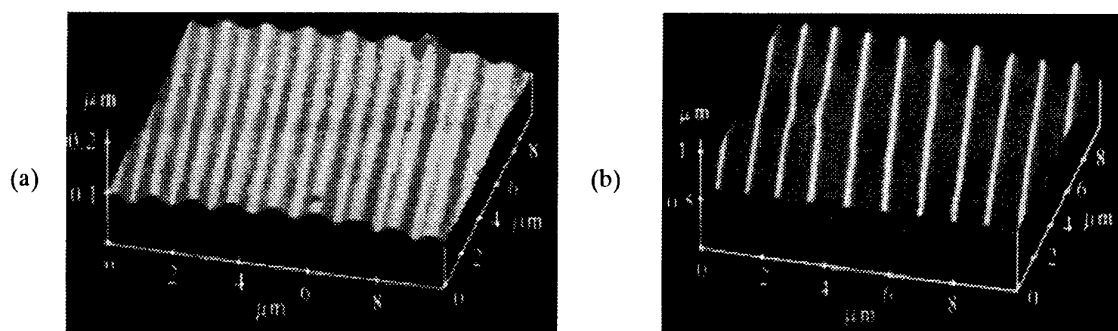


Fig. 1 AFM image of surface relief grating  
(a) before and (b) after corona discharge

Fig. 2 Reconstructed image of hologram  
(1.6cm × 2.3cm)



# Very Efficient Visible-Light-Induced Electron Transfer at Gold Electrodes Modified with Self-Assembled Monolayers of Various Metalporphyrin-Ferrocene-Thiol Linked Molecules

*Toshihiro Kondo, Masayuki Okamura, Takuya Masuda, and Kohei Uosaki*

*Physical Chemistry Laboratory, Division of Chemistry, Graduate School of Science,  
Hokkaido University, Sapporo 060-0810, Japan*

## Introduction

It is of great interest to mimic the elaborate molecular machinery of natural systems for the realization of a highly efficient artificial photosynthetic device. A self-assembly (SA) technique has been very widely used to construct ordered molecular layers of various functionalities and self-assembled monolayers (SAMs) of alkanethiols on gold have been the most well studied system. We have demonstrated that the photoinduced up-hill electron transfer can be achieved at gold electrodes modified with SAMs of molecules containing porphyrin and electron relay groups such as quinone and ferrocene [1-3]. Highest efficiency was observed at a gold electrode modified with a SAM of porphyrin-ferrocene-thiol linked molecule in an electrolyte solution containing methylviologen ( $MV^{2+}$ ) as an electron acceptor [3]. We have proposed that one of the most important reasons for the very high efficiency of this system is the effective inhibition of energy and/or reverse electron transfer from excited porphyrin to the gold as a result of the highly ordered structure of the SAM [3-6].

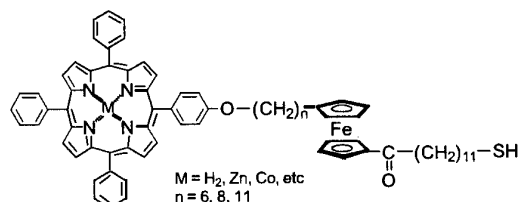


Fig. 1 Molecules containing porphyrin, ferrocene and thiol separated each other by alkylchains. ( $PC_nFcC_{11}SH$ ).

In this report, three compounds (Fig. 1), which have porphyrin, ferrocene and thiol groups as sensitizer, electron relay and surface binding groups, respectively, separated from each other by alkyl chains are studied. While the chain length between thiol and ferrocene was kept constant, that between ferrocene and porphyrin was varied. Quantum efficiency of photoinduced electron transfer at the gold electrode modified with SAMs of these molecules was examined. In addition, effects of introduction of various metals into porphyrin ring on photoelectrochemical characteristics was investigated.

## Experimental

$PC_nFcC_{11}SH$  ( $M = H_2$ ,  $n = 6, 8, 11$  in Fig. 1) were synthesized following the methods reported before [3,4]. The surface modification of the gold was carried out by dipping the substrate in dichloromethane solution containing 1 mM  $PC_nFcC_{11}SH$  at 20 °C for 15 h under Ar atmosphere. Photocurrent measurements were carried out by irradiating the electrode with a 500 W Xe lamp through a monochromator. Introduction of the metal into porphyrin ring was carried out by immersing the  $PC_nFcC_{11}SH$  SAM modified gold into methanol containing metal acetate.

## Results and Discussion

A highly efficient visible-light-induced photocurrent generation was achieved at a gold electrode modified with the SAM of  $\text{PC}_n\text{FcC}_{11}\text{SH}$  (Fig. 1) in a solution containing methylviologen ( $\text{MV}^{2+}$ ) as an electron acceptor. A cathodic photocurrent due to the reduction of  $\text{MV}^{2+}$  to the methylviologen radical cation ( $\text{MV}^{•+}$ ) was observed when the potential was more negative than the redox potential (+610 mV vs. Ag/AgCl) of the ferrocene moiety in the SAM (Fig. 2). The redox potential of the ferrocene moiety was more positive than that of  $\text{MV}^{2+}/\text{MV}^{•+}$  (-630 mV), indicating that we achieved photoinduced up-hill electron transfer of more than 1.0 eV. The photocurrent action spectrum matched well with the absorption spectrum of the  $\text{PC}_8\text{FcC}_{11}\text{SH}$  SAM (Inset of Fig. 2). These results indicate that porphyrin and ferrocene actually acted as a photosensitizer and electron relay groups, respectively.

Figure 3 shows the time course of the current measured at -200 mV in 0.1 M  $\text{NaClO}_4$  containing 5.0 mM  $\text{MV}^{2+}$  when the gold electrodes modified with the SAMs of  $\text{PC}_n\text{FcC}_{11}\text{SH}$  was illuminated with pulsed light at 430 nm. At all the SAM modified gold electrodes, cathodic photocurrent was observed. Quantum efficiencies based on the absorbed photons were 4.0 %, 11 % and 12 % at the gold electrodes modified with the SAMs of  $\text{PC}_6\text{FcC}_{11}\text{SH}$ ,  $\text{PC}_8\text{FcC}_{11}\text{SH}$  and  $\text{PC}_{11}\text{FcC}_{11}\text{SH}$ , respectively. The longer the alkylchain between porphyrin and ferrocene in the SAM, the larger the photocurrent. The present results indicate that energy and/or reverse electron transfer from excited porphyrin to ferrocene and/or gold play important roles for determining the efficiency.

## References.

1. T. Kondo, T. Ito, S. Nomura and K. Uosaki, *Thin Solid Films*, **284/285**, 652 (1996).
2. T. Kondo, M. Yanagida, S. Nomura, T. Ito and K. Uosaki, *J. Electroanal. Chem.*, **438**, 121 (1997).
3. K. Uosaki, T. Kondo, X.-Q. Zhang and M. Yanagida, *J. Am. Chem. Soc.*, **119**, 8367 (1997).
4. M. Yanagida, T. Kanai, X.-Q. Zhang, T. Kondo and K. Uosaki, *Bull. Chem. Soc. Jpn.*, **71**, 2555 (1998).
5. T. Kondo, T. Kanai, K. Iso-o, and K. Uosaki, *Z. Phys. Chem.*, **212**, 23 (1999).
6. T. Kondo, M. Yanagida, X.-Q. Zhang, and K. Uosaki, *Chem. Lett.*, **2000**, 964 (2000).

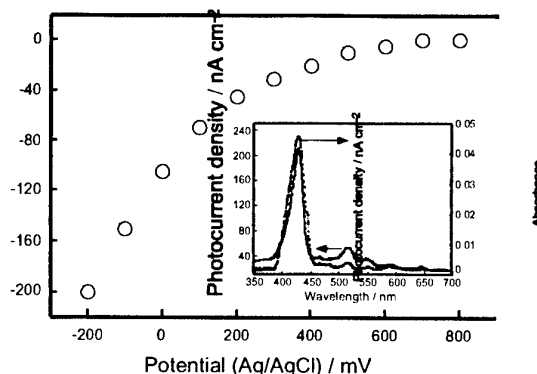


Fig. 2 Potential dependence of photocurrent at the  $\text{PC}_8\text{FcC}_{11}\text{SH}$  SAM modified gold electrode. Inset: Absorption spectrum of the  $\text{PC}_8\text{FcC}_{11}\text{SH}$  SAM on a transparent gold substrate observed in air (dotted line) and the photocurrent action spectrum of the  $\text{PC}_8\text{FcC}_{11}\text{SH}$  modified gold electrode. The electrode was illuminated with 430 nm pulsed light ( $40 \mu\text{W cm}^{-2}$ ;  $8.7 \times 10^{13} \text{ photons s}^{-1} \text{ cm}^{-2}$ ).

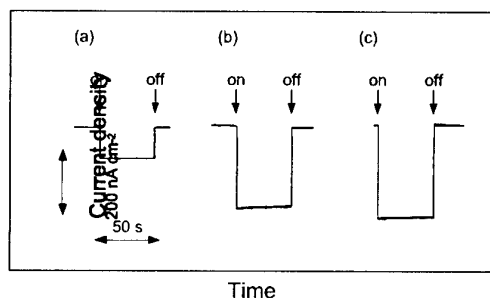


Fig. 3 Time course of currents at the gold electrodes modified with the SAMs of (a)  $\text{PC}_6\text{FcC}_{11}\text{SH}$ , (b)  $\text{PC}_8\text{FcC}_{11}\text{SH}$  and (c)  $\text{PC}_{11}\text{FcC}_{11}\text{SH}$  measured in 0.1 M  $\text{NaClO}_4$  containing 5.0 mM  $\text{MV}^{2+}$  as an electron acceptor when the electrodes kept at -200 mV were illuminated with 430 nm pulsed light.

## Optical and Optoelectronic Materials Derived from Deoxyribonucleic Acid (DNA)

Lili Wang, Hiroaki Takahashi, Gongjian Zhang, Jonichi Yoshida and Naoya Ogata\*  
Chitose Institute of Science and Technology, 758-65 Bibi, Chitose,  
Hokkaido 066-8655 Japan

Many of synthesized polymers have been used as host matrices in a variety of functional composites in order to achieve properties or processing advantages that were not possible without the synergism between the host polymer and guest materials. In this respect, a particularly ambitious goal has been the fabrication of composites, based on polymers and organic chromophores, for optical and optoelectronic applications. In principle, organic chromophores can exhibit fast response times, and are readily converted into films by self-assembly, by LB-techniques or, when included in polymer host matrices, films can be cast from solution or the melt. One of the greatest challenges in the polymer-based optoelectronic materials has been the preparation of materials with sustainable second harmonic generation, based on properties that relies on the absence of centrosymmetry that accompanies anisotropic ordering of the molecular chromophores

On the other hand, it is well known that the characteristic feature of a biopolymer, DNA structure is rod-like, double helix with  $\pi$ -electron-rich base pair stacking (the base separation is 0.34nm, diameter of the helix is about 2nm). Therefore, the double helix with  $\pi$ - $\pi$  stacking structure of nucleobase pairs of DNA not only forms a tunnel ready for electron transfer, but also makes the materials high optical transparency. Some of dyes can be easily intercalated in the helices, and intensity of the fluorescence is greatly enhanced. Some of dyes can be easily inserted into the grooves of DNA helix. Some of another dyes can be easily stacked on the surface of DNA helix. DNA has high affinity for various functional chromophores because that the intercalation and inserting is a relatively nonspecific interaction. We recently found DNA-Na fiber is thermostable up to 200 C°. It seems that the materials of DNA and DNA-dye complex are very promising for application of molecular optics and molecular optoelectronics. However, the film materials prepared from DNA or inorganic salts of DNA are too water-sensitive and poor mechanical strength to fabricate the devices.

We find that the self-assembled DNA-surfactant complex film is thermally stable up to 180°C, highly transparent and photostable. The DNA-surfactant complexes could be easily transformed into various functional optical and optoelectronic materials by doping functional dyes, such as NLO, laser, and photochromic organic dyes. Figure 1 shows a schematic road

**A Novel Photochromic Film Materials Derived from Supramolecules,  
DNA-Surfactant Complex: Spiropyran-DNA-CTMA Complex**

Lili Wang, Masahiro Fukushima, Junichi Yoshida and Naoya Ogata\*

Faculty of Photonic Sciences, Chitose Institute of Science and Technology,  
758-65 Bibi, Chitose, Hokkaido 066-8655. Japan

Tel: 0123-27-6001 Fax: 0123-27-6007 E-mail: [n-ogata@photon.chitose.ac.jp](mailto:n-ogata@photon.chitose.ac.jp)

Recently, we have reported that self-assembly of DNA-surfactant complexes produced high transparency, and thermostable film materials, having huge nano-size free volume (surfactant micelles, minor and major grooves and spaces between base-pairs). Therefore, it can be easily functioned by doping functional organic dyes such as laser and nonlinear optical dyes. On the other hand, an important class of functional dye, photochromic compound, has been studied extensively because of their potential use as optical and optoelectronic materials. Recently, photochromic materials are of great interest in molecular engineering. Any practical applications of photochromic materials require their inclusion in robust matrices such as polymers. The photochrome concentration is usually low in order to prevent phase separation. Due to interaction with other molecules in the system, new properties can be generated, thus allowing the performance of new functions. However, the persistent problem of photochemical degradation of photochromic dyes has limited and slowed their applications. The slow discoloration rate in solid matrices is also a disadvantage for commercial applications.

As a new approach, we aim to dope the photochromic compound into the DNA-surfactant complex film matrix because ordered free space such as minor and major grooves of DNA strands, and surfactant micelles can allow to trap the dye molecules. In this presentation we report on the preparation, optical and photoelectric characteristics of a typical photochromic compound, spiropyran, 6'-nitro-BIPS doped DNA-CTMA complex film.

The absorption peak of the photomerocyanine doped in DNA-CTMA was at 547 nm. This indicated that the zwitterions structure is stable in the DNA-CTMA solid matrix. Photomerocyanine is generally described as an equilibrium between the quinoid and zwitterions structures. In solution, it is well known that photomerocyanine forms of spiropyran are characterized by a positive solvatochromism corresponding to the increase of the red shift when the polarity of the solvent increases. The positive solvatochromism is characteristic of compounds having a weakly polar ground state, implying a small charge delocalization. Therefore, in apolar solution, the structure of the photomerocyanine form of spiropyran is much more quinoidal than zwitterionic.



Because the structure of the photomerocyanine is mainly zwitterions in the DNA-CTMA matrices, the polarity of the DNA-CTMA matrix should be stronger than general organic solvent such as dioxan, and solid PMMA matrix. The zwitterionic structure was stabilized by strong hydrogen bonds to grooves of the double helix of DNA-CTMA matrix cage, lowering the ground state of the merocyanine and increasing the gap to the first excited state. Therefore, in solid DNA-CTMA matrices, the photochromism is reversed with a stable open zwitterionic form.

All these results confirm our assumption concerning the presence of two chemical environments for the dye molecules in the DNA-CTMA matrices. A first part of spiropyran molecules was placed in major grooves, which did not stabilize the merocyanine form. A second part of spiropyran molecules was placed in minor grooves, which stabilized the merocyanine form. The reason that spiropyran molecules to aggregate to form helical structures, but does not aggregate in alkyl micelles can be explained in terms of the preference of like-like interactions over unlike interactions.

In the case of spiropiran contained in DNA-CTMA complex matrix, the film formed in the dark displayed pale yellow color. If the film was irradiated continuously during formation, resulting films consistently showed mocha color and a larger CD signal. These results could be interpreted in terms of the nature of the matrix; helical DNA part of DNA-CTMA solid film is expected to display excellent affinity for spiropyran dye thus aiding incorporation of the photochromic molecules in the films and orientation of the polar open forms.

A potentially useful property, alongside developing optically controllable molecular switches, is the photoluminescent behavior of photochromes. We will show the fluorescence properties of spiropyran, 6'-nitro-BIPS doped in DNA-CTMA accompanying ring-opening and ring-closing photoisomerization. The strong fluorescence is attributed to the production of the excited state of the opening-ring 6'-nitro-BIPS isomer via returning to ground state of the closed-ring isomer. In comparison with polymer media, such as PMMA, the orientation effect of the chiral environment greatly enhanced the fluorescence of the opening-ring 6'-nitro-BIPS isomer. This also indicated that aggregation and binding mode of spiropyran on the DNA formation were on monomer mode. Such aggregation was observed in the case of hemicyanine containing single alkyl substitution.

## Nanoparticle-Directed Crystallization of Calcium Carbonate

Inhyung Lee, Sang Woo Han, and Kwan Kim\*

*Laboratory of Intelligent Interface, School of Chemistry and Molecular Engineering  
and Center for Molecular Catalysis, Seoul National University, Seoul 151-742, Korea*

Natural organisms that produce biological composites exert exquisite control over the minerals they deposit, creating materials of myriad shapes and sizes that are often of high strength. Mineralized tissues are often found to contain polymorphs and individual minerals whose crystal morphology, size, and orientation are determined by local conditions and, in particular, the presence of matrix proteins or other macromolecules.<sup>[1]</sup> The processes and materials that control such crystal nucleation and growth are of great interest to materials scientists who seek to manufacture composite materials and crystalline forms analogous to those produced by nature.<sup>[2-5]</sup> In this respect, we have investigated the crystallization of calcium carbonate in the presence of monolayer-protected gold nanoparticles. In fact, spherically-shaped  $\text{CaCO}_3$  crystals (vaterite) were found to grow on the acid terminated gold nanoparticles (Figure 1). The spherical particles thus obtained were evidenced by TEM to consist in metal (core)-organic (linker)-inorganic (shell) hybrid structure. More surprisingly, in the presence of  $\text{Mg}^{2+}$  ions, needle-like  $\text{CaCO}_3$  crystals (aragonite) were formed (Figure 2). TEM images of these crystals indicated that the average diameter of  $\text{CaCO}_3$  needles is  $\sim 150$  nm and the size distribution is very narrow. The present observation thus suggests that organic-terminated metal nanoparticles can be used as a seed material for the growth of interesting biomimetic crystals.

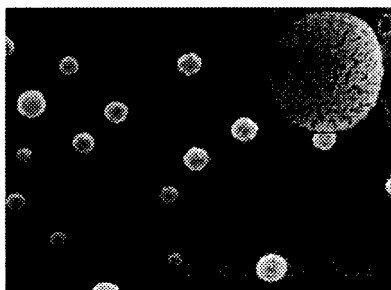


Figure 1

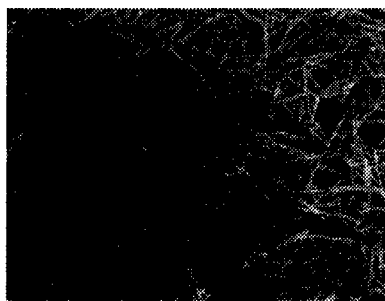


Figure 2

## REFERENCE

1. H. A. Lowenstam, S. Weiner, *On Biomineralization*, Oxford University Press, New York, 1989.
2. S. Mann, *Nature* **1988**, 332, 119.
3. S. Mann, *Nature* **1993**, 365, 499.
4. A. Berman, D. J. Ahn, A. Lio, M. Salmeron, A. Reichert, D. Charych, *Science* **1995**, 269, 515.
5. G. Falini, S. Albeck, S. Weiner, L. Addadi, *Science* **1996**, 271, 67.

## Nonlinear Optical Properties of Anisotropic Molecular Thin Films on Nanostructured poly(tetrafluoroethylene) surfaces

Gongjian Zhang, Kanna Uchikoshi, Toshihiko Tanaka\*, and Naoya Ogata

Chitose Institute of Science and Technology, 758-65 Bibi, Chitose, Hokaido, Japan

\*Tsukuba Research Lab., Sumitomo Chem. Co., Ltd., 6 Kitahara, Tsukuba, Ibaraki 300-32, Japan

The great progress made in recent years in the researches of the organic nonlinear optical materials is well established. Conjugated organic compounds have attracted considerable attention because their large optical nonlinearities suggest potential applications in integrated optical devices such as electro-optical modulators, all-optical modulators, and frequency converters. And, we noted that a promising application in short pulse nonlinear optical measurement was also reported recently. For most of these applications, high quality single-crystalline thin films are needed. Several attempts to prepare crystalline thin films have been reported by many research groups. The crystal growth was performed either from the melt by the Bridgman method, by slow cooling of a saturated solution, by thermal convection, or by vapor deposition on a glass substrate. Additionally, a Langmuir-Blodgett deposition technique is well known. Recently, a simple process by which the highly oriented nonlinear optical films seem to be epitaxially grown onto well-oriented polymer film surfaces, were reported in several articles.<sup>[1,2]</sup> It is well known that when PTFE is rubbed against a clean surface, under appropriate conditions, a highly oriented thin film is deposited onto the surface. PTFE chain axes in these so-called transfer films are oriented parallel to the surface and along the sliding direction. These films were shown to act as very effective substrates for promoting oriented growth of a variety of materials, for example, small organic molecules deposited onto them from solution, the melt, or vapor phases.

In this paper, we present results for the alignment growth of nonlinear optical materials on thin layers of oriented PTFE. These well-oriented PTFE substrates were prepared according to the friction transfer method. Subsequently, the organic material was deposited under vacuum through evaporation on it; the obtained films were characterized by means of the x-ray diffraction and nonlinear optical measurement technique. The results show that these films obtained by this method possess highly anisotropic optical properties and large nonlinearity, which are confirmed by the proposed molecular orientation. The compounds (see insertion of Fig.1 and Fig.2) used in the experiment were an organic nonlinear optical material 1-(2-thionyl)-3-(4-methylphenyl) propene-1-one (TMPP) and a bisazo dye (BZ-3) that shows large SHG activity and good optical quality of the film. For investigating the bisazo film, the polarized UV-visible spectra were applied. The absorption in the polarized spectra was significantly larger with incident light polarized parallel to the sliding direction of the thin PTFE films (from friction-transfer method). This means that the mean direction of long axes of the dye agrees with those of the PTFE chains, because the absorption

of dye film at the peak wavelength is maximized for the polarization direction exactly parallel to the sliding direction. The polarized IR spectra also support the same conclusion. This was done by observation of the peaks from vibration originating from asymmetric p-phenylene or from peaks combined with a C-N stretch through the azobenzene moiety. The investigation of x-ray diffraction, in which, a sharp peak appears located at  $2\theta$  of  $23.8^\circ$  shows the good effect of the molecular alignment (Fig.1).

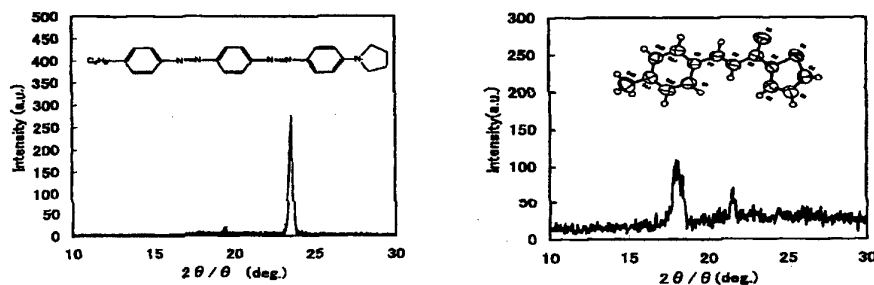


Fig.1 & 2 :  $\theta/2\theta$  x-ray diffraction from the film of BZ-3 and TMPP.

TMPP crystal was a well characterized, and reported in our previous work. [3] It shows a higher SHG activity and a better crystalline property in organic materials. However, the molecules of TMPP in crystal were not of planar structure, with respect to dihedral angles, the angle formed by the planes of the benzene ring and thiophene ring was about  $12^\circ$ , even though we can approximately see it as a planar molecule in crystal. The result shows that the film has two obvious diffraction peaks. We found that the peaks could be assigned as from the crystallographic planes (202) and (004). The (202) plane corresponds with somewhat molecular plane, and (004) is in a direction in where the crystal shows cleavage behaviors. However, the intensity from the plane (004) is smaller than that from (202) which is found almost corresponding with the molecular plane.

In conclusion, some mechanisms for interpretation of the molecular orientation were suggested. The alignment effect of crystals onto the PTFE surface can be considered as anisotropic surface interactions between oriented alignment polymer and the compound molecules. On other hand, the effect of selective nucleation of crystals is also resonantly considered. The BZ-3 could be considered as a planar and a long rod like molecule, while the TMPP is twisted in its molecular structure so that the alignment of the BZ-3 seem more similar to the former mechanism, and the TMPP orientation could be occurred by means of the selective nucleation. This method is very useful and can be expected applicable for preparation of the relevant nonlinear devices.

#### References:

- [1] P. Damman, R. Vallee, M. Dosiere, J. Wittmann, E. Toussaere, and J. Zyss, Opt. Mat., 9(1998)423.
- [2] R. Vallee, P. Damman, M. Dosiere, E. Toussaere, and J. Zyss, J. Am. Chem. Phys. 112, 23 (2000) 10556.
- [3] G.J.Zhang, S. Horinouchi, T. Kinoshita, and K. Sasaki, Appl. Opt., 34,24(1995)5301.

## Langmuir-Blodgett films of $\beta$ -carotene fabricated by the flow-orientation method

Toshihiko MATSUURA and Yuhei SHIMOYAMA\*

*Department of Applied Physics, Graduate School of Engineering,  
Hokkaido University, Sapporo 060-8628, Japan  
E-mail: mtoshi@eng.hokudai.ac.jp*

*\*Department of Physics, Hokkaido University of Education,  
Hakodate 040-8567, Japan  
E-mail: yuhei@cc.hokkyodai.ac.jp*

$\beta$ -Carotene, widely distributed in the botanical kingdom, is an optically active molecule at the visible region. Thus, Langmuir-Blodgett (LB) films of  $\beta$ -carotene have attracted attentions as photonic devices. Methods for the fabrication of well-ordered Langmuir (L) monolayers of  $\beta$ -carotene have not been well established [1]. The main problem in the conventional techniques was that the piling-up of the molecules on top of the lower layers. Hence, a well-defined monolayer could not be formed.

To fabricate well-defined  $\beta$ -carotene films, we employed the flow-orientation method [2, 3]. This method controls the flow of the developing solution on the subphase surface. In the conventional procedure, a constant surface area is normally used during the deposition of the developing solution on the subphase. In the present study, however, the developing solution is spread on the aqueous subphase while the surface area on trough is increased by means of a moving barrier. A laminar flow, caused by the movement of the moving barrier, enables the film molecule to diffuse in a definite direction, which induces the formation of well-ordered monolayers.

Figure 1 shows a surface pressure-area ( $\pi$ -A) isotherm for the  $\beta$ -carotene L-monolayer on the ultra-pure water at 290 K. The  $\pi$ -A curve gently rose for the range between 1.0-0.37 nm<sup>2</sup>/molecule. The limiting area, obtained by the extrapolation of the linear region to the zero surface pressure, was 0.37 nm<sup>2</sup>/molecule. This value is identical with the cross section of  $\beta$ -carotene. This suggests that  $\beta$ -carotene aligns its long axis perpendicular to the subphase. In the present experiment, the flow-orientation method promoted the surface diffusion of  $\beta$ -carotene on the subphase, and yielded the complete single monolayers. The

procedure provided a significant method to align  $\beta$ -carotene.

For the structural elucidation of LB films, we carried out X-ray diffraction (XRD), Fourier-transform infrared (FTIR), and ultraviolet visible (UV) measurements. The XRD observation yielded the Bragg diffractions of the (00 $l$ ) plane in the  $\beta$ -carotene LB films on the quartz glass. The plane separation at (001) reflection was larger than the molecular length of  $\beta$ -carotene. Hence, the  $\beta$ -carotene LB film possesses a periodic zigzag structure. In FTIR measurements, the peak corresponding to the C-H stretching vibration of  $\beta$ -carotene was observed at 3032  $\text{cm}^{-1}$ , when the incident beam was p-polarized. The observation suggests that the molecular plane orients almost perpendicular to the substrate surface. The UV measurements revealed that the peak position of the LB films shifted to the higher wavelength than that of the chloroform solution. The red shift demonstrates that the  $\beta$ -carotene LB film is a high-density packing film in the in-plane directions.

In conclusion, using the flow-orientation method that controls the flow of film materials on the subphase, we succeeded in fabricating the well-ordered L-monolayers and the LB films of  $\beta$ -carotene.

#### References

- [1] R. M. Leblanc and B. H. Orger, *Biochim. Biophys. Acta.* **275** (1972) 102.
- [2] T. Matsuura, T. Komatsu, E. Hatta and Y. Shimoyama, *Jpn. J. Appl. Phys.* **39** (2000) 1821
- [3] T. Matsuura, A. Nishimura and Y. Shimoyama, *Jpn. J. Appl. Phys.* **39** (2000) 3557.

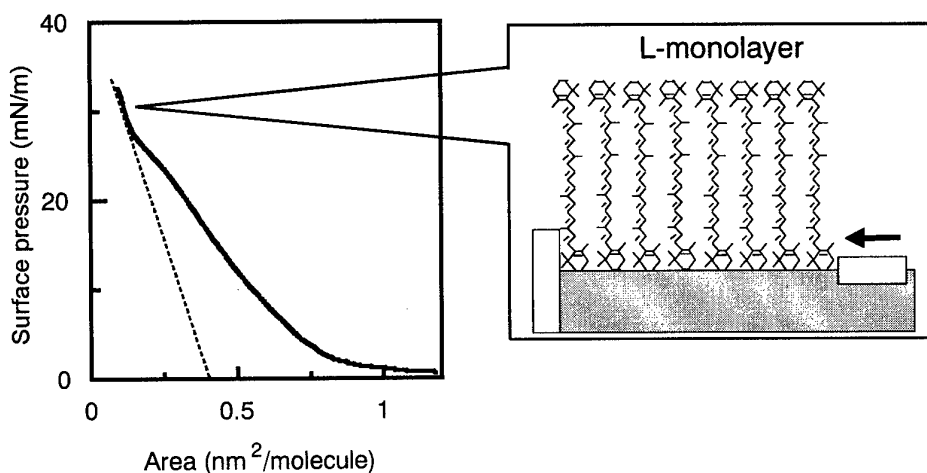


Fig. 1. The  $\pi$ -A isotherm for the  $\beta$ -carotene monolayer at 290 K.

## Formation and structure of self-assembled films of poly(3-alkylthiophene)

Toshihiko MATSUURA, Hiroshi SAKAGUCHI \*, and Yuhei SHIMOYAMA \*\*

*Department of Applied Physics, Graduate School of Engineering,  
Hokkaido University, Sapporo 060-8628, Japan*

*\* Institute for Electronic Engineering, Shizuoka University, Hamamatsu 432-8011, Japan*

*\*\* Department of Physics, Hokkaido University of Education, Hakodate 040-8567, Japan*

(yuhei@cc.hokkyodai.ac.jp)

Ultrathin films of poly(3-alkylthiophene) have potential applications in the future photonic devices. Recently, self-assembled monolayers (SAMs) have attracted considerable interests due to the simplicity of their preparation and stability of the films [1]. SAMs formed by spontaneous chemisorption of organic molecules on solid substrates (e.g., Au, GaAs, and Si) are new type of organic monolayers. Gao *et al.* have reported, for the first time, that poly(3-alkylthiophene) successfully forms SAMs on Au(111) through a immersion of the gold substrate in a chloroform solution for 10 h [2]. However, the growth process of the poly(3-alkylthiophene) SAMs has not been yet clarified. In the present study, we will reveal growth mechanism of SAMs of poly(3-alkylthiophene) on Au(111).

Poly(3-dodecylthiophene) (PDT) was used for the film molecule, as depicted in Fig. 1. To prepare the SAMs, we dipped the gold substrate into a chloroform solution of PDT at 17 °C. After removal from the solution, we rinsed the surface of the immersed substrate with chloroform. We measured them using Fourier-transform infrared reflection absorption spectroscopy (FTIR-RAS) and quartz crystal microbalance (QCM) method.

Figure 2 shows typical FTIR-RAS spectra of the PDT SAMs for the range of 3000-2800  $\text{cm}^{-1}$ . The spectra reflect the following C-H stretching vibrations: the in-plane  $\text{CH}_3$  asymmetric vibration  $\nu_a(\text{CH}_3; \text{ip})$  at 2965  $\text{cm}^{-1}$ , the out-of-plane  $\text{CH}_3$  asymmetric vibration  $\nu_a(\text{CH}_3; \text{op})$  at 2959  $\text{cm}^{-1}$ , the  $\text{CH}_2$  asymmetric vibration  $\nu_a(\text{CH}_2)$  at 2927  $\text{cm}^{-1}$ , and the  $\text{CH}_2$  symmetric vibration  $\nu_s(\text{CH}_2)$  at 2855  $\text{cm}^{-1}$ . The peak intensities of the  $\nu_a(\text{CH}_2)$  mode increased with the immersion period. The QCM measurements also reflected an increase of the PDT molecules adsorbed on the gold electrode with the immersion period. In order to describe the growth kinetics of the PDT SAMs, we employed the time-dependent Langmuir adsorption isotherm [3]. The theoretical curves reasonably fitted the data. The *time-dependent* Langmuir adsorption scheme turns out to reign over the formation process



of the PDT SAMs.

Our FTIR-RAS spectrum at 10 h of immersion was almost identical with that by Gao *et al.* at 10 h. Alkyl-chains in the PDT SAMs orient along normal to the substrate at 10 h. In the FTIR-RAS spectra beyond 120 h, on the other hand, we found the peak of the  $\nu_a(\text{CH}_3; \text{op})$  mode at  $2959 \text{ cm}^{-1}$ . Existence of the  $\nu_a(\text{CH}_3; \text{op})$  vibration implies that alkyl-chains in the PDT SAMs take a parallel configuration on Au(111). A transition of the molecular orientation was found during the SAM growth of PDT. The peak positions of the  $\nu_a(\text{CH}_2)$  mode shifted to a lower wave number region. The red-shift indicates that the immersion for the period longer than a week induces the close packed PDT SAMs.

In conclusion, we found that the formation process of the PDT SAMs obeys the *time-dependent* Langmuir adsorption scheme. The alkyl-chains undergo a transition of orientation from the standing-up to flat-lying states during the SAM growth.

- [1] A. Ulman, *An Introduction to Ultrathin Organic Films from Langmuir-Blodgett to Self-Assembly* (Academic Press, San Diego, 1991).
- [2] Z. Gao, K. S. Siow, H. S. O. Chan, *Synthetic Metals* **75** (1995) 5.
- [3] T. Matsuura, T. Takamura, Y. Shimoyama, *Jpn. J. Appl. Phys.* **38** (1999) 2874.

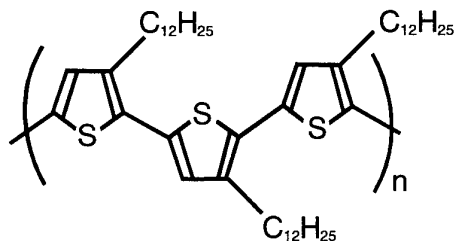


Fig. 1 Chemical formula of poly(3-dodecylthiophene)

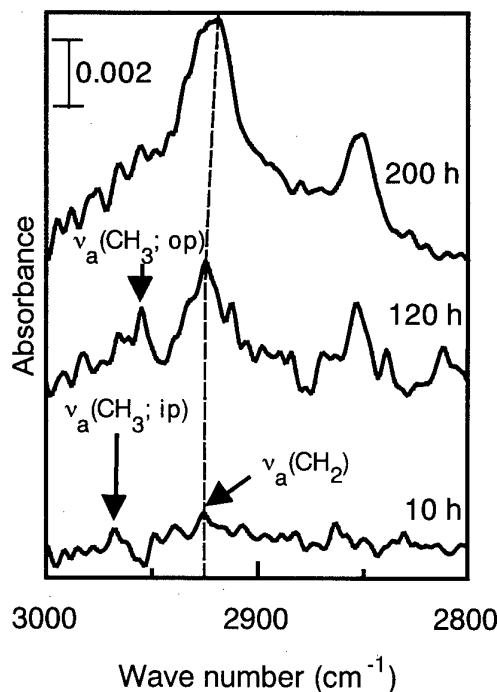


Fig. 2 FTIR-RAS spectra of SAMs of poly(3-dodecylthiophene).

## Langmuir-Blodgett Films of Nitrostilbene

Hiroyuki KAJI and Yuhei SHIMOYAMA

*Department of Physics, Hokkaido University of Education, Hakodate 040-8567, Japan.*

(e-mail: yuhei@cc.hokkyodai.ac.jp)

### Abstract

Nitrostilbene has been known as a functional organic molecule with the  $\pi$ -conjugated system, and possesses both the strong donor and acceptor moieties. Optical devices such as a doubler and a tripler of the laser frequency have been successfully fabricated by the organic films of nitrostilbene with the high hyperpolarizabilities [1]. A composite containing liquid crystalline polymer and nitrostilbene as the host-guest system was the first achievement of the second order nonlinear optical effect using nitrostilbene [2]. However, it is seldom to find reports on the fabrication method of well-ordered LB films of nitrostilbene. Fabrication of the LB films is difficult for nitrostilbene derivatives [1]. Therefore, it is of our intention to fabricate well-ordered LB films of nitrostilbene.

The reason for the ill-defined LB films of nitrostilbene is mainly due to the strong cohesive force among the molecule. A well-defined monolayer cannot be created by the simple compression of the nitrostilbene microcrystal. Thus, it is necessary to isolate each molecule, and to prevent the association of nitrostilbene which is strongly cohesive. Attempts have been made to develop novel fabrication methods for the well-ordered LB films of phthalocyanines [3]. Fabrication of a well-ordered Langmuir (L) monolayer has been done by the release of the aggregation through the dilution and the flow of developing solutions. Thus far, these methods have not yet been applied on the LB films of nitrostilbene.

We investigated the process of the L-monolayer formation by the surface pressure-area isotherm. A well-ordered L-monolayer of 4-dimethylamino-4'-nitrostilbene (DANS) has been formed by the flow-orientation method as well as the dilution technique. In the beginning, we have been searching for the most appropriate conditions to prepare L-monolayer by only the dilution technique. However, the limiting area increased, and hardly converged to a constant value, even though the developing solution was enough diluted at the micro-molar level. The micro domains of DANS were produced by dilution of the developing solution. Molecular

orientations of the domains are varied within the in-plane confinement. Thus, we had to control the molecular orientations of DANS by some artificial stimuli. Using the flow-orientation method at the extremely low concentrations we succeeded in converging the limiting area at a constant value. The shear stress applying DANS enforced to align along the flow direction, whereby promotes ordering of the L-monolayer. The aggregation state was released by the dilution which increases the distance between DANS. Furthermore the flow-orientation induces a laminar flow by the surface force on the subphase, and enhances the molecular ordering.

X-ray diffraction (XRD) and ultraviolet-visible (UV-VIS) spectroscopy revealed structure and orientation of the DANS LB films, respectively. The XRD showed that the DANS monolayers form the tilt stacking in the LB films. The UV-VIS spectra of the LB films indicated a peak shift to the shorter wavelength with respect to the DANS solution. The peak due to the  $\pi$ - $\pi^*$  transition in the UV-VIS spectrum showed the blue shift which reflects the intermolecular stacking of the nitrostilbene chromophore. This evokes the H-associations in which the molecule orients perpendicular to the substrate. The XRD as well as UV-VIS data indicated that DANS tilts *ca.*  $10^\circ$  to the normal of the substrate (Fig. 1).

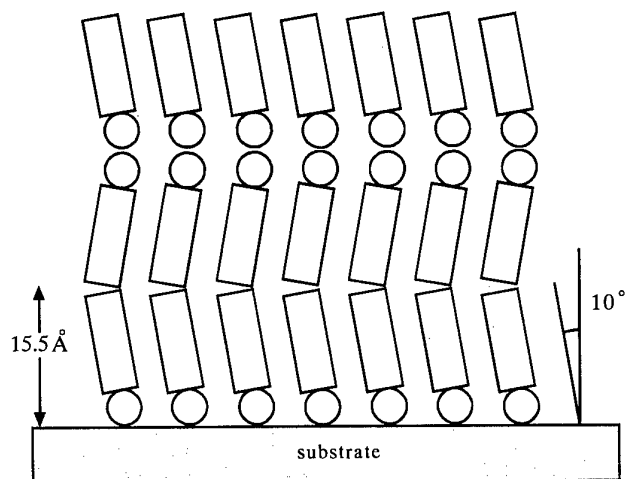


Fig. 1 A pictorial diagram of molecular organization of the DANS LB film.

## References

- [1] J. L. Oudar, *J. Chem. Phys.* **67** (1977) 446.
- [2] G. R. Meredith, J. G. VanDusen and D. J. Williams, *Macromolecules* **15** (1982) 1385.
- [3] T. Matsuura, T. Komatsu, E. Hatta and Y. Shimoyama, *Jpn. J. Appl. Phys.* **39** (2000) 1821.

## Enhanced electron injection in blue organic electroluminescent devices

Yuukou Matsuda, Chimed Ganzorig, and Masamichi Fujihira\*

*Department of Biomolecular Engineering, Tokyo Institute of Technology,  
4259 Nagatsuta, Midori-ku, Yokohama 226-8501, Japan*

Since the first report of efficient organic electroluminescent (EL) device by Tang and VanSlyke in 1987 [1], intensive researches have been carried out with the focus on its potential applications in display technology. Application to full-color, flat-panel displays has required red, green, and blue light emission. Only few blue-emitter materials like distyrylarene derivatives (DSA) [2,3] and silyl-substituted ter-(phenylene-vinylene) [4] appeared to be more significant, where the blue EL luminance is over  $10,000 \text{ cd m}^{-2}$ . Therefore, high EL efficiency, high carrier mobility, and thermally stable blue organic materials still remain to be developed. In addition, enhancing the carrier injection is one important way to improve device performance. Recently, Shaheen *et. al.* reported a two-layer blue organic EL device with a LiF/Al [5] cathode, i.e. ITO/TPD/DPVBi/Al, where ITO, TPD, and DPVBi are indium-tin-oxide, N,N'-diphenyl-N,N'-bis(3-methylphenyl)-1,1'-biphenyl-4,4'-diamine, and 1,4-bis(2,2-diphenylvinyl)biphenyl, respectively. This device has attracted considerable attention due to its impressive device performance [6].

In this work, we studied enhanced electron injection by introducing alkalimetal benzoates, such as  $\text{C}_6\text{H}_5\text{COOLi}$  [7], at emission layer (EML)/Al and electron transport layer (ETL)/Al interfaces in blue organic EL devices with DPVBi. Two different ETL materials, i.e. tris(8-hydroxyquinoline)aluminum ( $\text{Alq}_3$ ) and bathophenanthroline (Bphen) were examined. Here, as a hole transport layer (HTL) material, NPD (N,N'-bis-(1-naphthyl)-N,N'-diphenyl-1,1'-biphenyl-4,4'-diamine) was used. We found that cesium benzoate at the cathode interface exhibited the best device performance. We also found that the strong correlation between thickness of alkalimetal

benzoates or ETL and electron injection for reducing the power consumption and improving the EL efficiency. Improvement of electron injection might be attributed to lowering the work function of the Al cathode and doping of ETL with alkalimetal produced by interfacial chemical reactions during vapor-deposition of hot Al atoms.

#### References

- [1] C. W. Tang and S. A. VanSlyke, *Appl. Phys. Lett.* **51**, 913 (1987).
- [2] C. Hosokawa, H. Higashi, H. Nakamura, and T. Kusumoto, *Appl. Phys. Lett.* **67**, 3853 (1995).
- [3] H. Tokailin, M. Matsuura, H. Higashi, C. Hosokawa, and T. Kusumoto, *Proc. SPIE* **1910**, 38 (1993).
- [4] Z. Gao, C. S. Lee, I. Bello, S. T. Lee, R. M. Chen, T. Y. Lih, J. Shi, C. W. Tang, *Appl. Phys. Lett.* **74**, 865 (1999).
- [5] L. S. Hung, C. W. Tang, and M. G. Mason, *Appl. Phys. Lett.* **70**, 152 (1997).
- [6] S. E. Shaheen, G. E. Jabbour, M. M. Morrell, Y. Kawabe, B. Kippelen, N. Peyghambarian, M.-F. Nabor, R. Schlaf, E. A. Mash, and N. R. Armstrong, *J. Appl. Phys.* **84**, 2324 (1998).
- [7] C. Ganzorig and M. Fujihira, *Jpn. J. Appl. Phys.* **38**, L1348 (1999).

**Highly Efficient Organic Light-Emitting Diodes:  
Materials and Devices**

Yasunori Taga

## PHOTODYNAMICS OF MONO-L-ASPARTYL CHLORIN E6 FOR PHOTODYNAMIC THERAPY

Liming Li,<sup>1</sup> Kunihiro Kodama,<sup>1</sup> Koichi Saito<sup>2</sup> and Katsuo Aizawa<sup>3</sup>

<sup>1</sup>Chitose Institute of Science and Technology, 758-65 Bibi, Chitose, Hokkaido, 066-8655, Japan;

<sup>2</sup>Meiji Seika Kaisha Limited, 760 Morooka-cho, Kohoku-ku, Yokohama, 222-8567, Japan; and

<sup>3</sup>Tokyo Medical University, 6-1-1 Shinjuku, Tokyo, 160-8402, Japan

In recent years, significant advances have been made in the development of the photodynamic diagnosis (PDD) and photodynamic therapy (PDT). Currently the widely used photosensitizer in PDD and PDT is HpD. However, some problems with HpD remain to be resolved. First, HpD does not absorb photoradiation strongly in the red region of the spectrum where the radiation penetrates deeply into human tissue. Second, because HpD remains in normal tissue for a relatively long period, skin inflammation occurs. Thus, there has been extensive research into new photosensitizers with improved characteristics, such as optical absorption at longer wavelengths. A promising candidate is mono-L-aspartyl chlorin e6 (ME2906), in which long wavelength absorption is realized through a reduction of the double bond of a pyrrolic ring in the porphyrin macrocycle. However, photophysical information of ME2906 is very limited, and systematic studies are few.

In this letter, we report optical properties and photodynamics of ME2906 for PDD and PDT. In this study, ME2906 was dissolved in distilled water. Its concentration was varied between  $3.13 \times 10^{-7}$  and  $8.00 \times 10^{-5}$  M. Excitation and fluorescence spectra of the ME2906 water solutions were measured with a SPEX Fluorolog-3 fluorescence spectrophotometer (New Jersey, USA) equipped with a Tau-3 fluorescence lifetime measurement unit. The absorption spectra of the ME2906 solutions were measured with the Shimadzu UV-2500 UV-VIS spectrophotometer (Kyoto, Japan) to determine their molar extinction coefficients. Typical results of the excitation and the fluorescence spectrum for ME2906 water solution are shown in Fig. 1, where ME2906 concentration is  $2.50 \times 10^{-6}$  M. The excitation wavelength was measured, detecting at 662 nm, and the fluorescence was measured, exciting at 400 nm. The absorption peaks were observed at 400, 502, 600 and 655 nm for ME2906 dissolved with phosphate buffer saline solution (PH = 7.4). The fluorescence intensity, defined as the area of the fluorescence spectra plotted against wavelength, is shown as a function of ME2906 concentration in Fig. 2. The circles represent experimentally measured values. The solid line represents the linear dependence of the intensity upon ME2906 concentration. The intensity obtained in the present study is proportional to the concentration up to  $1.00 \times 10^{-5}$  M, and it tends to saturate above  $1.00 \times 10^{-5}$  M (black solid circles). These results clearly show that the emission observed below  $1.00 \times 10^{-5}$  M is assignable to the electronic transition from the lowest singlet excited state of an isolated ME2906 molecule to its ground state. This indicates suggests that a part of ME2906

molecules form dimers above  $1.00 \times 10^{-5}$  M.

The fluorescence decay time of the ME2906 water solutions was measured with the Fluorolog-Tau-3 fluorescence measurement system in the frequency domain. We carried out semiempirical molecular orbital (MO) calculation by the AM1 method to determine the optimized molecular configuration of ME2906 in the ground state and to have an insight into the experimental results obtained above. The calculation was done with WinMOPAC Ver.3. It showed that ME2906 is in isolate state in  $1.00 \times 10^{-5}$  M or less concentration range and is in dimer state in above  $1.00 \times 10^{-5}$  M concentration ranges.

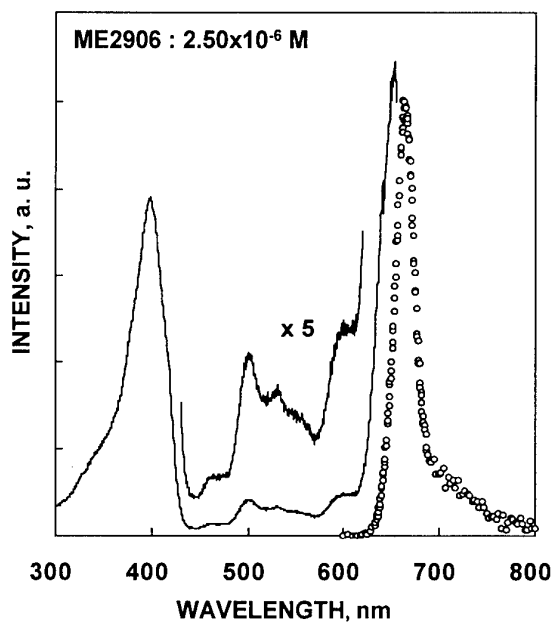


Fig.1. Excitation (solid lines) and fluorescence (open circles) spectrum of ME2906 water solution. The concentration of ME2906 is  $2.50 \times 10^{-6}$  M.

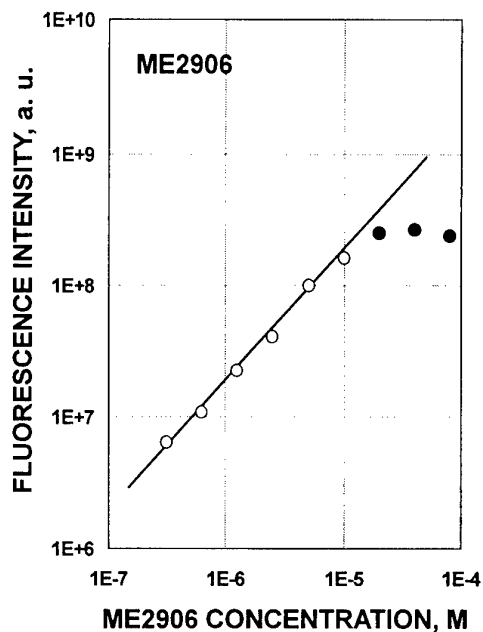


Fig.3. Fluorescence intensity as function of ME2906 Concentration. The circles stand for experimental results and the solid line for the linear relation between ME2906 concentration and fluorescence intensity.



## SPIDER and FROG apparatuses for amplitude and phase characterization of few-optical-cycle pulses

Liming Li,<sup>1</sup> Satoru Kusaka,<sup>2</sup> Ryuji Morita<sup>2</sup> and Mikio Yamashita<sup>2</sup>

<sup>1</sup>Chitose Institute of Science and Technology, Hokkaido University, and CREST, Japan Science and Technology Corporation, 758, Bibi 65, Chitose, 066-8655, Japan

<sup>2</sup>Department of Applied Physics, Hokkaido University, and CREST, Japan Science and Technology Corporation, Kita-13, Nishi-8, Kita-ku, Sapporo 060-8628, Japan

In recent years, significant advances have been made in the development of the ultrashort-pulse generation and measurement. To characterize ultra-short light pulses, especially for monocycle-like pulses, it is required to measure the pulse waveform and the time-dependent phase, which can be carried out using an SH-FROG technique or a more-recently-developed SPIDER technique. In this paper, we present characterization of  $\sim 5$  fs optical pulses using SH-FROG and SPIDER technique and compare between them.

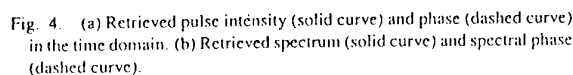
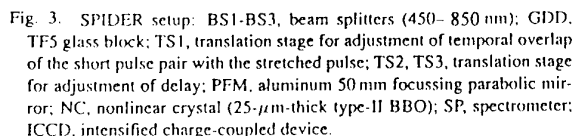
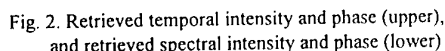
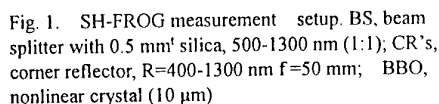
Ultrashort pulses ( $\sim 10$   $\mu$ J/pulse) to be characterized were generated from an optical pulse compressor of amplified Ti: sapphire laser pulses (1 kHz repetition rate) based on capillary-fiber self-phase modulation and spatial-light-modulator chirp compensation. The system generated 4.1 fs transform-limited pulses under the interferometric autocorrelation measurement.

The SH-FROG measurement set up is shown in Fig.1. The optical beam was passed through two pinholes and divided into two beams by using a broadband (500-1300 nm) dielectric multilayer coating beam splitter (BS) with a substrate thickness of 0.5 mm. Two corner reflectors (CR1, CR2) were used to make these beams parallel. These beams were then focused at a 10- $\mu$ m thick BBO nonlinear crystal (type I) using a parabolic mirror (PFM) with a spectral bandwidth of 400-1300 nm. The generated SH signal was passed through a filter (F) and then entered in a spectrometer. A CCD (1024x128 pixels) measured the SH spectra as a function of the delay time. One of the two corner reflectors was moved by a step motor and controlled by PC with every 0.1  $\mu$ m (0.6 fs) delay.

Using the SH-FROG apparatus, the amplitude and time-dependent phase of the light pulse were measured without any spectral compensation. Figure.2 shows the retrieved temporal intensity and phase and the retrieved spectral intensity and phase. The retrieved pulse duration is 5.7 fs and an error is 1.1%, through the 90 steps of the pulse retrieval program.

Next, we show a SPIDER apparatus in Fig. 3. The pulses were split by a 450-850 nm dielectric multiple-layer coated beamsplitter. One beam was input to a 450~850-nm-bandwidth Michelson-type interferometer to generate two pulse replicas,  $E_1$ ,  $E_2$ , with a delay of  $\tau$ . Another beam propagated twice a highly dispersive glass GDD (TF5: 100-mm length) and the duration of the output chirped pulse,  $E_C$ , was 25.2 ps. The two delayed pulses  $E_1$ ,  $E_2$ , were combined with the stretched pulse  $E_C$ . And all the pulses were focused on a 25- $\mu$ m-thick type-II BBO crystal by a 50-mm-focus-length aluminum parabolic mirror to generate interferometric sum-frequency beams (SFG). The two pulses  $E_1+E_C$  and  $E_2+E_C$  are two identical versions of the input pulse with a spectral shear  $\Omega$ , because of the delay time  $\tau$  of the two pulse replicas  $E_1$  and  $E_2$ . The spectral interferogram of the interference of the two SFG pulses was recorded by a 0.5-m spectrometer with a 150- $\mu$ m-width slit, a 1200 groove/mm grating and a 1024  $\times$  256 pixel U V-enhanced ICCD array allowing for rapid acquisition. The ICCD does not cover the full bandwidth of the SPIDER interferogram. Therefore, we were limited to updated times of  $7 \times 2.5$  s=17.5 s. A spectral shear  $\Omega$  is 2.81 THz corresponding to  $\Delta\lambda=1.31$  nm ( $\tau=860$  fs) and the present wavelength

Compared with the former SH-FROG, the latter SPIDER has several advantages of no moving components, noniterative reconstruction algorithm, the use of a thicker nonlinear crystal, the fast measurement time (17.5 s) and the measurement capability of monocycle-like pulses with ultrabroad spectra exceeding the one-octave.



## Solid state spectra and intermolecular interactions of tetrathiobenzoquinone derivatives

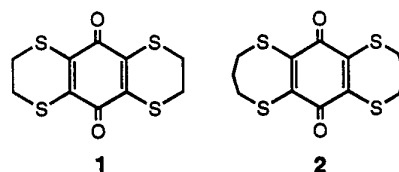
S. Matsumoto<sup>a, b, c</sup>, M. Matsuoka<sup>b</sup> and T. Wada<sup>c</sup>

<sup>a</sup> Research Fellow of the Japan Society for the Promotion of Science

<sup>b</sup> Laboratory of Material Science, Kyoto Women's University, 35 Kitahiyoshi, Imakumano, Higashiyama-ku, Kyoto 605-8501, Japan

<sup>c</sup> Supramolecular Science Laboratory, RIKEN (The Institute of Physical and Chemical Research), 2-1 Hirosawa, Wako, Saitama 351-0198, Japan

Tetrathiobenzoquinone derivatives **1** and **2** have a quinonoid structure with the sulfur atoms and the carbonyl groups as the donor and the acceptor, respectively, as shown in Scheme 1. They have attracted attention as a new organic pigment because of their poor solubility in various organic solvents as well as vivid coloration in the solid state.<sup>1</sup> **1** has also been known to have a large third-order non-linear susceptibility.<sup>2</sup> **1** was characterized by an extremely large bathochromic shift of about  $6612\text{ cm}^{-1}$  on going from a solution to the solid state as shown in Figure 1. The displacement energy of the bathochromic shift upon



Scheme 1.

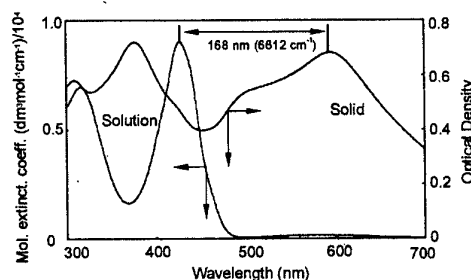


Figure 1. Solution and the solid state spectra of **1**.

crystallization depends considerably on the side-chain group, although no significant difference is recognized in their solution spectra. The bathochromic displacement of **2** (ca.  $2101\text{ cm}^{-1}$ ) corresponds to only about one-third of that of **1**.

X-ray structure analyses have revealed that there are profound differences in the intermolecular distance and the close intermolecular S-S atomic contacts, although their crystal structures are nearly isomorphous.<sup>3</sup> Then the electronic structures of above tetrathiabenzoquinone derivatives have been investigated on the basis of the crystal structure focusing on some intermolecular interactions in the solid state.<sup>4</sup> No significant difference was observed in the calculated results of the dipole-dipole interaction which depend on the intermolecular distance. However, the influence of the observed close S-S atomic contacts of **1** on the electronic state was found to be significant as compared with that of **2** by means of molecular-orbital calculations. These calculated results are in good agreement with the bathochromic shift upon crystallization as well as the polarized reflection spectra measured on single crystals.

References: (1) K. Takagi et al., *Dyes and Pigments*, 1997, **36**, 35., (2) M. Matsuoka et al., *Nonlinear Optics*, 1995, **10**, 109., (3) S. Matsumoto et al., *Acta Cryst.*, 2001, **B57**, 82., (4) S. Matsumoto et al., *Bull. Chem. Soc. Jpn.*, 2001, **74**, 471.

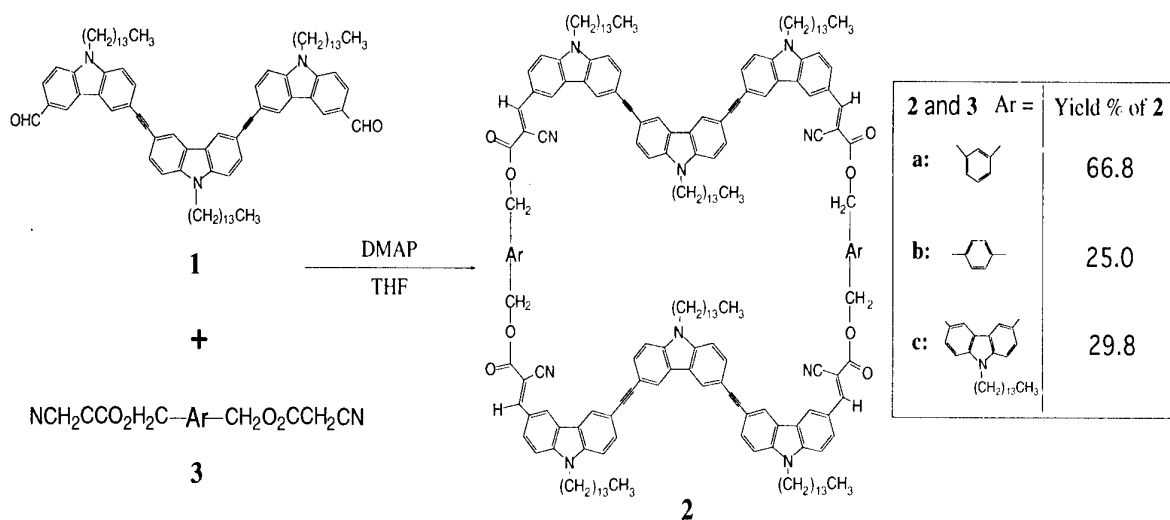
## DEVELOPMENT of NOVEL CARBAZOLE MACROCYCLES

Yoshihiro Imase<sup>a,b</sup>, Atsushi Gunji<sup>a</sup>, Tatsuo Wada<sup>a,b</sup><sup>a</sup>RIKEN(The Institute of Physical & Chemical Research), 2-1 Hirosawa, Wako-shi, Saitama 351-0198, Japan<sup>b</sup>Graduate School of Science and Engineering, Saitama University, 255 Shimo-ookubo, Urawa-shi, Saitama 338-8570, Japan

Various kinds of main chain polymers and oligomers containing multifunctional carbazole units have been synthesized in our laboratory. In particular, conjugated carbazole trimers with relatively low glass transition temperature have showed high efficient photorefractive response. Three carbazole rings share the requirement of photorefraction, that is, the central ring works as a photoconductor and terminal rings as a second-order nonlinear optical chromophore. On the other hand, we have also succeeded in syntheses of cyclic carbazole compounds by one-pot reaction in high yield. In this paper, we present the novel multifunctional carbazole macrocycles containing carbazole trimer units.

One-pot Knoevenagel condensation reaction of the conjugated carbazole trimer containing two formyl groups **1** with bis(cyanoacetoxymethyl)aryl **3** was carried out. The intended macrocyclic compounds **2** were obtained in relatively high yield.

<sup>1</sup>H-NMR spectra showed the absence of formyl group signals, which supported the cyclic structure of the obtained compounds **2**. The chemical structures were confirmed by mass spectrometry and element analysis as shown in scheme. From fluorescent spectra, it is suggested that the rigid structure in the carbazole trimer moieties of the macrocycles and its optical characteristics are maintained in analogy with main chain polymers. The studies on second-order nonlinear optical effect, etc. are now in progress.



Scheme

# Time-resolved photoluminescence spectrum of polythiophene derivative

T. Kobayashi<sup>A</sup>, J. Hamazaki<sup>B</sup>, M. Arakawa<sup>B</sup>, H. Kunugita<sup>B</sup>,  
T. Endo<sup>C</sup>, M. Rikukawa<sup>C</sup>, K. Sanui<sup>C</sup> and K. Ema<sup>B</sup>

<sup>A</sup> Supramolecule Science Laboratory, RIKEN (The Institute of Physical and Chemical Research),  
2-1 Hirosawa, Wako, Saitama 351-0198, Japan

<sup>B</sup> Department of Physics, Sophia University, 7-1 Kioi-cho, Chiyoda-ku, Tokyo 102-8554, Japan  
and CREST, Japan Science and Technology Corporation (JST)

<sup>C</sup> Department of Chemistry, Sophia University, 7-1 Kioi-cho, Chiyoda-ku, Tokyo 102-8554, Japan  
and CREST, Japan Science and Technology Corporation (JST)

**Abstract:** We measured the time-resolved photoluminescence (PL) spectrum of a polythiophene derivative, and found that the model that photoluminescence in polythiophene derivatives originates from the even-parity state as well as the odd-parity state can well explain the feature of their PL properties.

## 1. Introduction

Polythiophene derivatives (PT's) are considered as ones of the important materials for electroluminescence (EL) device because they are stable against both oxygen and moisture, and are relatively easy to prepare their thin film. The photoluminescence (PL) and EL usually originate from the same excited state, nevertheless the photoexcitation dynamics in PT's is not sufficiently investigated. In this study, we report the time-resolved photoluminescence experiments on a Langmuir-Blodgett film of poly(3-[2-((S)-2-methylbutoxy)ethyl]thiophene) (P(S)MBET) to reveal the photoexcitation dynamics and the electronic structure associated with PL and EL, and propose that the PL in PT's consists of the fluorescences from both even-parity and odd-parity states.

## 2. Experimental Results and Discussion

P(S)MBET has an ether coupling (R-O-R') in its sidechains. Because of hydrophilicity of oxygen atoms, LB films of P(S)MBET with high quality can be obtained. Figure 1 shows the absorption and photoluminescence spectra of the LB film of P(S)MBET, where the vibronic structure due to the C=C stretching mode is clearly observed. We measured the time-resolved photoluminescence spectra using a streak camera with a 7-ps time resolution. The PL spectra at various times after photoexcitation at 2.4 eV are shown in Fig. 2. The redshift of the PL spectrum is due to the migration of the self-trapped exciton (STE) to the lower energy segments.<sup>[1]</sup> A striking feature that we wish to highlight here is a spectral change, especially a prominent 1-phonon line at 500 ps. Such vibronic structure cannot be reproduced by usual Frank-Condon factor, which is valid for the dipole-allowed transition. On the other hand, the spectrum at 0 ps can be well reproduced by Frank-Condon factor. Therefore, the PL originates from different states at 0 and 500 ps, and that these states has opposite parity. In fact, from the experimental and theoretical research,<sup>[2]</sup> it is predicted that, in polythiophene, the even-parity  $2A_g$  state lies slightly below the odd-parity  $1B_u$  state. Generally, the system that has the  $2A_g$  state much lower than the  $1B_u$  state does not show PL because all excited states created in the  $1B_u$  state by absorption relax to the  $2A_g$  state nonradiatively, and the transition from the  $2A_g$  state to the ground state is dipole-forbidden. However, in PT's, since these states lie close to each other, the vibronic coupling between them allows the radiative transition from the  $2A_g$  state to the ground state. In this case, the vibronic structure of PL from the  $2A_g$  state differs from that from the  $1B_u$  state, and is described by<sup>[3]</sup>

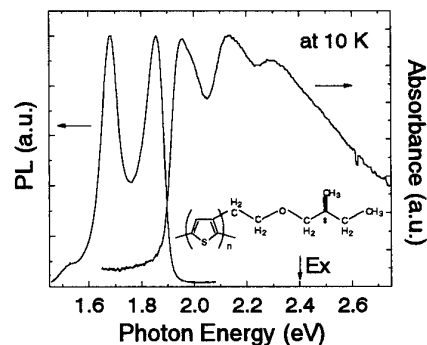


Fig. 1. Absorption and photoluminescence spectra of LB film of P(S)MBET at 10 K. Inset: the chemical structure of P(S)MBET.

$$F_{0m}(S) = \frac{e^{-S}}{m!} S^{m-1} (m-S)^2, \quad (1)$$

where  $S$  represents the strength of the electron-phonon interaction for the  $2A_g$  state, and  $m$  indicates the associate phonon number.  $F_{0m}$  can reproduce such a vibronic structure with a dominant 1-phonon line when  $S$  is extremely small. Therefore, we consider that the PL of P(S)MBET is contributed from not only the  $1B_u$  state but also the  $2A_g$  state. We also calculated the PL spectra by combination of the  $1B_u$  and the  $2A_g$  components using usual Frank-Condon factor and Eq. (1), and obtained the excellent agreement.<sup>[3]</sup> The  $1B_u$  state has a larger dipole moment than the  $2A_g$  state, thus, the PL spectrum loses the  $1B_u$  feature (a prominent 0-phonon line) as time evolves. This explains the spectral change observed in Fig. 2.

Recently, EL spectrum of a light-emitting diode utilizing spin-coated film of P(S)MBET was reported.<sup>[4]</sup> The EL spectrum shows a large 1-phonon line, and differs from PL spectrum of its spin-coated film.<sup>[4]</sup> This fact indicates that EL exclusively originates from the lowest excited state, i.e.  $2A_g$  state, while PL originates from both  $1B_u$  and  $2A_g$  states.

It is known that the PL property of PT's varies from sample to sample considerably. P(S)MBET shows sample dependence of PL spectrum, as well. (see Fig. 3) However, these spectra can be explained by the combination of PL from the  $1B_u$  and the  $2A_g$  states, and the spectral change discussed above was observed in these samples. Therefore, only the ratio between the  $1B_u$  and  $2A_g$  contributions might be sensitive to the structural disorder, oxidation and so on.

### 3. Conclusion

We reveal that the PL spectrum of P(S)MBET consists of two components from the  $1B_u$  and the  $2A_g$  states. The presence of the  $2A_g$  state below the  $1B_u$  state explains the spectral change in the time-resolved PL measurement, the spectral shape of the time-integrated PL, and EL spectrum. Therefore, we suggest that it is important taking the contribution from the  $2A_g$  state into consideration to discuss PL and EL of PT's. Since a prominent 1-phonon line is also observed in other PT derivative,<sup>[5]</sup> we consider that this model is valid for all PT derivatives.

### 4. References

- [1] T. Kobayashi, J. Hamazaki, M. Arakawa, H. Kunugita, K. Ema, K. Ochiai, M. Rikukawa, and K. Sanui, "Self-trapped exciton dynamics in highly ordered and disordered films of polythiophene derivative," *Phys. Rev. B* **62**, 8580 (2000).
- [2] D. Birnbaum and B. E. Kohler, "Location of a  $^1A_g$  state in bithiophene," *J. Chem. Phys.* **96**, 2492 (1992).
- [3] T. Kobayashi, J. Hamazaki, M. Arakawa, H. Kunugita, K. Endo, M. Rikukawa, K. Sanui, and K. Ema, "Photoluminescence from the even-parity state in polythiophene derivative," *J. Phys. Soc. Jpn.* (in press).
- [4] T. Endo, M. Rikukawa, and K. Sanui, "Regiocontrolled synthesis of poly(thiophene) derivatives: EL devices utilizing chiral poly(thiophene) derivatives," *Synth Met.* **119**, 191 (2001).
- [5] K. Sakurai, H. Tachibana, N. Shiga, C. Terakura, M. Matsumoto, and Y. Tokura, "Experimental determination of excitonic structure in polythiophene," *Phys. Rev. B* **56**, 9552 (1997).

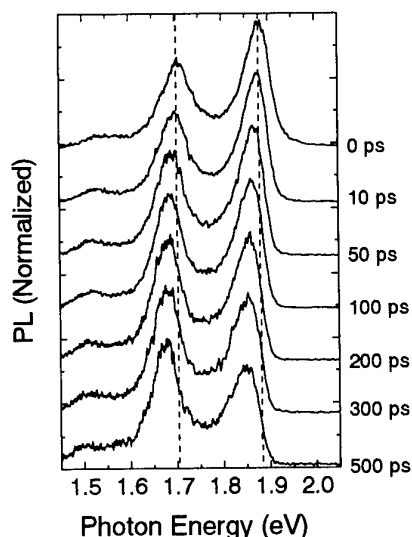


Fig. 2. PL spectra of P(S)MBET excited at 2.4 eV at various times after photoexcitation. The maximum of each spectrum was normalized to one and the time of maximum luminescence was taken as zero time.

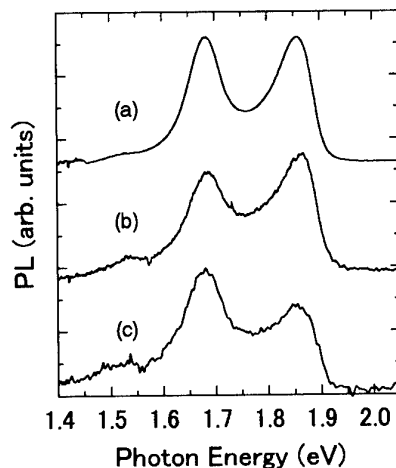


Fig. 3. Sample dependence of the time-integrated PL spectrum of LB films of P(S)MBET.

## **Electro-Optical Characteristics of Self-Organizing Molecular Semiconductor Aligned by Polyimide Film**

*Yasuo Toko, Masahiro Funahashi\*, and Jun-ichi Hanna\**

*R&D Laboratory, Stanley Electric Co., Ltd., 1-3-1 Eda-nishi, Aoba-ku,  
Yokohama, 225-0014, Japan*

*\*Imaging Science and Engineering Laboratory, Tokyo Institute of  
Technology, 4259 Nagatsuda, Midori-ku, Yokohama, 226-8053, Japan*

Electro-optical characteristics were studied on the organic semiconductor materials exhibiting molecular alignment based on molecular self-organization in their liquid crystal phases. It was confirmed that these organic semiconductor materials exhibit very fast electron transport in the smectic mesophases as well as hole transport, both of which were independent on electric field and temperature. Due to the direct transition from the isotropic to the smectic phases of the materials, a uniform orientation (mono-domain) had been difficult to obtain. However, we found that it is possible to realize the uniform orientation of the organic semiconductor materials by choosing polyimide film (thickness:  $< 10$  nm) and rubbing condition. In this paper, organic semiconductor materials which were uniformly orientated were examined on the anisotropy of electro-optical characteristics depending on the orientation direction. In the uniformly orientated cell using these organic semiconductor materials, the electrical characteristic drastically changes depending on the molecular orientation direction. In addition, the uniform orientation cell shows the linearly polarized light emission which originates from the molecular orientation when a DC bias is applied.

## Preparation of DNA optical fibers

Hidetomo Ashitaka, Kouki Ishihara and Naoya Ogata

Faculty of Photonics Sci. and Technol., Chitose Inst. of Sci. and Technol.  
758-65 Bibi, Chitose-shi, Hokkaido, 066-8655

Tel: 0123-27-6084 Fax: 0123-27-6084 e-mail: [h-ashita@photon.chitose.ac.jp](mailto:h-ashita@photon.chitose.ac.jp)

DNA/optical fibers/DNA-lipid complex/wet-spinning/Salmon testes/ Cetyltrimethylammonium chloride

The oriented DNA fibers, impregnated with organic dyes, are expected to be a promising optical material. The DNA fibers are prepared by wet-spinning by extruding ethanol solution of DNA-lipid complex derived from pure DNA sodium salts with high molecular weight and cetyltrimethylammonium chloride into water and stretching. The organic dye can be intercalated into or bonded to DNA double strands before or after the spinning. The DNA fibers were transparent and water insoluble, but weak in mechanical strength and humidity. An appropriate cladding material can improve a part of the fiber properties.

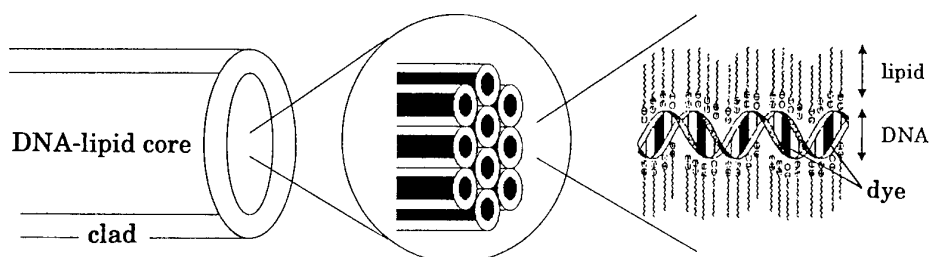


Figure 1 Schematic representation of the structure of a DNA-lipid optical fiber intercalated with organic dye



## Analysis of Mode Propagation in Plastic Optical Fibers

*Yoshiaki Ito, Takayuki Fukagawa, Yuichiro Kumakura, Masashi Eguchi,  
Hiroyuki Sasabe and Suguru Horinouchi*

758-65 Bibi, Chitose-shi, Hokkaido 066-8655 JAPAN

(Tel)+81-90-3545-4616 (Fax)+81-123-27-6119

(Email)SuguruHori@aol.com

A new method for analyzing multi-mode fibers is proposed in this paper. The beam quality factor (the  $M^2$  factor) has been used for defining the transverse laser beam quality. We applied the  $M^2$  factor to analyze mode propagation properties in Plastic Optical Fibers (POF). Brief review of the  $M^2$  factor and the results of beam quality measurements on a He-Ne laser propagating in a free-space and in POF are shown.

Gaussian beam theory<sup>1</sup> gives equations governing the variation with propagation distance of the beam radius and the wavefront radius of curvature for the fundamental  $TEM_{00}$  mode. The gaussian spot size  $\omega(z)$  which provides the transverse scale factor characteristic of any family of Hermite-gaussian or Laguerre-gaussian free-space modes propagates with distance in free space is given by

$$w^2(z) = w_0^2 + \left(\frac{\lambda}{\pi w_0}\right)^2 (z - z_0)^2 \equiv w_0^2 \left\{1 + \left(\frac{z - z_0}{z_R}\right)^2\right\} \quad (1)$$

where  $\omega_0$  is the waist spot size,  $\lambda$  is the wavelength of laser,  $z$  is arbitrary position and  $z_0$  is the waist location.  $z_R \equiv \pi \omega_0^2 / \lambda$  indicates the Rayleigh range of the Hermite-gaussian modes. The free space propagation of a gaussian beam is fully characterized by its waist spot size  $\omega_0$  and waist location  $z_0$  with far-field angular spread for  $\omega^2(z)$  being given by  $\lambda / \pi \omega_0$ .

In the case of higher order modes or mixtures of modes, equation (1) doesn't adequately describe how the beams propagate. The beam quality factor (the  $M^2$  factor)<sup>1-6</sup> clearly characterizes the propagation properties of multi-mode laser beams. It is a very general and useful formalism for defining the transverse beam quality, as well as other propagation parameters<sup>7-11</sup> of arbitrary real laser beams. The formalism for describing arbitrary and highly nongaussian real laser beams is given by

$$W^2(z) = W_0^2 + M^4 \left(\frac{\lambda}{\pi W_0}\right)^2 (z - z_0)^2 \equiv W_0^2 \left\{1 + \left(\frac{z - z_0}{z_R}\right)^2\right\} \quad (2).$$

The propagation of the real beam depends on the beam quality factor (the  $M^2$  factor) in addition to being dependent on the inverse waist size. The physical interpretation of the  $M^2$  factor is a measure of the near-field times far-field space-beamwidth<sup>1</sup> product of the arbitrary real beam normalized to the space-beam width product for an ideal  $TEM_{00}$  gaussian. The beam quality factor always has  $M^2 \geq 1$  and the far-field beam spread is given by  $M^2(\lambda / \pi \omega_0)$ . The  $M^2$  value serves as a rigorous definition of the times diffraction limited value for an arbitrary real beam compared to a  $TEM_{00}$  gaussian beam.

The  $M^2$  factors of light propagating in a free space or in POF were respectively measured and evaluated by the knife-edge measurement technique<sup>2,4</sup>. Fig. 1 shows the experimental setup of the knife-edge measuring for determining the factor. Light source is coupled into fibers by lens. The knife-edge is mounted on a stepping motor stage. The stage is controlled by a computer and can move towards  $x$ ,  $y$  and  $z$  direction. At any point  $z_i$ , the stage is moved through

transverse direction of the sample (x and y direction) to determine the square of beam spot size. The factor of He-Ne laser was measured by the system as shown in Fig. 1. The obtained values of  $M^2$  was 1.07, the beam waist  $\omega_0=0.04$  (mm) and the waist location  $z_0=30.3$  (mm). This results shows the validity of this experimental configuration of Fig.1.

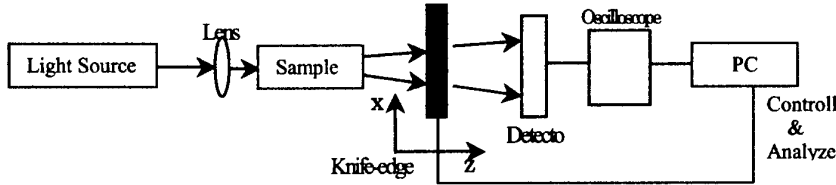


Fig. 1 The experimental setup of the knife-edge measurement for determining the beam quality factor.

The laser light was coupled into a commercially available step-index low NA POF and the beam quality measurement through POF was carried out. The measured value of  $M^2$  is shown in Table 1. The larger number means the higher order modes propagates in the fiber. The  $M^2$  factor clearly shows the transverse beam quality with higher order modes or the complex mixtures of modes. This factor is useful for investigating propagation properties of multi-mode fibers.

Table1 Measured value of  $M^2$

	Measured sample	Measured value of $M^2$
1	POF (2m) without mode scrambler	599
2	POF (2m) with mode scrambler	1221
3	POF (50m) without mode scrambler	1259
4	POF (50m) with mode scrambler	1263

#### References

1. A. E. Siegman, SPIE Vol.1868, pp.2 (1994)
2. A. E. Siegman, SPIE Vol.1224, pp.2 (1990)
3. A. E. Siegman, IEEE Jour. Quant. Electron. Vol.27, pp.1098 (1991)
4. D. Wright, Optical and Quantum Electron. 24, pp.993 (1992)
5. R. D. Jones, Laser Focus, pp.123 (1991 January)
6. L. Marshall, Laser Focus, pp.26 (1971 April)
7. H. Kogelnik and T. Li, Appl. Opt. 5, pp.1550 (1966)
8. J. T. Luxon, D. E. Parker and J. Karkheck, Appl. Opt. 23, pp.2088 (1984)
9. W. H. Carter, Appl. Opt. 19, pp.1027 (1980)
10. W. B. Bridges, Appl. Opt. 14, pp.2345 (1975)

#### Acknowledgement

This research is supported by the fund of Telecommunications Advancement Organization of Japan (TAO). The authors are grateful to TAO.

## Development of Optical Module for Plastic Optical Fiber Link System

*Takayuki Fukagawa, Yoshiaki Ito, Masashi Eguchi,  
Hiroyuki Sasabe and Suguru Horinouchi*

758-65 Bibi, Chitose-shi, Hokkaido 066-8655 JAPAN

(Tel)+81-90-3545-4616 (Fax)+81-123-27-6119  
(Email)SuguruHori@aol.com

The characteristics of Plastic Optical Fiber (POF) has been drastically developed for high speed data communication for 10 years by Prof. Koike with Keio University. Thanks to the professor's effort, two types of graded index type POF, poly methyl methacrylate (PMMA) based POF and perfluorinated (PF) based POF are commercially available. The POF is expected to play an important role in the field of high speed digital data transmission system. POF is applicable various types of networking system because of its nature of low cost and easy handling. Two types of standardizations; ATM and IEEE 1394 using POF have been established. PMMA based POF is expected as the media of home networking or automobile networking. The transmission window of PMMA based POF is around the wavelength of 650nm and the theoretical attenuation limit of the material is about 100 dB/km. Increasing demand to transmit high volume data, maximum data rate of IEEE 1394 was upgraded to 400Mbps from 100Mbps, where 4.5m metallic cable has been used. Recently the committee organized by the electronics industries and Keio University mentioned the importance of the long distance (up to 100m) with higher speed data transmission.

In this study we have developed high speed (the data rate more than 400Mbps) optical transceivers for PMMA based POF data link system and investigated the property of physical layer. The implementation conditions such as fiber length and power margin were examined to optimize the system configuration of the POF-LAN system.

### *References*

- 1 Y. Koike, Polymer 32, 1737 (1991).
- 2 Y. Koike, and E. Nihei, ACS Polymer Preprints 32, 111 (1991).
- 3 T. Ishigure, E. Nihei and Y. Koike, Appl. Opt. Vol.35, 2048 (1996)
- 4 E. Nihei, T. Ishigure, N. Tanio and Y. Koike, IEICE Electron., Vol.E80-C, 117 (1997)
- 5 Y. Koike, T. Ishigure, and E. Nihei, J. Lightwave Tech., Vol.13, 1475 (1995)
- 6 A. Tagaya, Y. Koike, E. Nihei, K. Fujii, and K. Sasaki, IEEE J Quantum. Electron. 31, 2215 (1995).
- 7 K. Fujii, A. Tagaya and Y. Koike, Journal of Nonlinear Optical Physics and Materials 5, 73 (1996).
- 8 K. Fujii, A. Tagaya and Y. Koike, Electronics and Communications in Japan Part 2 78, 36 (1995).

### *Acknowledgement*

This research is supported by the fund of Dohgitomakomai (Douousangyougijutusinkoukikou). The authors are grateful to Dohgitomakomai. The url of Dohgitomakomai is <http://dohgi.tomakomai.or.jp>.

## New Model for CW Amplification in Plastic Optical

*Mitsuhiro Koda, Masatoshi Gyoten, Keitaro Koguchi, Masashi Eguchi,  
Kazuhito Fujii, Hiroyuki Sasabe and Suguru Horinouchi*

758-65 Bibi, Chitose-shi, Hokkaido 066-8655 JAPAN

(Tel)+81-90-3545-4616 (Fax)+81-123-27-6119

(Email)SuguruHori@aol.com

We propose the theoretical analysis of a rare-earth chelate doped plastic optical fiber amplifier (POFA). Our new model for CW amplification utilize the side excitation of pump light source. From the calculation for a Nd-chelate doped POFA, the maximum signal gain of 21 dB can be achieved by only 20 W of pumping power and the POFA length of 20 cm. Moreover, there is obviously an optimal radius of doped area which is about the half of the core radius.

The proposed POFA system and its cross sectional view is schematically displayed in Figure 1 (a) and (b), respectively. The POFA is pumped from the direction normal to the propagation

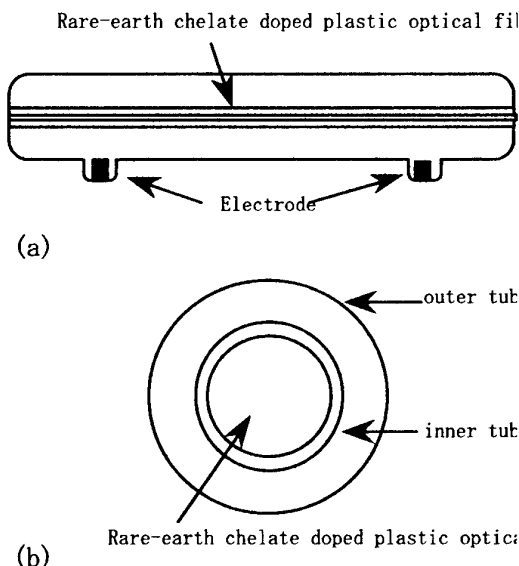


Fig. 1 (a) Schematic structure of the proposed POFA. The excitation tube has double tube structure. The Nd chelate doped plastic optical fiber is in the inner tube and excited around from the side. (b) Cross sectional view of the POFA. The core diameter is 0.5 mm and the diameter of the Nd chelate doped area is smaller than that diameter.

direction of the signal light by the cw-excitation tube, e.g. like a considerably monochromatic fluorescence lamp, with the length of  $L$ . The cw-excitation tube has a double tube structure and the rare-earth chelate doped plastic optical fiber is inside the inner tube. As the fluorescence materials, we choose a Nd-chelate because the energy level of  $\text{Nd}^{3+}$  is known a typical 4-level system, and the absorption of the signal light is negligible. Additionally, we assume that  $\text{C}_{14}\text{H}_8\text{O}_3\text{Br}^-$  as a ligand<sup>7</sup> makes an organic complex with  $\text{Nd}^{3+}$ . The wavelength of the pump light is selected within an absorption range of the ligand. As for a rare-earth chelate, the maximum absorption cross section of the ligand is several orders larger than the maximum emission cross section of the rare-earth ion, and the term on the signal light is negligible compared with the term on the pump light in rate equations for each level. It also shows to neglect the depletion of the upper laser level due to the signal light. Moreover, decay time from other

excited levels to the upper laser level is very short compared with that from the upper laser level to the ground state, and there is no Nd-chelate concentration at other energy states. Furthermore, we assume that the influence of amplified spontaneous emission on each level is negligible due to using a sufficiently low intensity input of the signal light. In the case, a population density of the ground state  $n_1(r)$  and the upper laser level  $n_2(r)$  of the chelate is given by the following equations as a function of the radial direction of  $r$ .

$$n_1(r) = N/\tau / (\sigma_p^a I_p(r)/h\nu + 1/\tau), \quad \dots\dots\dots(1)$$

$$n_2(r) = N\sigma_p^a I_p(r)/h\nu / (\sigma_p^a I_p(r)/h\nu + 1/\tau), \quad \dots\dots\dots(2)$$

where  $N$ ,  $I_p(r)$ ,  $\sigma_p^a$ ,  $\tau$ ,  $h$ , and  $\nu$  denotes doping density of the rare-earth chelate, the pump power density, absorption cross section for the pump light, lifetime of the upper laser level, Planck's constant, and frequency of the pump light, respectively. Here,  $r_d$  denotes a radius of dope area, and a region  $0 \leq r \leq r_d$  is enough to calculate the signal gain.  $I_p(r)$  for this region is defined, according to the assumption for the pump light direction, by

$$I_p(r) = w/(2\pi L r n_p) \exp(-n_1(r) \sigma_p^a (r_d - r)), \quad \dots\dots\dots(3)$$

where,  $n_p$  and  $w$  is refractive index of PMMA for the pump light and total power of an excitation tube, respectively. But, considering that actual situation,  $I_p(r)$  saturates inside from a radius  $r_s$  due to aberrations. If  $r_s < r_d$ , Equation 3 is rewritten as follows:

$$\begin{aligned} I_p(r) &= w/(2\pi L r_s n_p) \exp(-n_1(r) \sigma_p^a (r_d - r)) \quad (0 \leq r \leq r_s) \\ &= w/(2\pi L r n_p) \exp(-n_1(r) \sigma_p^a (r_d - r)) \quad (r_s \leq r \leq r_d). \quad \dots\dots\dots(4) \end{aligned}$$

Because  $n_1(r)$  and  $n_2(r)$  are constant along the direction of the signal light propagation, the signal gain  $G(L)$  is given by

$$G(L) = \exp((2\pi c \int_0^{r_d} I_s(r) n_2(r) \sigma_s^e r dr - \alpha) L) \quad \dots\dots\dots(5)$$

where  $c$ , and  $\sigma_s^e$  is a constant for normalizing the power density distribution of an initial signal light, and emission cross section for the signal light, respectively. Considering  $r$  dependence of  $n_2(r)$  according to Equations (1)-(3), the integration in Equation (5) is calculated. Here,  $\alpha$  is absorption coefficient by the main material of the plastic optical fiber (POF), that is, PMMA. Also,  $I_s(r)$  shows a power density distribution of the initial signal light which originally comes from a propagation mode in the POFA but, for simplification, it is defined as the Gaussian function instead of that<sup>7</sup>, in which 95% of the total power is in the core region.

In the calculation,  $r_s$  is assumed to be 0.1 mm. Emission wavelength from  $\text{Nd}^{3+}$  is 1.064  $\mu\text{m}$ , where  $\alpha$  is about  $9.2 \times 10^{-3} \text{ cm}^{-1}$ . The emission cross section  $\sigma_s^e$  at 1.064  $\mu\text{m}$  and life time  $\tau$  is about  $5 \times 10^{-20} \text{ cm}^2$  and 3 msec, respectively. As for  $\sigma_p^a$ , we use the value from the absorption cross section spectrum of  $\text{C}_{14}\text{H}_8\text{O}_3\text{Br}$  reported in Reference 7. There are two peaks at 280 nm and 330 nm in the spectrum. The maximum value of  $\sigma_p^a$  is  $0.27 \times 10^{-16} \text{ cm}^2$ , which is 3 orders higher than  $\sigma_s^e$  of  $\text{Nd}^{3+}$ .

### References

- 1 Y. Koike, Polymer 32, 1737 (1991).
- 2 Y. Koike, and E. Nihei, ACS Polymer Preprints 32, 111 (1991).
- 3 A. Tagaya, Y. Koike, E. Nihei, K. Fujii, and K. Sasaki, IEEE J Quantum. Electron. 31, 2215 (1995).
- 4 K. Fujii, A. Tagaya and Y. Koike, Journal of Nonlinear Optical Physics and Materials 5, 73 (1996).
- 5 K. Fujii, A. Tagaya and Y. Koike, Electronics and Communications in Japan Part 2 78, 36 (1995).

### Acknowledgement

This research is supported by the fund of Northern Advancement Center for Science and Technology (NOASTEC). The authors are grateful to NOASTEC. The url of NOASTEC is <http://www.noastec.jp>.

## $\pi$ -Conjugated Nanohole Columnar of Substituted Phenylacetylenes Prepared with a Rh Complex Catalyst

Yasuteru Mawatari, Takeyuki Sone, Yoshikazu Sadahiro, and Masayoshi Tabata

Department of Molecular Chemistry, Graduate School of Engineering,

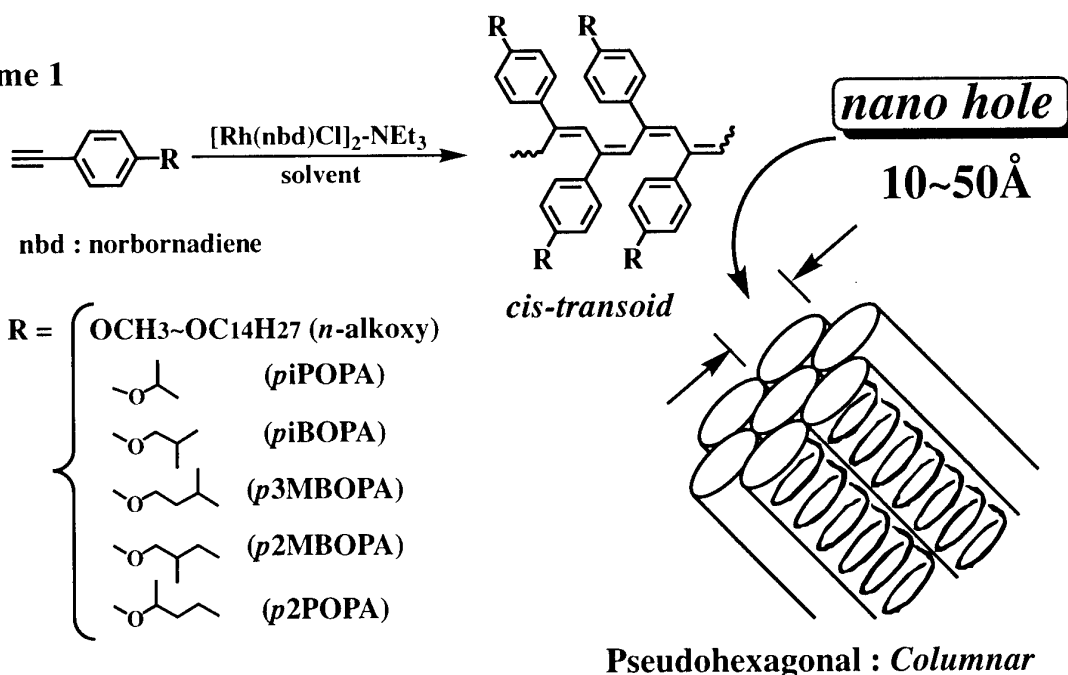
Hokkaido University, Sapporo 060-8628, Japan

Tel. & FAX : +81-11-706-6603 e-mail yasuyasu@poly.eng.hokudai.ac.jp

We have reported<sup>1)</sup> the highly stereoregular polymerization of *para* alkoxy phenylacetylenes is induced by a Rh complex catalyst:  $[\text{Rh}(\text{nbd})\text{Cl}]_2$  when EtOH or triethylamine (TEA) was used as the polymerization solvent to selectively produce *cis-transoid* polymers in high yield. These polymers were found to produce pseudo-hexagonal structure called columnar and undergo isomerization from *cis* form to *trans* form by compression. The columnar is considered as self-assembly in which helical main chain polymers were packed tightly and nanometer holes are created.

In this study we report a new syntheses of poly (*p*-alkoxyphenylacetylene)s, PpROPA having a normal or branched chain which is initiated by the Rh complex catalyst together with influences of the alkoxy chains with respect to not only the diameter and content of columnar but also the color of polymer.

**Scheme 1**



Polymerization reaction of these monomers was rapidly initiated when monomer solution and catalyst solution were mixed at room temp.. The yields of polymers were around 60~90%. These polymers were soluble in  $\text{CHCl}_3$  and THF so that the molecular weights :  $M_n$  were estimated as *ca.*  $5.0 \times 10^4 \sim 4.0 \times 10^5$  using GPC method, and characterized in detail using NMR, Laser Raman, ESR, X-ray diffraction (XRD) and diffuse reflective UV-VIS (DRUV) methods.

Fig. 1 shows the relationship between the carbon number and columnar diameters which were calculated from (100) reflection of the XRD patterns. From the XRD patterns of these polymers, each peaks were found to be shifted to lower angle region when the carbon number of *n*-alkoxy chain was increased. This means that the columnar diameter can be controlled by the carbon number in the *n*-alkoxy chain (see Fig. 1).

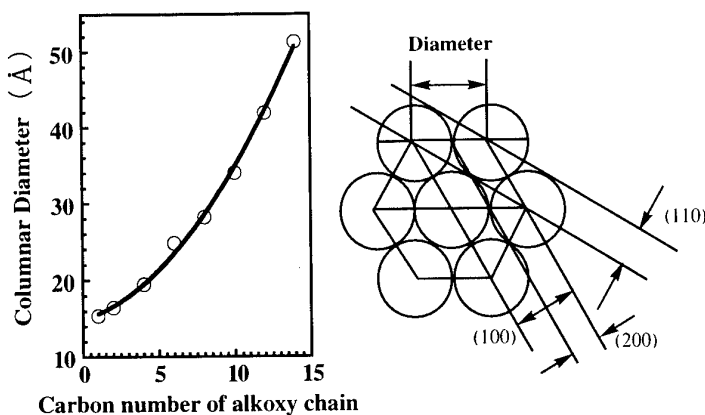


Fig. 1. Diameter of Columnar dependence on the carbon number of *n*-alkoxy chain in PpROPA.

Fig. 2 shows the X-ray diffraction patterns of Poly(*p*3MBOPA) prepared in TEA(a) or in EtOH(b). The (100) reflection peak intensity of (a) is extremely larger than that of (b). This shows that the content of columnar depends on the polymerization solvent used. Previously<sup>2)</sup>, we showed that the columnar contents can be increased by solvent treatment using  $\text{CHCl}_3$  or toluene. It is concluded, therefore, that the content of the columnar can be controlled by the polymerization solvent as well as the solvent treatment of the pristine polymers, although the effect on the columnarization is larger in the latter case.

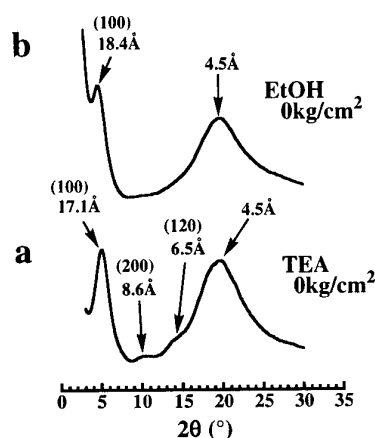


Fig. 2. X-ray diffraction patterns of the Poly(*p*3MBOPA) observed at room temperature using  $\text{CuK}_\alpha$  radiation.

Fig. 3 shows the DRUV spectra of Poly(*p*3MBOPA) prepared in EtOH(a) and in TEA(b), in which a large red-shift of the absorption maximum is induced by the increase of the columnar content together with extension of absorption up to longer wavelength region, irrespective of cis-transoid structure<sup>3)</sup>. Thus, the color of conjugated polymers is determined by the content of the columnar which is also controlled by the polymerization solvent as well as the solvent treatment after the polymerization.

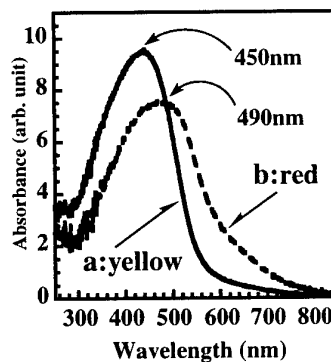


Fig. 3. Diffuse reflective spectra of Poly(*p*3MBOPA) observed at room temperature. (a) in EtOH and (b) in TEA.

- 1) M. Tabata, Y. Sadahiro, Y. Nozaki, Y. Inaba, and K. Yokota. *Macromolecules*, **1996**, 29, 6673-6675.
- 2) M. Tabata, T. Some, Y. Sadahiro. *Macromol. Chem. Phys.* **1999**, 200, 265-282.
- 3) Y. Mawatari, M. Tabata, T. Sone, K. Ito, and Y. Sadahiro. *Macromolecules*, **2001**, 34, 3776-3782.

## Improvement of Reprecipitation Method for Fabrication of Organic Microcrystals

○Koichi BABA, Eiji SARASHINA, Hitoshi KASAI, Shuji OKADA, Hidetoshi OIKAWA, Hachiro NAKANISHI

Institute of Multidisciplinary Research for Advanced Materials, Tohoku University, CREST, Katahira 2 chome, Aoba-ku, Sendai 980-8577, Japan

### Introduction

Inorganic nanocrystals have been investigated extensively from the viewpoints of both fundamental science and some applications. In particular, it is worth noting that several reports have described the enhancement of nonlinear optics (NLO) properties, due to the quantum confinement effect, in nanocrystals of semiconductor below 10 nm in size. Fabrication techniques for these inorganic nanocrystals are almost established thus far. On the other hand, we have proposed the "reprecipitation method"<sup>1)</sup> for preparing many kinds of  $\pi$ -conjugated organic nanocrystals as a dispersion, and discussed their optical properties, depending on crystal size<sup>2)</sup>. In the present study, we have applied the microwave irradiation process to the conventional reprecipitation method, called "the microwave irradiation method"<sup>3)</sup>, for the purpose of fabricating further well-defined organic nanocrystals. In addition, we attempted to collect organic nanocrystals dispersed in a liquid by applying electric fields, since nanocrystals have highly minus  $\zeta$ -potential. The electrophoreses effect would be useful technique to adsorption of nanocrystals on ITO electrode.

### Experimental

First, 1,6-di(*N*-carbazolyl)-2,4-hexadiyne) (DCHD) nanocrystals were prepared by the conventional reprecipitation method: 200  $\mu$ l of 5 mM DCHD acetone solution was injected into vigorously stirred water (20 ml) with using microsyringe. After 20 min of retention time for nanocrystallization, UV ( $\lambda = 254$  nm) light was irradiated for 20 minutes to convert solid-state polymerizable DCHD nanocrystals into poly (DCHD) nanocrystals. In the case of microwave irradiation method, just after reprecipitation, the DCHD dispersion liquid was immediately placed in a Teflon vessel, and then was irradiated with microwave (2.45 GHz, 500 W) for a given intervals. Afterwards, UV light was irradiated in a similar manner.

On the other hand, Tris (8-quinolinolate) aluminum (Alq) fibrous nanocrystals prepared by the reprecipitation method were employed to perform the collection experiments of organic nanocrystals dispersed in a liquid. The 150  $\mu$ l of Alq dichloroethane solution (8.7 mM) was injected into vigorously stirred cyclohexane (10 ml). To apply DC electric field, the ITO electrode pair was insert parallelly with spacing 2 mm into the quartz cell, which was filled out with Alq fibrous nanocrystals dispersion. The applied electric field was of the order of  $10^3$  V/cm. The adsorption of Alq fibrous nanocrystals on ITO electrode was detected by UV-VIS absorption spectrum.

### Result and discussion

Figure 1. shows the UV-VIS absorption spectra changes of poly (DCHD) nanocrystals with different irradiation time of microwave. The excitonic absorption peaks increased with microwave irradiation time. The absorbance was roughly the maximum at 35 s of microwave irradiation time. As shown in Fig. 2, the shapes of resulting poly (DCHD) nanocrystals were fibrous and the crystal size along the long-axis was about 500 nm. If the similar poly (DCHD) fibrous nanocrystals would be prepared by the conventional reprecipitation method, it takes about 60 minutes at 60 °C. On the contrary, microwave irradiation method could provide well-defined monodispersed poly (DCHD) fibrous nanocrystals reproducibly in a short time, compared with the conventional reprecipitation method.

Figure 3. indicates the absorbance changes at  $\lambda_{\max} = 400$  nm of Alq fibrous nanocrystals dispersed in cyclohexane with applying electric field. As Alq fibrous nanocrystals were adsorpted electrostatically on ITO electrode, the absorbance decreased evidently. The total amount of adsorption and its kinetics were remarkably influenced by the applied electric field. Thus, total amount and the rate became high with increasing the electric field. Figure 4. exhibits the reversible changes of UV-VIS absorption spectra for Alq nanocrystals dispersed in cyclohexane through the following processes: the electric field (5000 V/cm) was applied for 3 minutes, and then the



ultrasonic wave (120 W) was subsequently irradiated for 10 second. These results imply the possibility of collection and re-dispersion of organic nanocrystals, and are noted as a basic technology for mass-production of organic nanocrystals.

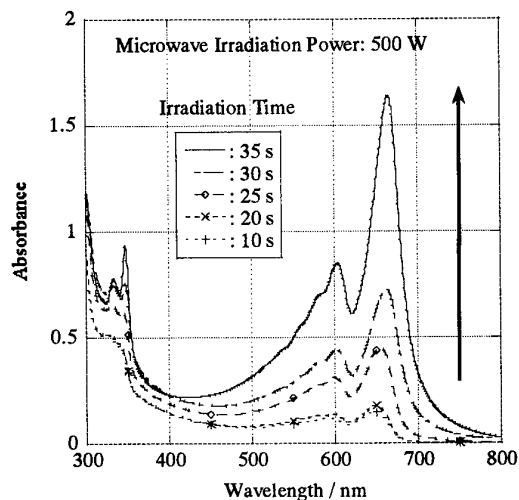


Fig. 1. UV-VIS absorption spectra changes of Poly (DCHD) nanocrystals prepared by the microwave irradiation method.



Fig. 2. SEM photograph of Poly (DCHD) fibrous nanocrystals prepared by the microwave irradiation method.

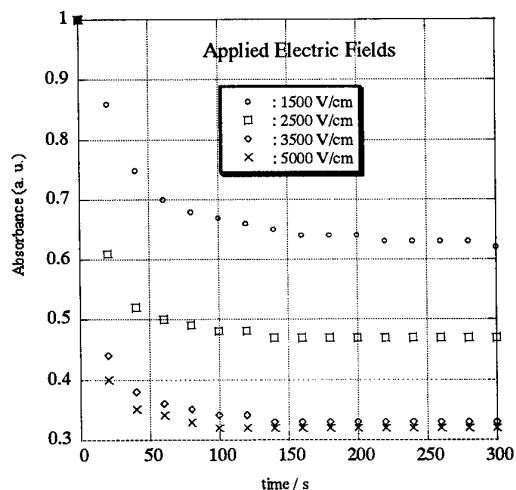


Fig. 3. Absorbance changes of Alq fibrous nanocrystals with the applied electric fields. The absorbance was detected at  $\lambda_{\max} = 400$  nm.

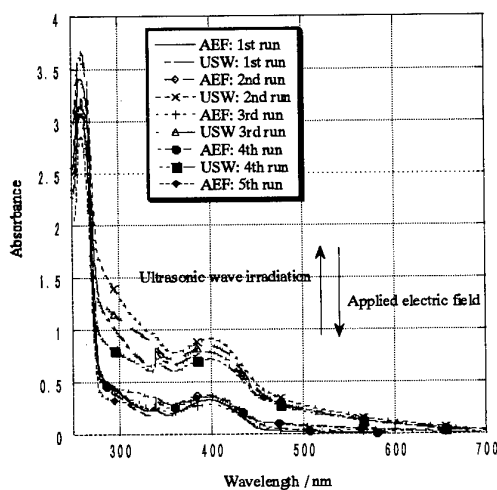


Fig. 4. UV-VIS absorption spectra changes of Alq fibrous nanocrystals with the applied electric fields (AEF), afterward with the subsequent ultrasonic wave irradiation (USW).

#### Reference

- 1) H. Kasai *et al.*, *Jpn. J. Appl. Phys.*, 31, L1132 (1992).
- 2) *Handbook Nanostructured Materials & Nanotechnology*, ed. H. S. Nalwa (Academic Press, U.S.A., 2000) 1 st ed., Vol. 5, Chap. 8, p. 433.
- 3) K. Baba *et al.*, *Jpn. J. Appl. Phys.*, 39, L1256 (2000).

## Fabrications of Polyimide Nanoparticles

Masao Suzuki, Hitoshi Kasai, Shuji Okada, Hidetoshi Oikawa,  
Takayasu Nihira\*, Hiroyoshi Fukuro\* and Hachiro Nakanishi

Institute of Multidisciplinary Research for Advanced Materials, Tohoku University, CREST  
2-1-1 Katahira, Aoba-ku, Sendai 980-8577, Japan

Tel: 022-217-5645 Fax: 022-217-5645 e-mail: soccer@icrs.tohoku.ac.jp

\*Central Research Institute, Nissan Chemical Ind., LTD., CREST  
722-1, Tsuboi-cho, Funabashi 74-8507, Japan

Aromatic polyimide (PI) is one of the processing high performance materials, *i.e.*, high thermal stability, mechanical properties, and low dielectric constant, and is widely used in the fields of electronics. In general, most of the studies on PI have been focused on film, adhesives and varnish, and few data on particles were published so far [1, 2]. Recently, organic nanoparticles, ranging from several tens to hundreds of nanometers in size, and reported to be exhibited specific optical and electronic properties, which appeared neither in a molecule nor in bulk state [3, 4]. Such the improvement of its properties will be expected similarly in case of PI nanoparticle. In the present work, we have prepared poly(amic acid) (PAA) precursor nanoparticles successfully by the reprecipitation method [5] for fabricating aromatic PI nanoparticles through thermal imidization, and the relationship between reprecipitation conditions, such as concentration of the injected solution, the temperature of poor solvent, molecular weight of PAA and poor solvent species, and nanoparticle morphology will be discussed.

PAA used as a precursor polymer was produced by polyaddition of 4,4'-oxydianiline (ODA) and 4,4'-(hexafluoroisopropylidene)diphthalic anhydride (6FDA) in *N*-methyl-2-pyrrolidinone (NMP), and the average molecular weight and polydispersity of PAA are summarized in Table 1. According to the reprecipitation procedure, a given amount of the diluted NMP solution of PAA was rapidly injected into a vigorously stirred poor solvent [5]. In our case, three kind of poor solvent were used : carbon disulfide (CS<sub>2</sub>), cyclohexane and their mixture (miscibility for NMP : cyclohexane < mixture < CS<sub>2</sub>). To obtain PI nanoparticle through thermal imidization procedure, PAA nanoparticle dispersion was spin-coated on slide glass and then heated successively at 100, 200 and 300°C for 1 h at each step. The size and morphology of nanoparticles were evaluated by means of DLS and SEM.

Figure 1a indicates the SEM photograph of typical PAA2 nanoparticles prepared by reprecipitating into CS<sub>2</sub>. PAA nanoparticles seem to be all spherical and monodispersed, and ca. 40nm in size. The resulting PI nanoparticles are also displayed in Figure 1b. This result implies that nanoparticle morphology was not changed before and after thermal treatment. Figure 2 shows the dependence of the size of PAA2 nanoparticles on volume ratio ( $\phi$ ) of CS<sub>2</sub> in the CS<sub>2</sub>/cyclohexane mixture. According to these results, the nanoparticle size was found to increase with decreasing  $\phi$ , and the nanoparticle size distribution became remarkably wide around  $\phi < 0.1$ . However the spherical morphology was not influenced in any crystal size. In the case of only cyclohexane as a poor solvent, the size distribution was around  $\pm 100$ nm, and some PAA nanoparticles were more than 500nm in size. The relationship between concentration of the injected solutions and size of PAA1 nanoparticles is shown in Figure 3. It has become apparent that the nanoparticle size increased with concentration, and this tendency became remarkable with increasing molecular weight. Figure 4 shows the dependence of size of PAA4 nanoparticles on temperature of the poor solvent. It was proved that the nanoparticle size decreased with raising the poor solvent temperature, regardless of molecular weight.

Table 1. Average molecular weight of PAA

Sample Code	$M_w$	$M_w/M_n$
PAA1	$4.5 \times 10^4$	2.86
PAA2	$6.9 \times 10^4$	1.84
PAA3	$9.3 \times 10^4$	1.70
PAA4	$1.2 \times 10^5$	1.66

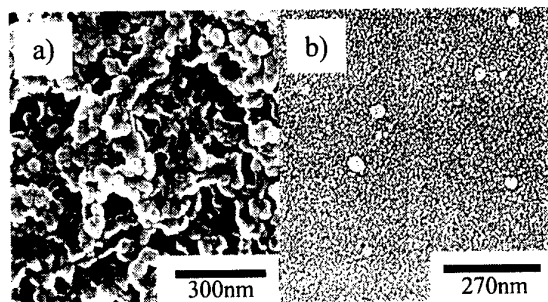


Fig. 1. SEM photograph of a) PAA2 nanoparticles prepared by the reprecipitation method, poor solvent :  $\text{CS}_2$ , conc. : 0.49wt%,  $T_{\text{poor}}$  : 22°C, and b) the corresponding PI nanoparticles.

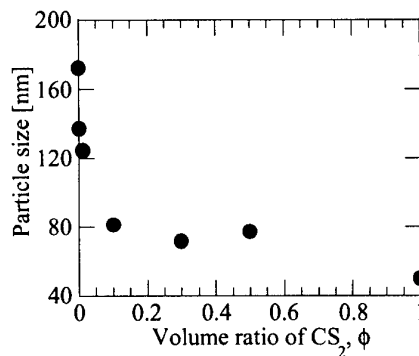


Fig. 2. Dependence of the size of PAA2 nanoparticles on volume ratio of  $\text{CS}_2$  ( $\phi$ ) in the mixed poor solvent of  $\text{CS}_2$  and cyclohexane. conc. : 0.49wt%,  $T_{\text{poor}}$  : 22°C.

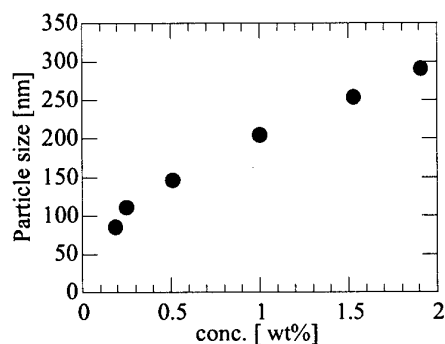


Fig. 3. Relationship between concentration of the injected PAA1-NMP solutions and particle size, poor solvent : cyclohexane/ $\text{CS}_2$  ( $\phi=0.002$ ),  $T_{\text{poor}}$  : 22°C.

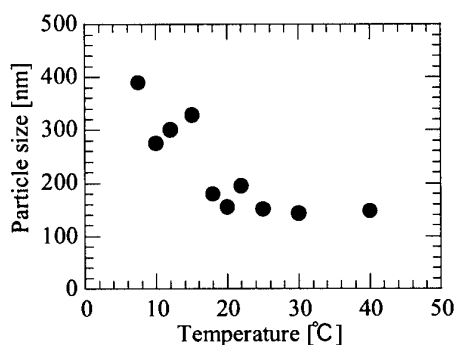


Fig. 4. Dependence of the size of PAA4 nanoparticles on temperature of the poor solvent. poor solvent : cyclohexane/ $\text{CS}_2$  ( $\phi=0.002$ ), conc.: 0.5wt%.

## References

- [1] Y. Nagata, Y. Ohnishi, T. Kajiyama, *Polym. J.*, **28**, 980 (1996)
- [2] K. Asao, H. Ohnishi, H. Morita, *Kobunshi Ronbunshu*, **57**, 271 (2000)
- [3] H. Katagi, H. Kasai, S. Okada, H. Oikawa, H. Matsuda, H. Nakanishi, *J. Macromol. Sci.-Pure Appl. Chem.*, **A34**, 2013 (1997).
- [4] H. B. Fu and J. N. Yao, *J. Am. Chem. Soc.*, **123**, 1434 (2001)
- [5] H. Kasai, H. S. Nalwa, H. Oikawa, S. Okada, H. Matsuda, N. Minami, A. Kakuta, K. Ono, A. Mukoh, H. Nakanishi, *Jpn. J. Appl. Phys.*, **31**, L1132 (1992).

## Effect of Polymeric Stabilizers on the Catalytic Activity of Pt Nanoparticles

Nam Hoon Kim, Sang Woo Han, Inhyung Lee, and Kwan Kim

*Laboratory of Intelligent Interface, School of Chemistry and Molecular Engineering  
and Center for Molecular Catalysis, Seoul National University, Seoul 151-742, Korea*

Pt nanoparticles can be readily prepared by laser ablation of platinum foil in distilled water. To explore their possible application, we are currently examining their catalytic activity, after capping with polymers, for an electron transfer reaction between hexacyanoferrate (III) and thiosulfate ions. Herein, we report the effect of three typical capping polymers on the catalytic activity of the Pt nanoparticles; three typical polymers used were poly(N-vinyl-2-pyrrolidone) (PVP), polyvinyl alcohol (PVA), and polyethylenimine (PEI). We observed first of all that the electron transfer reaction occurs much faster in the presence of PEI-stabilized Pt nanoparticles than in the presence of PVP- or PVA-stabilized particles (see Fig. 1). Secondly, the catalytic activity of the PEI-stabilized Pt nanoparticles was observed to be highly dependent on the pH of the reaction medium (see Fig. 2). This clearly demonstrates that the net charge of the capping molecules plays a decisive role for the efficient Pt-mediated electron transfer between charged reactants.

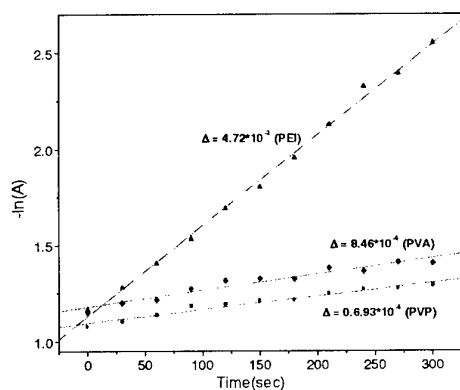


Fig. 1

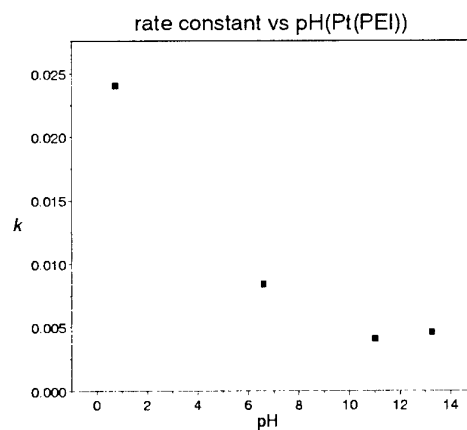


Fig. 2

## Surface potential difference measurements on indium-tin-oxide substrates modified with various organic molecules

Chimed Ganzorig and Masamichi Fujihira\*

*Department of Biomolecular Engineering, Tokyo Institute of Technology,  
4259 Nagatsuta, Midori-ku, Yokohama 226-8501, Japan*

Indium-tin-oxide (ITO) is the most widely used material as a transparent electrode due to its excellent transparency and high conductivity. It has been used as an anode in organic electroluminescent (EL) devices. The devices based on a bare ITO, however, exhibited inefficient hole injection due to insufficient high work function and required high drive voltages. Thus, various surface treatments of ITO have been attempted to change the work function (surface potential) of ITO in order to reduce the hole injection barrier height. In this paper, we report chemical modification of ITO with various organic molecules in which one end is binding groups (-COCl, -SO<sub>2</sub>Cl, and -PO<sub>2</sub>Cl<sub>2</sub>), the other end is terminal groups with different permanent dipole moment (H-, Cl-, and CF<sub>3</sub>-), and these two ends are linked by *p*-phenylene group. We also demonstrate the correlation between the change in contact potential difference (CPD) of various chemically modified ITO surfaces and the performance of the organic EL devices by using the chemical modification. We find that the enormous increase in ITO work function up to 0.9 eV is possible using phenylphosphoryl dichloride with a terminal group with high permanent dipole as CF<sub>3</sub>- in *para*-position. As we would expect, the molecular control of ITO work function can be applicable widely to other fields such as molecular electronics and solar cells.

---

\*Electronic mail: [mfujihir@bio.titech.ac.jp](mailto:mfujihir@bio.titech.ac.jp)

## Construction and Electron Transfer Characteristics of Multilayers of Au Nanoclusters Modified with Self-Assembled Monolayers Containing Ferrocene Group

Masayuki Okamura, Toshihiro Kondo, and Kohei Uosaki

Physical Chemistry Laboratory, Division of Chemistry, Graduate School of Science,  
Hokkaido University, Sapporo 060-0810, Japan

The formation of ordered multilayers of metal and semiconductor nanoclusters has attracted significant interest in view of the wide variety of the applications in nanotechnology and nanodevices. Although the attachment of the functional groups to the nanoclusters is expected to significantly increase the possible applications of nanocluster assemblies, the multilayer formation of the nanocluster with functionalities have not been reported. Here we report the successful formation of the multilayers of the Au nanoclusters protected by the mixed SAMs with three kinds of alkanethiols containing a methyl, ferrocene, or carboxylate terminal group, based on the electrostatic interaction between carboxylate and metal cation.<sup>1</sup> Electrochemical characteristics of the multilayers of the mixed alkanethiol SAM-protected Au nanoclusters on Au(111) electrodes were investigated.

The hexanethiol ( $C_6$ ) SAM-protected Au nanocluster (average core diameter: 2.4 nm) was synthesized using literature method.<sup>2</sup> Ferrocenylhexanethiol ( $FcC_6$ ) and 11-mercaptoundecanoic acid (MUA) were introduced into the Au nanocluster surface by the place-exchange method.<sup>2</sup> Deposition of the mixed SAM-protected Au nanocluster was carried out by alternate two-step dips of the carboxylate-terminated Au(111) substrate in an ethanol solution containing 1 mM  $Cu(ClO_4)_2$  and the 0.15 wt% mixed SAM-protected Au nanocluster with a rinse cycle.

Figure 1 shows the cyclic voltammograms (CVs) of the carboxylate-terminated Au(111) electrodes, which were prepared by repeating the above two-step dip and rinse cycles for 1, 2, 3, 5, and 10 times, measured in dichloromethane containing 0.1 M tetrabutylammonium perchlorate (TBAP) at a scan rate of 100 mV s<sup>-1</sup>. The oxidation and reduction peaks at +420 mV (vs. Ag/AgCl) due to the redox reaction of the ferrocene /ferricenium cation couple were observed in all cases. If the dipping of the substrate in the ethanol solution containing  $Cu^{2+}$  before the dip in the Au nanocluster solution was omitted, no current peaks were observed, showing that the carboxylate/ $Cu^{2+}$ /carboxylate electrostatic interaction is essential for the mixed SAM-protected Au nanocluster attachment. The greater the number of alternate two-step dip and rinse cycles, the greater the charge of the redox peaks, showing that multilayers of the mixed SAM-protected Au nanoclusters formed on the carboxylate-terminated Au(111) electrode surface. Based on the consideration of the structure, the present results showed that electron is transferred between ferrocene and the Au(111) electrode through the Au nanocluster cores and/or the ferrocene groups.

### References

1. T. Kondo, M. Okamura, and K. Uosaki, *Chem. Lett.*, in press (2001).
2. M. Brust et al., *J. Chem. Soc., Chem. Commun.*, 801 (1994).
3. S. J. Green et al., *J. Phys. Chem. B*, **101**, 1997 (1997).

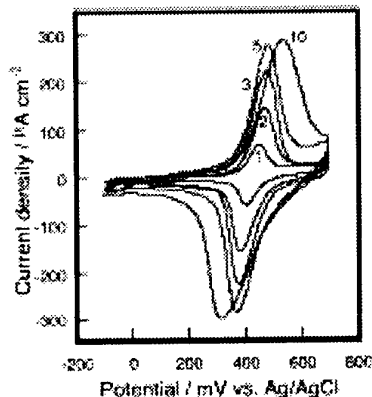


**Fig. 1** Cyclic voltammograms of carboxylate-terminated Au(111) electrode prepared by two-step dips and rinse cycles for 1, 2, 3, 5, and 10 times measured in dichloromethane containing 0.1 M TBAP at a scan rate of 100 mV s<sup>-1</sup>. Number of cycles is described in the figure.

**Control of the Charge Transfer Rate at a Gold Electrode Modified with a Self-Assembled Monolayer Containing Ferrocene and Azobenzene by Electro- and Photochemical Structural Conversion of *cis*- and *trans*-forms of the Azobenzene Moiety**

***Toshihiro Kondo, Toshihito Kanai, and Kohei Uosaki***

*Physical Chemistry Laboratory, Division of Chemistry, Graduate School of Science,  
Hokkaido University, Sapporo 060-0810, Japan*

Self-assembled monolayers (SAMs) of alkanethiols on gold have been extensively studied because of their potential applications in wide fields such as sensors, corrosion inhibition, wetting control, and biomolecular and molecular electronic devices. For these applications, SAM-modified electrodes play very important roles. It is important to control the redox properties of the redox group in the SAMs. In this report,<sup>1</sup> we constructed SAMs of a novel molecule, which contains ferrocene and azobenzene, 4-nitro-(1-azobenzyl)-1'-(6-mercaptohexyl) ferrocene (NAzFcC<sub>6</sub>SH) shown in Fig. 1, on gold and demonstrated that the charge transfer rate of the ferrocene group in the SAM can be reversibly controlled by electro- and photochemical structural conversion between *cis*/*trans* forms of the azobenzene moiety in the SAM.

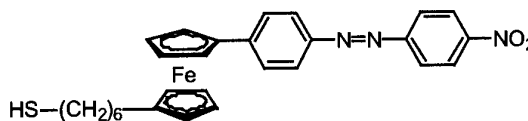


Fig. 1 NAzFcC<sub>6</sub>SH.

Figure 2 (a) shows the cyclic voltammogram (CV) of the gold electrode, which was prepared by dipping in the solution containing *trans*- and *cis*-forms of NAzFcC<sub>6</sub>SH with (4 : 1), measured in 0.1 M HClO<sub>4</sub> solution at a potential sweep rate of 50 mV s<sup>-1</sup> between +200 and +750 mV. Oxidation and reduction peaks due to the redox of the ferrocene/ferricenium cation were observed at +500 mV and +375 mV. When the potential was scanned to more negative than +200 mV, a pair of waves appeared around +100 mV in the first scan (solid line in Fig. 2 (b)). The charge in these waves was 15.4 μC cm<sup>-2</sup>, which corresponded to 38 % of the charge in the wave due to the redox of ferrocene. In the second scan, these waves disappeared, as shown by the dotted line in Fig. 2 (b). After the first potential scan to 0 mV, the redox potential of ferrocene became more negative (378 mV). The redox waves due to the redox of ferrocene were stably observed during many cycles between 0 and +750 mV. After the electrode surface was irradiated with UV light for more than 1 week, the CV completely returned to the original characteristics (Fig. 2 (a)). Based on the structural analysis by FT-IR spectroscopy, we concluded that the reversible change of electrochemical characteristics is due to the electro- and photochemical structural change of the azobenzene moiety.

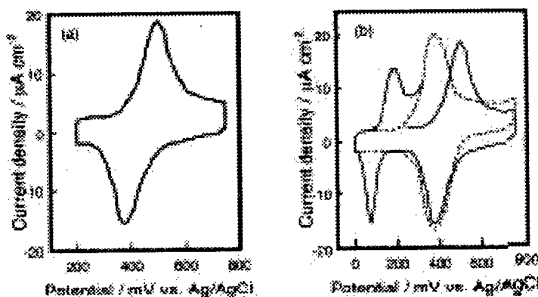


Fig. 2 (a) CV of the NAzFcC<sub>6</sub>SH SAM-modified gold electrode measured in 0.1 M HClO<sub>4</sub> in the potential range between +200 and +750 mV at a scan rate of 50 mV s<sup>-1</sup>. (b) The first scan (solid line) and second scan (dotted line) of the CVs measured in the potential region between 0 mV and +750 mV in 0.1 M HClO<sub>4</sub> at a scan rate of 50 mV s<sup>-1</sup>. Noted that the potential scan was started from +200 mV toward the positive direction.

**Reference**

1. T. Kondo, T. Kanai, and K. Uosaki, *Langmuir*, in press (2001).

## PREPARATION AND CHARACTERIZATION OF MESOSCOPIC PATTERNS OF NANOPARTICLES

Tetsuro Sawadaishi<sup>1</sup>, Kuniharu Ijio<sup>2</sup> and Masatsugu Shimomura<sup>1,2</sup>

<sup>1</sup>Spatio-Temporal Functional Materials Group, Frontier Research System, the Institute of Physical and Chemical Research (RIKEN, JAPAN); <sup>2</sup>Research Institute of Electronic Science, Hokkaido University, Sapporo 060-0812 Japan

e-mail: tetsuro@poly.es.hokudai.ac.jp

Arrangement of colloidal nanoparticles is important for the application of photonic devices, electronic devices and biosensors. Recently, we have reported that some types of submicrometer-sized regular patterns were formed in cast films by simple casting of polymer solution or ultra-fine particles dispersion. For example, regular stripe patterns were formed parallel to the receding direction of casting solution, when ultra-diluted solution was cast onto freshly cleaved mica surfaces (Fig. 1)<sup>1, 2</sup>. The purpose of this research is preparation of two-dimensional patterns of ultra-fine particles by self-assembly, and investigation of the structures in the patterns as the basic research for the application of novel functional electric or photonics materials.

Silica particles (NISSAN CHEMICAL INDUSTRIES, LTD.) , polystyrene beads (POLYSCIENCE, INC.), etc. were employed. Five  $\mu\text{l}$  of ultra-fine particles dispersion was cast onto freshly cleaved mica surface. Solvent was evaporated at various temperature

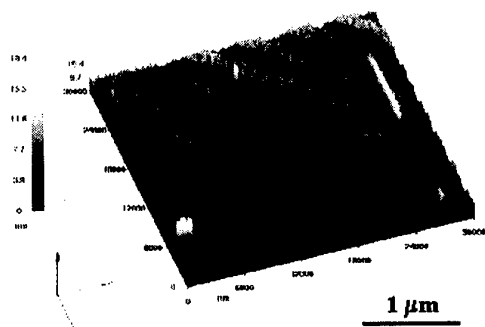


Figure 1 AFM image of cast film of cationic gold nanoparticles.

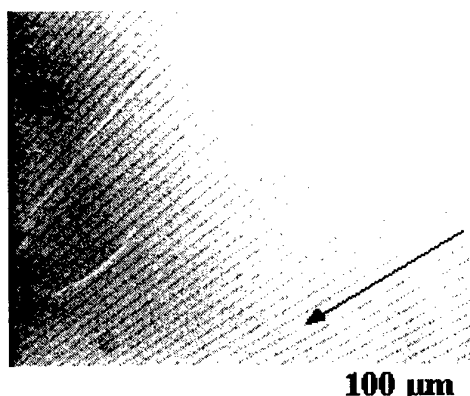


Figure 2 Optical micrograph of cast film of silica particles.



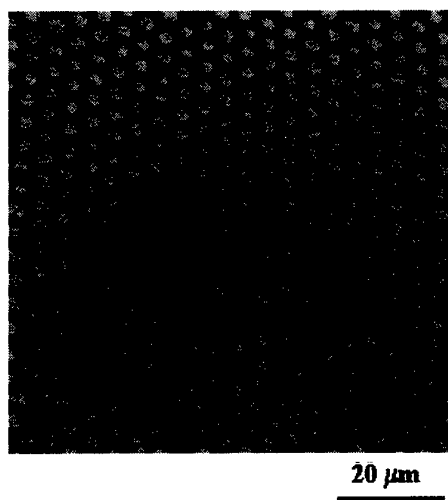


Figure 3 SEM image of honeycomb-patterned polymer film.

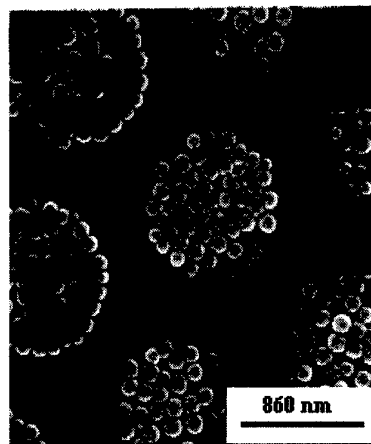


Figure 4 SEM image of silica particles (diameter: 100 nm) on honeycomb-patterned polymer film.

condition. When diluted dispersion (0.004 %) of silica particles was cast, stripe patterns were observed parallel to the receding direction by dissipative structures. However, by using highly concentrated dispersion (4.1 %) of silica particles, regular stripe crack patterns were formed parallel to the receding direction (Fig. 2). Next, we employed patterned cast films consisting of polymers as a substrate. Firstly, 30  $\mu$ l of amphiphilic polymer chloroform solution (1 mg/ml) was cast onto water surface in highly humid condition. After solvent was evaporated, polymer film was deposited on glass substrate, which were not modified, or modified by aminopropyltriethoxysilane or methyltriethoxysilane. As we have already reported<sup>3,4</sup>, the cast film obtained was having regular honeycomb structures (Fig. 3). After 1  $\mu$ l of silica particles dispersion was dropped onto the patterned film, solvent was naturally evaporated at 25 °C. Scanning electron micrograph of the cast film was shown in Fig. 4. Densely packed particles were observed in the hollow of honeycomb patterns. We will also report about the effect of temperature and chemical property of substrate, and patterning of ultra-fine particles in wide range by dip-coating.

1. T. Sawadaishi, K. Ijro, M. Shimomura, Y. Shiraishi, N. Toshima, T. Yonezawa, T. Kunitake, *Abstract of International Conference on Colloid and Surface Science (Tokyo, Japan)*, 173 (2000)
2. M. Shimomura, T. Sawadaishi, *Current Opinion in Colloid & Interface Science*, **6**, 11-16 (2001).
3. N. Maruyama, T. Koito, J. Nishida, S.-I. Nishimura, X. Cieren, O. Karthaus, M. Shimomura, *Thin Solid Films*, **327-329**, 854-856 (1998)
4. T. Nishikawa, J. Nishida, R. Ookura, S.-I. Nishimura, S. Wada, T. Karino, M. Shimomura, *Materials Science and Engineering C*, **10**, 141 (1999)

## Template Polymerization of Diacetylene Assemblies Based on DNA-Mimetics at the Air-Water Interface

**Jin Matsumoto,<sup>1</sup> Kuniharu Ijio,<sup>1,2</sup> S.-I. Nishimura<sup>3</sup> and Masatsugu Shimomura<sup>2</sup>**

<sup>1</sup> PRESTO, Japan Science and Technology Corporation (JST)

<sup>2</sup> Research Institute for Electronic Science, Hokkaido University

<sup>3</sup> Graduate School of Science, Hokkaido University

N12W6, Kita-ku, Sapporo, Japan, 060-0812

Tel : 81-11-706-3665, Fax : 81-11-706-4974, E-mail : matsu@poly.es.hokudai.ac.jp

DNA has a double helical supramolecular structure composed of complementary base pairs between adenine-thymine and guanine-cytosine. We have reported that the nucleobase amphiphiles formed base pairs and base trimers at the air-water interface,<sup>1,2</sup> which were similar to the structure of natural DNA duplex and triplex. In order to realize the template polymerization of nucleobase monomers based on base trimer formation at the air-water interface, photopolymerization of two-dimensional assemblies of the nucleobase amphiphiles with diacetylene (DA-Ade and DA-Thy) have been studied.<sup>3,4</sup> Here we prepared the mixed monolayer of DA-Ade, DA-Thy and C<sub>18</sub>-Cyt, which have no-polymerizable group, on an oligonucleotide solution to confirm that the DA-Ade/DA-Thy base pairs were organized along the template oligonucleotide dissolved in the water subphase at the air-water interface. The molecular weight of the polymerized DA-Ade/DA-Thy base pairs was determined by matrix-assisted laser desorption ionization mass spectrometry (MALDI-TOF-MS).

The 1:1:10 mixtures of DA-Ade, DA-Thy and C<sub>18</sub>-Cyt were spread on various oligonucleotide solutions containing poly(G). The mixed monolayers were irradiated with UV light (254 nm) on each subphase and the reflection spectra were measured by a fiber-optics spectrophotometer (Fig. 1). The mixed monolayer on the aqueous dT<sub>30</sub> subphase gave the blue form of polydiacetylene with the absorption maximum at ca. 620 nm. Because the Ade-Thy base pairs of DA-Ade and DA-Thy can form the base trimer with thymine of template dT<sub>30</sub>, DA-Ade/DA-Thy base pairs could be organized along the dT<sub>30</sub> and the diacetylenes could be photopolymerized (Fig. 2a). On the contrary the mixed monolayers on the d(GT)<sub>15</sub> and d(GGT)<sub>10</sub> subphase were not polymerized. C<sub>18</sub>-Cyt amphiphiles, which formed base pair with guanine of the d(GT)<sub>15</sub> and d(GGT)<sub>10</sub>, could be inserted between DA-Ade/DA-Thy base pairs (Fig. 2b). Moreover, the C<sub>18</sub>-Cyt complexed with poly(G) can act as a matrix to isolate the

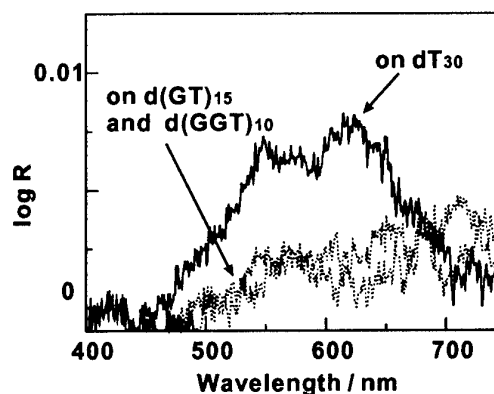


Fig. 1 Reflection spectra of the mixed monolayers on various oligonucleotide subphases with poly(G) after UV irradiation for 20 min.



## Sum frequency generation study on the structure of interfacial molecules and dynamics

S. Nihonyanagi, S. Ye\* and K. Uosaki

Physical Chemistry Laboratory, Division of Chemistry, Graduate School of Science, Hokkaido University,  
Sapporo 060, JAPAN

### INTRODUCTION

For the development of nano-technology, it is important to clarify the static and dynamic structure of interfacial molecules. Recently, sum frequency generation (SFG) spectroscopy has been demonstrated to be an ideal tool for the investigation of the structure of interfacial molecules as described well in a number of reviews published recently<sup>1</sup>. As a second-order nonlinear optical process, SFG is forbidden in a medium with inversion symmetry and is only active at an interface where the inversion symmetry is broken. In the infrared-visible SFG spectroscopy, one can obtain vibrational spectra of various interfaces.

We have been investigating the structures of self-assembled monolayers (SAMs) and interfacial water molecules at the interface between SAM modified quartz and electrolyte solution<sup>2-4</sup>. Here, we present some of the results on molecular structures at the quartz/SAM/solution interfaces by SFG spectroscopy as well as the SFG dynamics GaAs studied by pump and probe technique.

### EXPERIMENTAL

SFG system is schematically shown in Fig. 1. Tunable infrared radiation from 2.3 to 8.5  $\mu\text{m}$  was generated by OPG/OPA/DFG system pumped by a Nd:YAG laser (25 ps, 10 Hz). The SHG output at 532 nm of the Nd:YAG laser was used as visible light. The infrared and visible beams were overlapped at the sample surface with incident angle of 70 and 50 degrees, respectively. The SFG signal was detected by a photomultiplier tube and averaged by a gated electronic system<sup>2, 5</sup>. The vibrational spectroscopy was carried out by scanning the IR wavelength. In the pump and probe measurement, another 532 nm (or 355 nm) was incident to the sample as a pump beam after passing the delay line. Sum frequency of visible + IR with fixed wavelength was plotted against the pump delay time.

Clean fused quartz prisms were modified with silane molecules (N-(2-amino-ethyl)-3-aminopropyl-trimethoxy-silane: AAS or octadecyltrichlorosilane: OTS). SFG characterization was carried out in air and in electrolyte solution.

As received Si or Zn doped GaAs wafers (Mitsubishi Chemicals) were used for dynamics study.

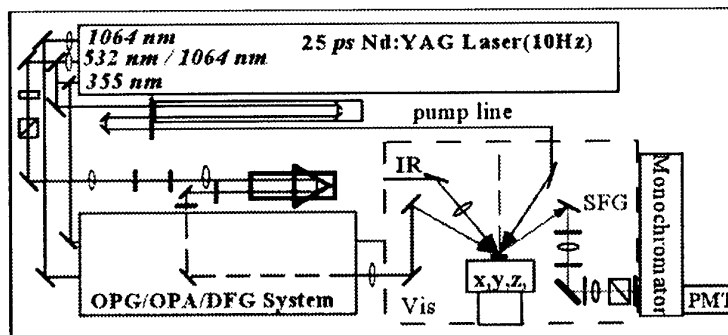


Figure 1. Schematics of SFG system.

\*Present address: Catalysis Research Center, Hokkaido University.

## RESULTS AND DISCUSSION

Figure 2 shows SFG spectra of AAS monolayers on the fused quartz in the phosphate buffer solutions with various pH ( $I=10$  mM). A small peak appeared at  $\sim 2900$   $\text{cm}^{-1}$  was assigned to the C-H stretching of  $\text{CH}_2$  group in AAS. Two broad bands observed at 3200 and 3450  $\text{cm}^{-1}$  were assigned to the symmetric O-H stretching of tetrahedrally and asymmetrically coordinated water molecules, respectively. The SFG intensity dramatically changed with pH. SFG signal was stronger at pH=2 than that at pH=7. Since this type of pH dependence was not observed at a bare quartz/electrolyte solution interface, this dependence should be due to an effect of the amino group in AAS monolayer. Thus, firstly in acidic solution,  $\text{NH}_2$  group was protonated to form positive charge at the interface. As a result, layers of water molecules should be aligned with their OH group facing to the bulk side of the solution. SFG intensity was also very strong in solution of higher pH. This behavior was similar to that observed at bare quartz surface. This should be due to the unreacted silanol ( $-\text{OH}$ ) group on the quartz surface. The detailed results will be discussed accompanied with the results of OTS case.

Results of the dynamics at GaAs will be also presented.

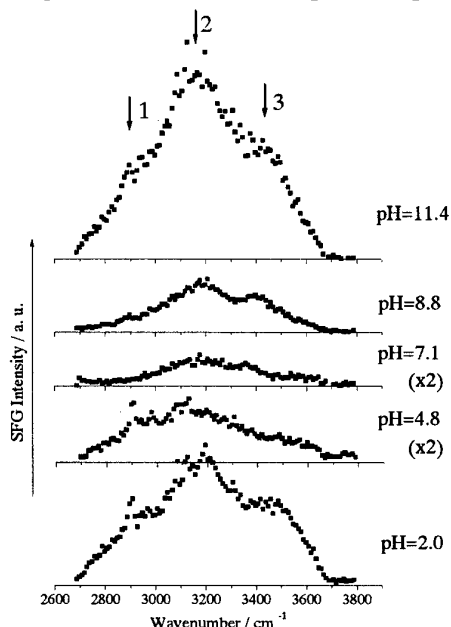


Figure 2. SFG spectra of AAS monolayer/fused quartz surface in buffer solutions of various pH.

## REFERENCES

1. P. B. Miranda and Y. R. Shen, *J. Phys. Chem. B* 103 (1999) 3292. See the reference of this article.
2. S. Ye, S. Nihonyanagi and K. Uosaki, *Chem. Lett.*, (2000) 734.
3. S. Nihonyanagi, S. Ye and K. Uosaki, *Electrochim. Acta*, in press, (2001).
4. S. Ye, S. Nihonyanagi and K. Uosaki, *PCCP*, 3 (2001) 3463.
5. S. Ye, T. Saito, S. Nihonyanagi, K. Uosaki, P. B. Miranda, D. Kim and Y. R. Shen, *Surf. Sci.*, 476 (2001) 121.

## Dynamics of Photogenerated Carriers at Surface-modified GaAs

*Ichizo YAGI, Kojiro EBINA, Satoru IDOJIRI and Kohei UOSAKI*

*Physical Chemistry Laboratory, Division of Chemistry, Graduate School of Science,  
Hokkaido University, Sapporo 060-0810, Japan ;E-mail: [yagi@pchem.sci.hokudai.ac.jp](mailto:yagi@pchem.sci.hokudai.ac.jp)*

### INTRODUCTION

Metal deposition at semiconductor surfaces has been carried out to improve the surface stability and the catalytic properties under photo-illumination. Metal deposit can accelerate charge separation in the semiconductor, but it can also work as a recombination center. Thus, the surface distribution and the shape of metal deposit are expected to affect the dynamics of photoexcited carrier. In the present study Cu cluster was electrodeposited on n-GaAs wafer and, the carrier dynamics was monitored by using femtosecond VIS-pump-IR-probe spectroscopy. The size and the spatial distribution of Cu cluster on GaAs surface was controlled by the electrochemical parameters during electrodeposition.

### EXPERIMENTAL

GaAs(001) substrate(n-type) with and without Cu electrodeposition were used as samples for the dynamics measurement. The wafer of n-GaAs(001) was prepared by etching in dilute HCl solution and rinsed with Millipore water before each experiment. Electrodeposition of Cu on n-GaAs was carried out by holding the electrode potential at -200 or -500 mV vs. Ag/AgCl reference electrode in 0.1 M H<sub>2</sub>SO<sub>4</sub> solution containing 1 mM CuSO<sub>4</sub>. Morphology of deposited Cu was examined by AFM. For the femtosecond VIS-pump-IR-probe measurement, pulsed light from two OPG/OPAs pumped by the regenerated Ti:S laser system was used. VIS-pump beam was generated by SHG of the signal light from an OPG/OPA and IR -probe beam was generated by DFG between the signal and idler light from the other OPG/OPA. These beams were overlapped at sample surface and the intensity of transmitted IR-probe light was detected by InSb detector (Fig. 1).

### RESULTS&DISCUSSION

In Fig. 2, transient absorption change of the n-GaAs samples (a) without and (b) with Cu electrodeposited at -500 mV. Cu particles with diameters of >50 nm covered the surface. The pump wavelength of 620 nm and the probe wavelength of 3.8  $\mu$ m were employed. Transient absorption by photoexcited carrier showed faster decay at the Cu-modified sample, which was due to the faster relaxation of photogenerated free electron. To estimate the effect of metal deposit on the photoexcited carrier dynamics, pump-probe measurements at the GaAs samples with both the different size and spatial distribution of Cu. Effects of the morphology of Cu deposit and the IRprobe wavelength on transient absorption of GaAs are currently under investigation.

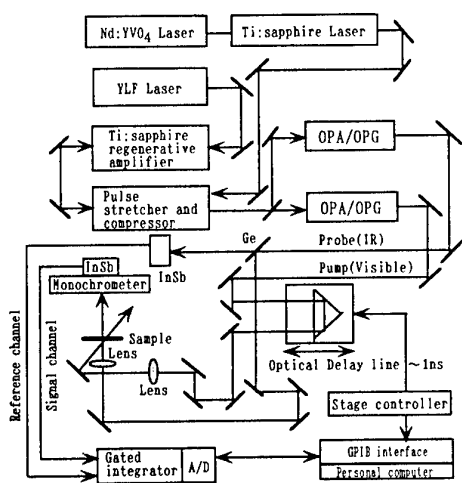


Figure 1. Optical arrangement for the VIS-pump-IR-probe spectroscopic measurement.

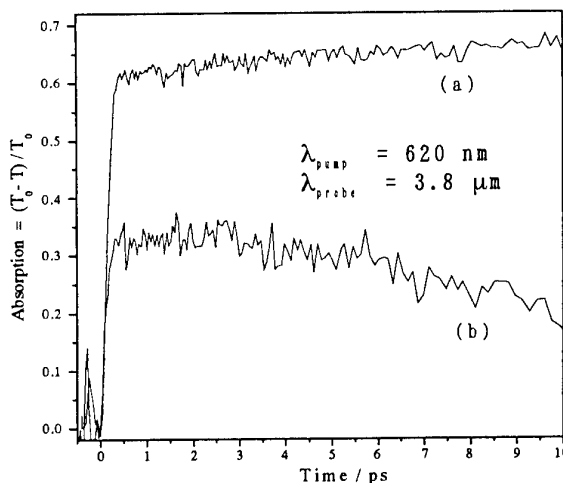


Figure 2. Transient absorption change at (a) GaAs and (b) Cu-modified GaAs.

# RIGID DENDRIMERS FOR LIGHT HARVESTING

Hiroyuki Sasabe <sup>1,2</sup>, Hirofumi Hokari <sup>1</sup>, Masahisa Osawa <sup>1,3</sup>, and Takashi Isoshima <sup>1,3</sup>

<sup>1</sup> Core Research for Evolutional Science and Technology (CREST),  
Japan Science and Technology Corporation (JST)  
2-1 Hirosawa, Wako, Saitama 351-0198, Japan

<sup>2</sup> Chitose Institute of Science and Technology  
758-65 Bibi, Chitose, Hokkaido 066-8655, Japan

<sup>3</sup> RIKEN (The Institute of Physical and Chemical Research)  
2-1 Hirosawa, Wako, Saitama 351-0198, Japan

Tel & Fax : +81-123-27-6109  
e-mail: sasabeh@photon.chitose.ac.jp

Dendrimers are macromolecules with regular branch structure emanating from the core. They are attractive platforms for molecular photonic and electronic devices, since they can include a number of functional groups in a well-defined structure. Light-harvesting is one of the most important functions to be achieved by a dendrimer. Light-harvesting is realized by antenna units which absorb light and focal component which emits light at a different wavelength or generates photocarrier. In order to realize efficient light-harvesting, energy transfer from the antenna units to the focal component should be maximized. Structural rigidity is essential to this purpose, since if the dendrimer is flexible the optimal arrangement of functional groups for energy transfer cannot be kept so that the averaged efficiency will be degraded severely. Therefore, we designed and synthesized two types of light-harvesting dendrimers, both with rigid structure.

The first ones are dendrimers based on carbazole and anthracene moieties shown in Fig. 1. (Rigorously speaking, they are dendrons rather than dendrimers since only one dendritic branch is attached to the core unit.) Carbazoles are used as rigid branch units which also work as antenna units. It is beneficial to introduce the ethynyl benzene groups at the peripheral part of the carbazole dendrons in order to increase the molecular extinction coefficient by the dendrons. Diethynylantracene is chosen as the energy acceptor at the focal point (core), due to large spectral overlap of its absorption band with the emission band of the carbazole units, and also due to its spectral window around 340 nm which is ideal for selective excitation of the carbazole units. Therefore, excitation of carbazole units at 340 nm is expected to result in intense emission at 470 nm from the anthracene unit via efficient energy transfer between them.

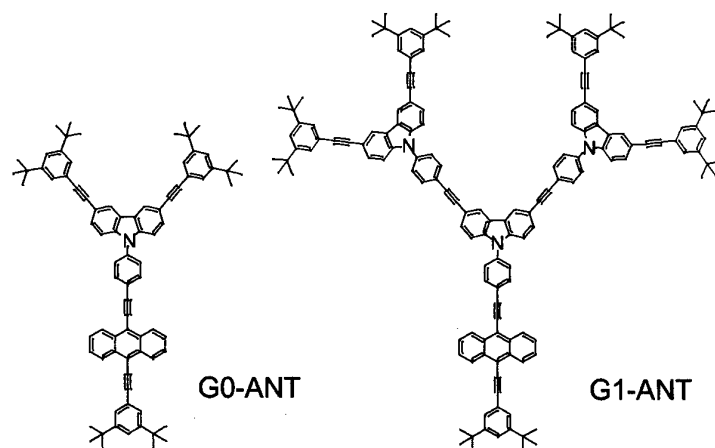


Fig. 1. Molecular structures of carbazole/anthracene-based light-harvesting dendrons

Both cw and time-resolved emission measurements at room temperature showed quench of carbazole emission by introduction of anthracene unit. As shown in Fig.2, emission from the anthracene unit significantly increased with the generation of the dendron, demonstrating efficient light-harvesting in this dendritic system.

The second ones are rigid dendrimers based on Ru(terpyridine)<sub>2</sub> links and Ni(bipyridine)<sub>3</sub> core, as shown in Fig.3. Rigidity of the Ni(bipyridine)<sub>3</sub> core unit with octahedral six-point coordination and the Ru(terpyridine)<sub>2</sub> units linked by 1,3,5-triethynylene benzene branches provides well-defined three-dimensional structure of the dendrimer<sup>1,2</sup>. The Ru(terpyridine)<sub>2</sub> units work as antenna and the core Ni(bipyridine)<sub>3</sub> unit as energy acceptor for light-harvesting.

Time-resolved emission of the dendrimer D-13-Ni was compared with a Ru-complex trimer 3-D which had no energy acceptor. Decay time constant of the emission from Ru-complex unit of D-13-Ni was 30 ns at room temperature, which was nearly identical to that of 3-D. This result suggests no significant energy transfer from Ru-complex units to Ni-complex core at room temperature. However, at low temperature of 150K, emission from Ru-complex unit was quenched by *ca.* 50 % in the dendrimers, suggesting energy transfer<sup>3</sup>.

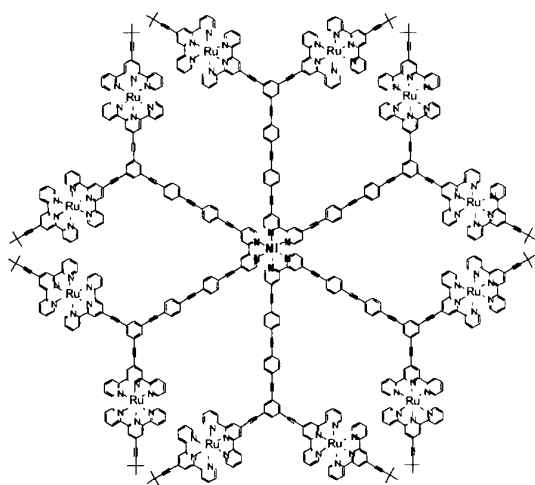


Fig.3. Molecular structure of D-13-Ni dendrimer

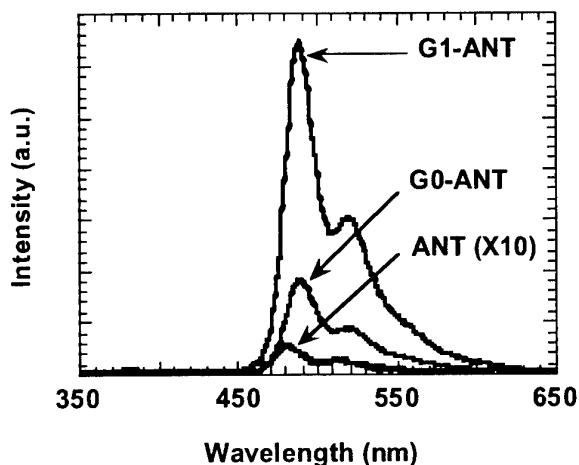


Fig.2. cw emission spectra of carbazole/anthracene-based dendrons. The intensity was normalized by the concentration. The excitation wavelength was 340 nm.

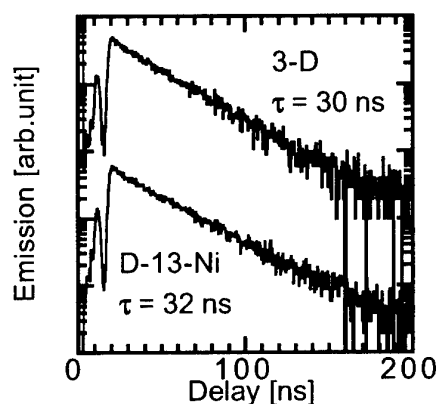


Fig.4. Decay profile of emission from Ru-complex unit. D-13-Ni is the dendrimer with Ni-complex core and 3-D is a trimer without an energy acceptor.

<sup>1</sup> M. Osawa et al., *Organometallics*, **18**, 112 (1999)

<sup>2</sup> M. Osawa et al., *4th Int. Symp. on Functional Dyes (IUPAC)*, Osaka (1999)

<sup>3</sup> M. Osawa et al., in *Hyper Structured Molecules III: Chemistry, physics and applications* (H. Sasabe, ed.), Gordon and Breach Science Publisher, New York (in press).



## Nanoimprint technology for the formation of high resolution periodic structure in electrooptic polymers

**Okiihiro Sugihara**

Faculty of Engineering, Shizuoka University 3-5-1 Johoku, Hamamatsu 432-8561 Japan

Simple fabrication technique of high resolution nonlinear gratings in electrooptic (EO) polymer films based on simultaneous embossing and poling at elevated temperature (SEPET) was proposed and demonstrated. The master gratings whose period ranges from  $\mu\text{m}$  to sub- $\mu\text{m}$  order which consist of polyimide die and metal base were fabricated by a single pulse two-beam interference technique using UV laser ablation, and the stability of the grating was investigated both thermally and mechanically. It was found that the master grating was stable enough against heat and imprint treatment cycles. The master molded several EO polymers (Disperse Red 1 (DR1) doped PMMA, Disperse Red 1 doped U-100, etc.) at around their glass transition temperatures ( $T_g$ s). At the same time, high voltage was applied to the polymers to induce the second-order nonlinearity. The grating profiles as well as the induced nonlinearity were estimated by changing the molding and removal conditions of the master grating. The mass-productivity of nonlinear gratings was also investigated. Moreover, formation of other waveguide components, for example, channel waveguide and fiber guide based on the SEPET process were also fabricated. SEPET method made it possible to form a channel waveguide having diffraction gratings as well as the fiber guide. The several advantages of this technique, high resolution, simple and cost-effective way, make it useful for several polymer waveguide devices.

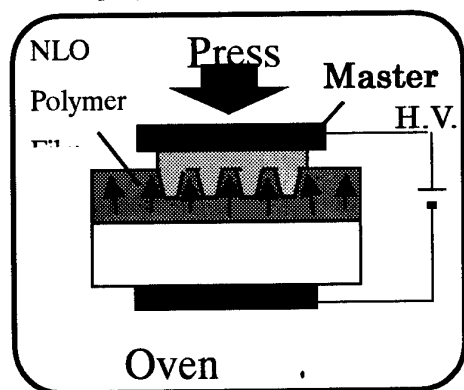


Fig.1 SEPET technique.

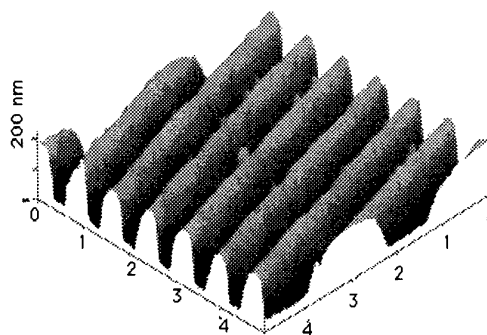


Fig.2 AFM Photograph of grating profile with  $0.7\mu\text{m}$  period in DR1/U-100 film.